Effects of Plasma Proteins on the Sieving of Macromolecular Tracers in the Kidney

by

Matthew Jordan Lazzara

B.S. Chemical Engineering
University of Florida, Gainesville, 1997

SUBMITTED TO THE DEPARTMENT OF CHEMICAL ENGINEERING IN PARTIAL FULFILLMENT OF THE REQUIREMENTS FOR THE DEGREE OF

DOCTOR OF PHILOSOPHY IN CHEMICAL ENGINEERING
AT THE
MASSACHUSETTS INSTITUTE OF TECHNOLOGY

FEBRUARY 2003

Signature of Author: .....
Department of Chemical Engineering
January 7, 2003

Certified by: .....
William M. Deen
Carbon P. Dubbs Professor of Chemical Engineering and Bioengineering
Thesis Supervisor

Accepted by: .....
Daniel Blankschtein
Professor of Chemical Engineering
Chairman, Committee for Graduate Students

Effects of Plasma Proteins on the Sieving of Macromolecular Tracers in the Kidney

by

Matthew Jordan Lazzara

Submitted to the Department of Chemical Engineering
on January 7, 2003, in partial fulfillment of the
requirements for the degree of
Doctor of Philosophy

ABSTRACT

The ultrafiltration of plasma in the mammalian glomerulus is the first step in the processing of blood by the kidney. Proper functioning of this process is critical to the kidney's ability to effectively eliminate waste and retain desirable substances. The glomerular barrier has long been regarded as both a size and charge selective screen for plasma solutes. The origin of this selectivity is found in the unique three-layered structure of the glomerular capillary wall (GCW), consisting of a fenestrated endothelium, the interdigitating foot processes of the glomerular epithelium, and the shared glomerular basement membrane (GBM). The selectivity properties of the GCW have commonly been probed by measuring the sieving coefficients of a variety of tracers, both proteins and exogenous polymers, across the intact glomerular barrier and across isolated components of the GCW. It was found previously that the sieving coefficients of the tracers Ficoll and Ficoll sulfate across isolated GBM were greatly elevated when BSA was present at physiological levels (Bolton et al. 1998). It was suggested that most of this increase was the result of steric interactions between BSA and the tracers which increased tracer partitioning from the bulk into the GBM. Such an effect, if present, would have important implications for the interpretation of macromolecular sieving studies, both *in vivo* and *in vitro.* The goals of this thesis research were to model the effect of an abundant protein on the partitioning of a dissimilar tracer molecule, to incorporate that effect into models for glomerular sieving, and to test the partitioning model by measuring the effect of protein concentration on the partitioning of protein and Ficoll in agarose gels.

The theoretical effects of solute size on partition coefficients in straight pores or randomly oriented fiber matrices have been investigated previously for very dilute solutions, where solute-solute interactions are negligible, and also for more concentrated solutions consisting of spherical solutes of uniform size. For concentrated solutions it has been found that steric and other repulsive interactions among solutes increase the partition coefficient above the dilute limit. To extend the results for porous or fibrous media to include concentrated mixtures of solutes with different sizes or shapes, we used an excluded volume approach. In this formulation, which describes steric interactions only, partition coefficients were computed by summing all volumes excluded to a solute molecule by virtue of its finite size, the finite size of other solutes, and the presence of fixed obstacles (pore walls or fibers). For a mixture of two spherical solutes, the addition of any second solute at finite concentration increased the partition coefficient of the first solute. That increase was sensitive to the size of the second solute; for a given volume fraction of the second solute, the smaller its radius, the larger the effect. When the

total volume fraction of solutes was fixed, an increase in the amount of a second, *smaller* solute increased the partition coefficient of the first solute, whereas an increase in the amount of a second, *larger* solute had the opposite effect. Results were obtained also for oblate or prolate spheroidal solutes and for fibrous media with multiple fiber radii. For constant total fiber volume fraction, an increase in the amount of a second, *smaller* fiber decreased the partition coefficient of a spherical solute, whereas an increase in the amount of a second, *larger* fiber had the opposite effect. Overall, the theory suggests that the introduction of heterogeneity, whether as mixtures of solute sizes or mixtures of fiber sizes, may cause partition coefficients to differ markedly from those of uniform systems.

Using the excluded volume partitioning model, the theory for the sieving of macromolecular tracers was extended to account for the presence of a second, abundant solute. Using that theory, we returned to the experimental data of Bolton et al. (1998) and attempted to model the effect of protein concentration on Ficoll sieving. The osmotic reduction in filtrate velocity caused by an abundant, mostly retained solute will also tend to elevate the tracer sieving coefficient. The osmotic effect alone explained only about one third of the observed increase in the sieving coefficients of Ficoll and Ficoll sulfate, whereas the effect of BSA on tracer partitioning was sufficient to account for the remainder. At physiological concentrations, predictions for tracer sieving in the presence of BSA were found to be insensitive to the assumed shape of the protein (sphere or prolate spheroid). The effect of plasma proteins on tracer partitioning is expected to influence sieving not only in isolated GBM, but also in intact glomerular capillaries *in vivo*.

To test the predicted effects of solute concentration on the equilibrium partitioning of single macromolecules and macromolecule mixtures, measurements of the equilibrium partition coefficients of BSA and four narrow fractions of Ficoll were made in agarose. Solutions of each test macromolecule were equilibrated with a known volume of gel, final liquid concentrations measured, and partition coefficients calculated by applying a material balance. The partition coefficient of each molecule was measured under dilute conditions and under conditions where BSA was present at concentrated levels. All measurements were made for two different gel solid volume fractions (4 and 6%). As expected, the partition coefficients decreased with increasing gel solid volume fraction and with increasing molecular size. Increasing BSA concentration caused an increase in the partitioning of BSA itself and that of all four sizes of Ficoll. This effect was most significant for the largest molecules. A subset of the measurements repeated at a higher ionic strength demonstrated that electrostatic interactions were unimportant. The experimental results were compared with predictions generated from the excluded volume partitioning theory. Agarose was represented as a randomly oriented array of cylindrical fibers, BSA was modeled as a prolate spheroid, and Ficoll was treated as a sphere. Comparisons of the theoretical predictions with the experimental data produced generally good agreement, indicating that steric interactions among solute molecules and between solute molecules and gel fibers could explain the partitioning behavior.

Thesis Supervisor: William M. Deen
Title: Carbon P. Dubbs Professor of Chemical Engineering and Bioengineering

ACKNOWLEDGEMENTS

My time as a graduate student at MIT has been extremely rewarding. I would like to thank here some of the individuals who have made it such a memorable and valuable experience.

I would first like to thank my advisor, Professor William Deen, for providing a very challenging and stimulating research environment and for his example of excellence and integrity in academic research. From his example, I have learned much which I am certain will serve me well into the future.

I would also like to thank the members of my thesis committee, Professors Ken Smith and Daniel Blankschtein, for their good advice, guidance, and support during the completion of my thesis. Their assistance was extremely valuable.

I would like to thank Professors Ken Smith and Clark Colton for providing a wonderful teaching opportunity for me as a graduate student. My experience as an instructor for the undergraduate course in heat and mass transfer will be one of my best memories of my time here.

Thanks to my labmates , Glen Bolton, Jeff White, Pat Gwynne, Scott Johnston, Bo Chen, Stephanie Homer, Chen Wang, Kim Kosto, Ian Zacharia, Greg Zugates, and Nitesh Nalwaya, for their insight and help along the way and for making lab an enjoyable place to spend so much time. Thanks also to my other MIT friends who made the journey with me and have provided necessary comic relief along the way.

Finally I would like to extend a special note of gratitude to all of my family and friends in Tampa for the tremendous support they have shown me during my years away from Florida. In a special way, I would like to thank my parents, Gwen and Philip, and my older brother, Philip Tyler, for their good example, constant love, and encouragement.

CONTENTS

LIST OF FIGURES

[the Anderson and Brannon (1981) theory] or from the excluded volume theory are shown for three ratios of solute radius to pore radius (r_i/R_p).

Figure 2-4 Partition coefficient for uniform spherical solutes in a fiber matrix, as a function of the ratio of solute radius to fiber radius (r_i/R_f) and the volume fraction of fibers (ϕ). Results are shown for infinite dilution ($\chi_i = 0$) and finite concentration ($\chi_i = 0.1$).

Figure 2-5 Partition coefficient for uniform spheroidal solutes in a fiber matrix, as a function of the axial ratio of the solute, η_i. Oblate spheroids have $\eta_i < 1$; spheres have $\eta_i = 1$; prolate spheroids have $\eta_i > 1$. Results are shown for two ratios of characteristic solute size to fiber radius (r_i/R_f), both for infinite dilution and for finite concentration. In all cases $\phi = 0.1$.

Figure 2-6 The partition coefficient of a tracer (Φ_1) as a function of the volume fraction of an abundant solute (χ_2), for a mixture of two spherical solutes in equilibrium with a random fiber matrix. Results are shown for various values of the ratio of solute radii (r_2/r_1). In each case $\phi = 0.1$ and $r_1/R_f = 2$.

Figure 2-7 The partition coefficient of one solute (Φ_1) as a function of the volume fraction of the other solute (χ_2), for a mixture of two spherical solutes in equilibrium with a random fiber matrix. Both solutes were assumed to be present at finite concentration, such that their total volume fraction was fixed at $\chi_t = \chi_1 + \chi_2 = 0.1$. In each case $\phi = 0.1$ and $r_1/R_f = 2$.

Figure 2-8 The partition coefficient of a spherical solute in a fibrous material containing two types of fibers with different radii. The partition coefficient is plotted as a function of the volume fraction of one fiber (ϕ_2), with the total volume fraction of fibers fixed at $\phi_t = \phi_1 + \phi_2 = 0.2$. Results are shown for various values of the ratio of fiber radii (R_2/R_1). In each case $\chi_i = 0.1$ and $r_i/R_1 = 2$.

Figure 2-9 The partition coefficient of a tracer (Φ_1) as a function of the volume fraction of an abundant solute (χ_2), for a mixture of two spherical solutes in equilibrium with cylindrical pores of radius R_p. Results are shown for various values of the ratio of solute radii (r_2/r_1). In each case $r_1/R_p = 0.2$.

Figure 2-10 The partition coefficient of one solute (Φ_1) as a function of the volume fraction of the other solute (χ_2), for a mixture of two spherical solutes in equilibrium with cylindrical pores of radius R_p. Both solutes were assumed to be present at finite concentration, such that their total volume fraction was fixed at $\chi_t = \chi_1 + \chi_2 = 0.2$. In all cases $r_1/R_p = 0.2$.

Figure 2-11 Partition coefficients predicted for spherical particles in agarose, in which the agarose gel was represented as a random fiber array having either uniform fibers

generated from the FFT model for an agarose "cube" of dimensions $3 \times 3 \times 2.3$ mm^3.

Figure 4-2 BSA partition coefficient (Φ_{BSA}) measured in 4% gels using 0.4 g/dL BSA solutions for gels which were used immediately after a three hr casting or which were first stored at 7 °C between one and seven days. All samples were equilibrated for 24 hr. Data are shown as mean ± s.e., with $n = 4$ for all measurements.

Figure 4-3 Absorbance of 2 g/dL BSA stored between one and seven days relative to the absorbance of a freshly prepared BSA solution. Samples were stored at 7 °C, 25 °C, or 25 °C on an orbital shaker.

Figure 4-4 Representative size exclusion chromatogram of BSA The second, larger peak corresponds to an $r_s = 36$ Å, equivalent to the known r_s of monomeric BSA. The smaller leading peak corresponds to an $r_s = 49$ Å, which is close to a value of $r_s = 47$ Å for dimeric BSA cited by Squire et al. (1968).

Figure 4-5 Comparison of experimental and theoretical results for BSA partition coefficient (Φ_{BSA}) versus bulk volume fraction of BSA (χ_{BSA}) in 4% agarose gels. The most dilute data point is taken from the experiments using a prewashed gel ($n = 4$). For all other points, $n = 8$, except the most concentrated point for which $n = 12$. Φ_{BSA} and χ_{BSA} values are shown as mean ± s.e.

Figure 4-6 Comparison of experimental and theoretical results for BSA partition coefficient (Φ_{BSA}) versus bulk volume fraction of BSA (χ_{BSA}) in 6% agarose gels. The most dilute data point is taken from the experiments using a prewashed gel ($n = 4$). For all other points, $n = 8$. Φ_{BSA} and χ_{BSA} values are shown as mean ± s.e.

Figure 4-7 Comparison of experimental and theoretical results for partition coefficients (Φ_i) of Ficolls in 4% agarose. Values are shown as mean ± s.e., with $n = 8$ for all Ficoll data, $n = 16$ for BSA points from Ficoll experiments, and $n = 8$ for BSA points from experiments with BSA alone.

Figure 4-8 Comparison of experimental and theoretical results for partition coefficients (Φ_i) of Ficolls in 6% agarose. Values are shown as mean ± s.e., with $n = 8$ for all Ficoll data, $n = 16$ for BSA points from Ficoll experiments, and $n = 8$ for BSA points from experiments with BSA alone.

Figure 4-9 Comparison of dilute Ficoll partition coefficients (Φ_i) as a function of Stokes radius (r_s) in 4 and 6% agarose with data obtained by Laurent et al. (1967) using a chromatography method. The lines shown for the present, narrow fraction data are best fits to the four data points obtained at each agarose solid volume fraction.

LIST OF TABLES

Chapter 1

Background

1.1 Introduction to Renal Physiology and Pathophysiology

The primary function of the mammalian kidney is the clearance of toxic metabolic waste products from the blood and the maintenance of water and electrolyte homeostasis. The functional units in the kidney responsible for the processing of blood and the formation of urine are the nephrons, of which there are roughly one million per human kidney (Tisher and Madsen 1986). A schematic of a mammalian nephron is shown in Fig. 1-1. The processing of blood and formation of urine by the nephrons is essentially a two-part process involving the ultrafiltration of plasma and subsequent reabsorption of desirable substances from the ultrafiltrate. The site of plasma ultrafiltration is the glomerulus, an anastomosing network of capillaries surrounded by Bowman's capsule. As will be discussed in further detail, the walls of the glomerular capillaries have a unique structure which is responsible for its special permeability properties. Blood enters the glomerulus through the afferent arteriole, and is ultrafiltered across the walls of the glomerular capillaries. The retained portion of the plasma exits via the efferent arteriole. The glomerular ultrafiltrate collects in Bowman's space and passes through the various sections of the tubule where water and salts are reabsorbed by the tubular cells at a homeostatic rate. In humans, the tubule can be up to 55 mm in

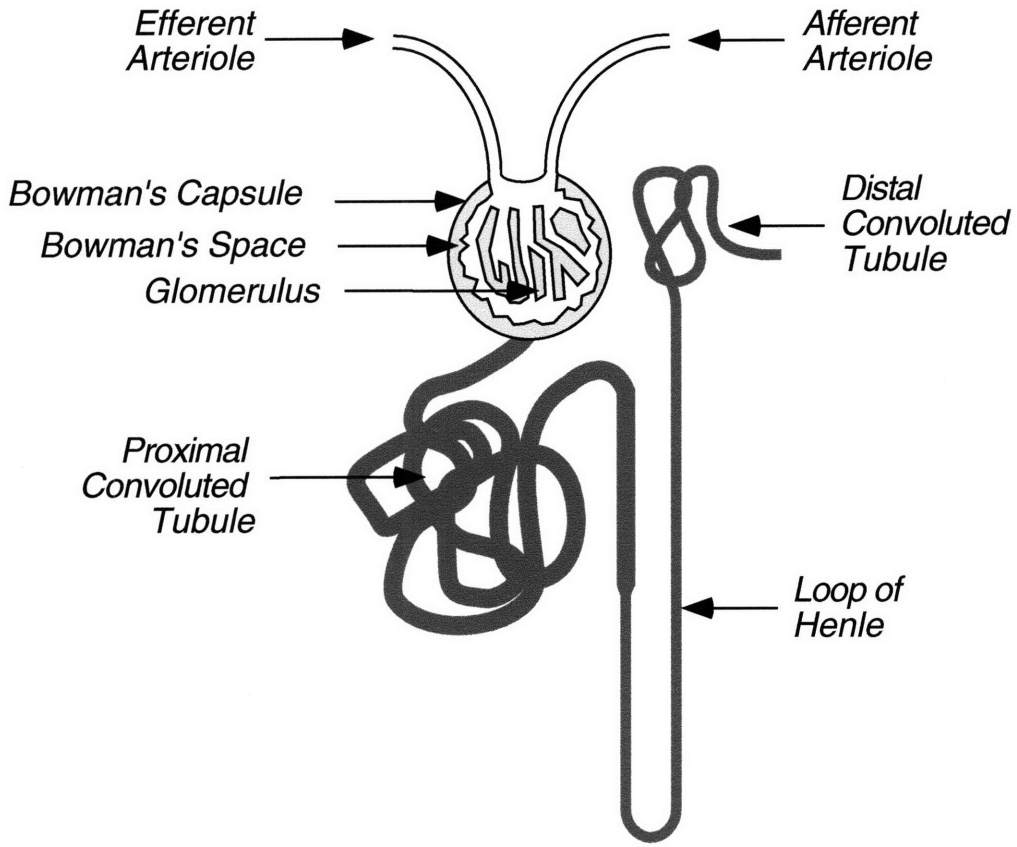

Figure 1-1: Schematic of the mammalian nephron. Blood enters the glomerulus through the afferent arteriole and exits via the efferent arteriole. In the glomerulus, plasma is ultrafiltered across the walls of the capillaries. The glomerular ultrafiltrate collects in Bowman's space and then passes through the tubule where water and salts are reabsorbed and other substances are secreted directly into the tubular fluid for excretion.

length, beginning at Bowman's capsule and ending at its junction with the urinary collecting ducts (Burkitt et al. 1993). The proximal convoluted tubule is responsible for the bulk of the reabsorption of water and electrolytes from the glomerular ultrafiltrate (Burkitt et al. 1993). At its distal end, the proximal tubule gives rise to the loop of Henle, a section of the tubule which is initially very thin and abruptly widens near its end. The loop begins in the outer region, or cortex, of the kidney, descends down into the inner region, or medulla, and then returns to the cortex where it empties into a collecting tubule. The collecting tubules of multiple nephrons empty into a common collecting duct. Other substances are secreted into the tubule lumen for excretion. In humans, approximately 150 L of glomerular ultrafiltrate is produced per day. Approximately 99% of that volume is reabsorbed by the tubule, so that the daily urine volume is roughly 1.5 L (Campbell 1990). In addition to its separatory function, the kidney is also involved in several hormone-regulated processes (Burkitt et al. 1993). For example, the kidney is responsible for the secretion of renin and angiotensin, which are involved in the maintenance of proper blood pressure, and the secretion of erythropoetin, a hematopoetic factor that stimulates the production of red blood cells in the bone marrow.

Renal diseases affect every major structural component of the kidney and result in a complex set of symptoms. The structure and function of the individual components of the renal microanatomy predisposes each to particular types of injury (Cotran et al. 1999). For example, many glomerular diseases are caused by the deposition of immune complexes which are trapped by the glomerular barrier, while tubular disorders are frequently caused by the action of toxic substances which are endocytosed by the cells which line the tubule (Cotran et al. 1999). Here we will briefly discuss some aspects of the clinical manifestations and pathology of glomerular disease. As a result of the interdependence of the various structures in the kidney, however, injury to one component often results in secondary damage to the other components. Glomerular diseases constitute a significant grouping of disorders in renal physiology and are common forerunners of chronic renal failure (Cotran et al. 1999). In some cases, glomerular injury is the result of a disorder in which the kidney is the primary site of involvement. In other cases, however, glomerular

injury is the secondary result of some systemic disease, such as lupus erythematosus or diabetes mellitus. Whether the glomerular injury is secondary or primary, the clinical manifestations and structural alterations to the glomerular architecture are often very similar. One of the most common results of glomerular disease is the nephrotic syndrome. Clinical manifestations of the nephrotic syndrome are proteinuria (elevated levels of protein in the urine), hypoalbuminemia (low plasma levels of albumin), edema (accumulation of fluid in the interstitial spaces in the body), hyperlidemia (elevated lipid levels in the blood) and lipiduria (elevated lipid in the urine). In all cases, the initial event that precipitates this constellation of symptoms is a structural change to the glomerular capillary wall, resulting in an increased permeability to marcomolecules. The direct result of that increase in permeability is proteinuria. Protein loss in the urine is so high that it exceeds the ability of the liver to replace albumin in the blood, resulting in albuminemia. Edema is the direct result of the loss of plasma oncotic pressure, causing fluid accumulation in the interstitial spaces of the body.

1.2 Structure and Composition of the Glomerular Capillary Wall

1.2.1 Microstructre. The glomerular capillary wall is unusual in having three layers: a fenestrated endothelium, the glomerular basement membrane (GBM), and the foot processes of glomerular epithelial cells. Between the epithelial foot processes are "filtration slits" bridged by slit diaphragms. Because of the low water permeability of most cell membranes, it is generally accepted that glomerular filtrate follows an extracellular path: through the fenestrae, across the GBM, and through the slits (passing through the slit diaphragms). To describe this flow, Drummond and Deen (1994b) proposed that the glomerular capillary wall be viewed as an assembly consisting of many repeating subunits. The basic structural subunit, as shown in Fig. 1-2, consisted of a single filtration slit, an associated area of GBM, and several fenestrae. The key geometric quantities in this model are the width of the structural unit (W), the thickness of the GBM (L), the width of the filtration slit (w), the dimensions of a fenestra, and the number of fenestrae per filtration slit. Representative values gleaned from various morphometric studies in rats

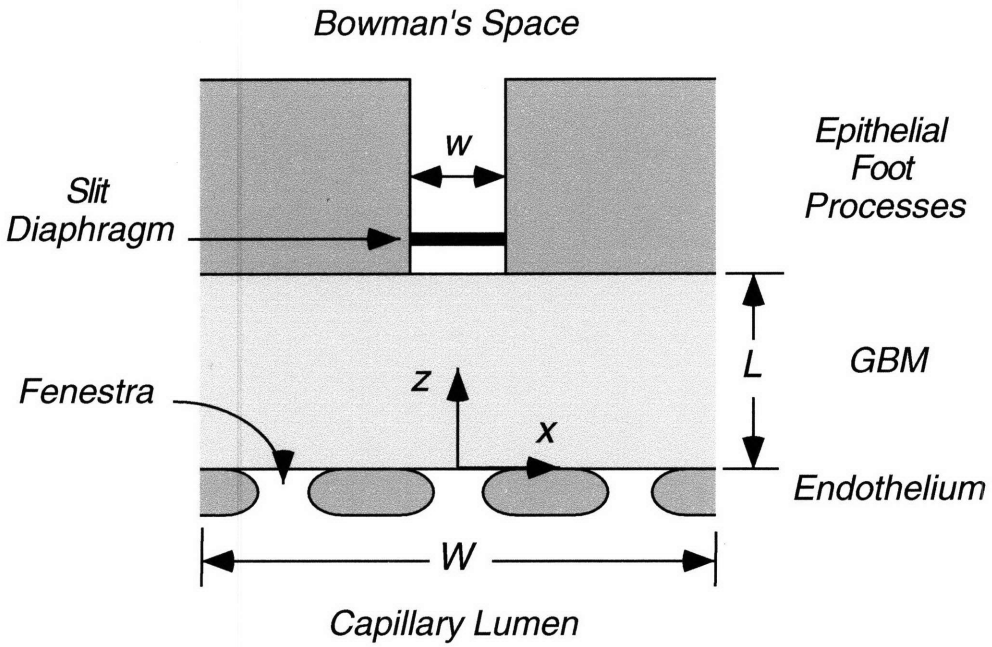

Figure 1-2: Idealized structural unit of the glomerular capillary wall, corresponding to one filtration slit. Modified from Edwards et al. (1999).

(Abrhamson 1987; Furukawa et al. 1991; Kondo 1990; Lea et al. 1989; Rodewald and Karnovsky 1974; Ryan 1986; Shea and Morrison 1975; Takami et al. 1991; Webber and Blackbourne 1970) are summarized in Table 1-1. Typical dimensions for rats are $W = 360$ nm, $L = 200$ nm, and $w = 39$ nm. The extent to which the GBM surfaces are blocked by cells is described by the fraction of the surface area occupied by slits ($\varepsilon_s = w/W = 0.11$) and the fraction of the area occupied by fenestral openings ($\varepsilon_f = 0.20$). As depicted in Fig. 1-2, the fenestrae have been reported to have an hourglass shape (Lea et al. 1989). The value of ε_f is based on the minimum cross-sectional area. Other information needed to model the fenestrae is discussed in Drummond and Deen (1994b).

Data for healthy humans suggest a slit width similar to that in rats, $w = 43$ nm (Ellis et al. 1987), but a significantly larger subunit width and GBM thickness, $W = 500$ nm and $L = 400$ nm (Lafayette et al. 1998; Squarer et al. 1998). A morphometric index used to describe slit spacing is the filtration slit frequency (FSF), which is related to the subunit width by $W = (2/\pi)(1/\text{FSF})$; the factor $2/\pi$ accounts for the random angle of sectioning (Drummond et al. 1994). A much more comprehensive discussion of glomerular anatomy is available elsewhere (Kanwar and Venkatachalam 1992).

1.2.2 Slit diaphragm. Among the key nanostructural dimensions are those which describe the openings in the slit diaphragm. Figure 1-3(a) shows an enlarged view of the slit diaphragm, oriented as in Fig. 1-2. The most frequently cited configuration for the slit diaphragm is that of Rodewald and Karnovsky (1974), who described a structure consisting of a central filament oriented parallel to the podocyte membranes, and regularly spaced bridge fibers, alternating from side to side, that connect the central filament to the membranes. This arrangement, which we term the "zipper" structure, is depicted in Fig. 1-3(b). The reported dimensions of the openings were 40×140 Å. These dimensions are problematic in that they imply a much more size-selective barrier than that shown by functional measurements, as will be discussed. A simpler structure, motivated by the observations of Hora et al. (1990), is shown in Fig. 1-3(c). This "ladder" structure remains quite tentative, and specific dimensions for it are not available from electron microscopy.

Width of structural unit, W, nm	360
Thickness of GBM, L, nm	200
Width of filtration slit, w, nm	39
Fractional area of fenestrae, ε_f	0.20
Fractional area of filtration slits, ε_s	0.11
Number of fenestral openings per slit, n_f	3

Table 1-1: Microstructural parameters representative of normal rats.

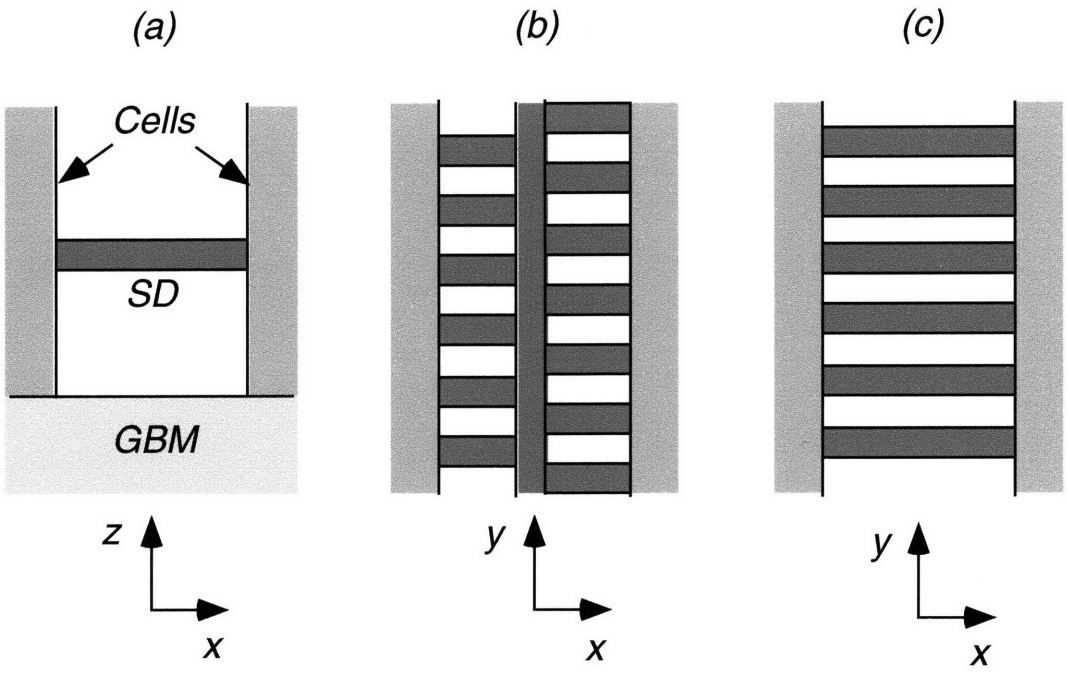

Figure 1-3: Representations of the epithelial slit diaphragm: (a) view perpendicular to the flow direction, as in Fig. 1-1; (b) view parallel to the flow direction, showing the "zipper" configuration; (c) another view parallel to the flow direction, showing the "ladder" configuration. From Edwards et al. (1997).

Recent efforts to elucidate the structure of the slit diaphragm have centered on its component molecules, particularly the newly identified protein nephrin. Nephrin has a molecular weight of ~150 kD and has been shown to be expressed exclusively by glomerular podocytes in the slit diaphragm region (Holthofer et al. 1999; Ruotsalainen et al. 1999). Lack of proper expression of the nephrin gene has been shown by Tryggvason and co-workers (Lenkkeri et al. 1999; Tryggvason 1999) to be linked to congenital nephrotic syndrome of the Finnish type, a glomerular disorder which results in severe proteinuria and which is associated with normal GBM and the loss of foot processes and slit diaphragms. Genetic analysis of the coding region of the nephrin gene has demonstrated that it is a single-pass membrane spanning protein with 8 Ig motifs and a type III fibronectin domain (Tryggvason 1999). It has been hypothesized that nephrin molecules extending out from adjacent podocytes might interact in a homophilic manner to form the zipper structure (Tryggvason 1999). Such proposals remain speculative, as the interaction of nephrin with other protein components of the slit diaphragm is not yet known. It has been demonstrated that cultured podocytes form linking structures which are similar to filtration slits *in vivo*, and that these intercellular linking structures contain the proteins zonula occludens-1, P-cadherin, and α, β and γ-catenin (Reisner et al. 2000).

1.2.3 Glomerular basement membrane. The GBM is a gel-like material which is 90-93% water by volume (Comper et al. 1993; Robinson and Walton 1987). Structural integrity is conferred by a heteropolymeric network of type IV collagen, laminin, fibronectin, entactin and heparan sulfate proteoglycan (Laurie et al. 1984; Maddox et al. 1992). Collagen IV, a triple helical polypeptide, is thought to form an interconnected network of fibers within the GBM, to which other matrix components are attached. Laminin, an asymmetrical four-armed structure, is thought to play an important role in the structural integrity of the GBM and in its interactions with the cellular layers of the glomerular capillary wall. The sulfated glycoprotein entactin, or nidogen, binds to collagen IV, heparan sulfate proteoglycan, and laminin, and thus may play an important role in linking GBM components to one another. Similarly, fibronectin, a 500 kD glycoprotein, binds to laminin, collagen IV, and heparan sulfate proteoglycan, suggesting that it too may have a role in

linking GBM constituents together. Heparan sulfate proteoglycan has been shown to comprise approximately 1% of the dry weight of the GBM (Kanwar and Farquhar 1979). The predominant GBM proteoglycan is made up of a 400 kD core protein called perlecan and four to five heparan sulfate chains bound to one end of the core protein (Vogel 1994). These anionic heparan sulfate chains are made of repeating disaccharide units of glucosamine and glucuronic acid (Kanwar and Venkatachalam 1992).

1.2.4 Endothelial glycocalyx. The glycocalyx that covers the luminal surface of the endothelial cells and fills the fenestrae may also be an important determinant of glomerular permeability. This layer is thought to be composed principally of sulfated proteoglycans (Sorensson 2000) and glycoproteins (Simionescu and Siomionescu 1986). Recent electron microscopy studies (Rostgaard and Qvortrup 1997) demonstrated a 300 nm thick filamentous surface coating which appeared to be present over both fenestral and interfenestral surfaces. The thicknesses of endothelial surface coatings reported by Rostgaard and Qvortrup (1997) exceed those previously observed by other authors (Luft 1966; Shirahama and Cohen 1972) by a factor of three to five. This difference was attributed to a novel method of tissue fixation, combined with a treatment that enhanced micrograph contrast.

1.3 Water Permeability of the Glomerular Capillary Wall

1.3.1 Structure-based model. The structural unit depicted in Fig. 1-2 was used by Drummond and Deen (1994b) to formulate a hydrodynamic model for the filtration of water across the glomerular capillary wall. The objective of the model was to predict values of the effective hydraulic permeability (k). Because the three layers of the capillary wall act as resistances in series, the overall hydraulic permeability is related to those of the individual layers by

$$\frac{1}{k} = \frac{1}{k_{en}} + \frac{1}{k_{bm}} + \frac{1}{k_{ep}} \qquad \textbf{[1-1]}$$

where k_{en}, k_{bm}, and k_{ep} are the hydraulic permeabilities of the endothelium, GBM, and epithelium, respectively. Thus, the problem is reduced to that of analyzing each layer in turn, and adding the results as shown in Eq. [1-1].

Finite-element solutions of Stokes' equation (the low-Reynolds-number form of the Navier-Stokes equation) have been used to characterize flow in the epithelial filtration slits (Drummond and Deen 1994a). The results indicated that the slit diaphragm is the dominant resistance to water flow between the foot processes, implying that the slit length is not an important parameter for water filtration. Using the zipper structure, with all dimensions as given in Rodewald and Karnovsky (1974), the permeability of the slit diaphragm (in SI units) was estimated as $k_s = 7.9 \times 10^{-8}$ m/s/Pa. Because what is desired is a filtrate velocity (or volume flux) averaged over an entire structural unit, and because the slits only occupy a fraction ε_s of the surface area, the epithelial permeability is $k_{ep} = \varepsilon_s k_s$. Using the representative dimensions for the rat given above, $\varepsilon_s = 0.11$ and $k_{ep} = 8.6 \times 10^{-9}$ m/s/Pa. It was shown that the resistances to water flow of the zipper and ladder structures are similar, provided they are assumed to have the same ratio of wetted cylinder area to cross-sectional area (Drummond and Deen 1994a).

Finite element solutions of Stokes' equation were used also to characterize the hydraulic resistance of a water-filled fenestra (Drummond and Deen 1994b). Using the dimensions given in Lea et al. (1989), the permeability of a single fenestra was estimated as $k_f = 1.0 \times 10^{-6}$ m/s/Pa. With the fenestrae occupying 20% of the filtering surface ($\varepsilon_f = 0.20$), it was found that $k_{en} = \varepsilon_f k_f = 2.0 \times 10^{-7}$ m/s/Pa. Comparing this with the epithelial result, it is found that $k_{en}/k_{ep} \cong 20$. This suggests that the dominant cellular contribution to k is that of the slit diaphragms, and that the water flow resistance of the fenestrae is negligible. This assumes, however, that the flow resistance of the glycocalyx is unimportant.

Water flow through the GBM was described by Drummond and Deen (1994b) using Darcy's law,

$$\mathbf{v} = -\frac{\kappa}{\mu}\nabla P \qquad [1\text{-}2]$$

where $\mathbf{v}$ is the local fluid velocity vector, κ is the Darcy permeability, μ is the fluid viscosity, and ∇P is the local pressure gradient. This relation is commonly used to model flow through porous or fibrous materials in situations where the pore spacings or interfiber spacings are much smaller than the dimensions of the sample. Microstructural details such as fiber concentration and fiber size are ignored, except as they influence the value of κ (units of m^2). This approach is suitable when the underlying structure is complex, but pressure-flow data are available from which κ can be evaluated. Such data are provided by studies of filters made by consolidating isolated GBM, an approach used by Robinson and co-workers (Robinson and Walton 1989; Walton et al. 1992) and by Daniels and her associates (Bolton et al. 1998; Daniels et al. 1992; Edwards et al. 1997a). Typical results are κ = 1-3 nm^2.

Equation [1-2] was combined with that which describes local conservation of mass ($\nabla \cdot \mathbf{v}$) and solved for the idealized GBM geometry showin in Fig. 1-2 (Drummon and Deen 1994b). Setting $\kappa = 2.7$ nm^2 and using the dimensions for the rat, it was found that $k_{bm} = 8.3 \times 10^{-9}$ m/s/Pa (Drummond and Deen 1994b). Because $k_{bm} \cong k_{ep} >> k_{en}$, it was concluded that the GBM and epithelial resistances to water filtration in the normal rat are about equal, and that the resistance of the endothelium is negligible. From Eq. [1-1], the overall hydraulic permeability was predicted to be $k = 4.1 \times 10^{-9}$ m/s/Pa. This is well within the range of values estimated from micropuncture measurements, which is roughly 3×10^{-9} to 5×10^{-9} m/s/Pa (Drummond and Deen 1994b).

The hydraulic resistance of the GBM is proportional to $1/\kappa$ (Drummon and Deen 1994b), and the Darcy permeability used above is larger than more recent estimates, including $\kappa = 1.5$ nm^2 (Edwards et al. 1997a) and $\kappa = 1.2$ nm^2 (Bolton et al. 1998). Thus, the GBM may actually account for somewhat more of the overall resistance than indicated. Using $\kappa = 1.2$ nm^2 instead of $\kappa = 2.7$ nm^2, the contribution of the GBM increases from 50% to 69% of the total resistance. Although the

overall hydraulic permeability is then reduced by 38% to $k = 2.5 \times 10^{-9}$ m/s/Pa, the predicted value is still in reasonable agreement with the experimental range.

There are uncertainties also in the cellular contributions to the hydraulic permeability. The value of k_{en} quoted above was computed by assuming that a fenestra is a short, water-filled channel of varying radius. An alternative model is that it is a gel-filled channel, due to the endothelial glycocalyx. When that possibility was explored by solving Brinkman's equation (related to Darcy's law) in a fenestra, with $\kappa = 2.7$ nm^2 as for the GBM, k_{en} was decreased to 1.3×10^{-8} m/s/Pa (Drummond and Deen 1994b). That change alone decreases the overall hydraulic permeability from 4.1×10^{-9} to 3.2×10^{-9} m/s/Pa, with the endothelium now accounting for 24% (instead of just 2%) of the total resistance. The main obstacle to refining the estimate of k_{en} is the unknown Darcy permeability of the glycocalyx.

Whereas the hydraulic resistance of the endothelium may have been underestimated, depending on the actual properties of the glycocalyx, that of the epithelium may have been overestimated. As already mentioned, the zipper structure is far too "tight" a barrier to be consistent with the relatively large test macromolecules that appear in normal glomerular filtrate. Larger openings in the slit diaphragm would also tend to increase the value of k_{ep}. To refine models either for water flow or for macromolecule movement through the filtration slits, an improved representation of the slit diaphragm geometry is needed.

Uncertainties in the individual contributions notwithstanding, the success of the water flow model in predicting the overall hydraulic permeability suggests that the overall balance between the GBM and cellular resistances is approximately correct. Indeed, the tendency to underestimate the endothelial contribution may well have canceled a tendency to overestimate the epithelial contribution.

1.3.2 GBM nanostructure and Darcy permeability. The Darcy permeability (κ) of a fibrous membrane or gel can be evaluated by using Eq. [1-2] to interpret measurements of fluid velocity as a function of applied pressure, as done in deriving the values for rat GBM used above. The value of κ can also be predicted, in principle, from nanostructural information. Numerous

theoretical results are available to predict κ for media consisting of arrays of cylindrical fibers with fluid-filled interstices; in some, the fibers are assumed to have a regular, spatially periodic arrangement, whereas in others the fiber orientation is random. The results of several approaches are reviewed in Jackson and James (1986). More recent results for random arrays of fibers include those of Clague and Phillips (1997) and Clague et al. (2000). A model developed specifically for the GBM is that of Palassini and Remuzzi (1998), who adopted a tetrahedral fiber arrangement, based on the structure of collagen IV. The application of several theories to GBM is discussed in Bolton and Deen (2001). For fibers of uniform radius (r_f), the results for regular or random arrays are typically of the form

$$\frac{\kappa}{r_f^2} = f(\phi) \qquad \textbf{[1-3]}$$

where ϕ is the volume fraction of fibers and the theory provides the specific function $f(\phi)$, which always decreases as ϕ increases. This implies that, for a fibrous material with a specified solids content, $\kappa \propto r_f^2$. In other words, the predicted value of κ is extremely sensitive to the value chosen for the fiber radius.

With ϕ 0.1, as has been reported for GBM (Comper et al. 1993; Robinson and Walton 1987), realistic values for κ (in the range 1-2 nm^2) are obtained from any of the theoretical expressions if the fiber radius is assumed to be about 1 nm (Bolton and Deen 2001). However, if r_f = 3-4 nm is employed, corresponding to the radii of fibers visible in electron microscopic images, the predicted value of κ is an order of magnitude too large. This led to the suggestion that GBM be modeled as a mixture of coarse and fine fibers, the former corresponding roughly to collagen IV fibrils and the latter to glycosaminoglycan chains (Bolton and Deen 2001; Edwards et al. 1997a). Underlying this suggestion is the presumption that the fine fibers would not have been resolved in the electron micrographs. With coarse and fine fiber radii of 3.5 nm and 0.5 nm, respectively, and roughly a 1:1 mixture (by volume) of the two fiber types, it was possible to reconcile the measured

values of κ and ϕ with the electron microscopic appearance of GBM. Parameter values for this two-fiber model of the GBM, which should be viewed as quite tentative, are summarized in Table1-2.

Additional quantitative information on the composition and the spatial arrangement of proteins and proteoglycans would be invaluable in efforts to reach more definite conclusions about the nanostructural basis for κ in the GBM. Analogous information is needed to estimate κ in the endothelial glycocalyx, and thereby better define the endothelial resistance to water flow.

1.4 Macromolecular Permeability of the Glomerular Capillary Wall

1.4.1 General relationships. This section begins with a discussion of physical phenomena that underlie efforts to relate macromolecule permeability to the structure of the glomerular capillary wall. Several key quantities are defined. In keeping with the microscopic viewpoint adopted for water filtration, this discussion focuses on the local sieving coefficient, which is the filtrate-to-plasma concentration ratio at a particular point along a capillary. This must be distinguished from the sieving coefficient for a whole kidney (or representative capillary), which is the average concentration in Bowman's space divided by that in afferent plasma. It is the average sieving coefficient which is accessible experimentally (e.g., from the fractional clearances of exogenous tracers). Even if the structure of the capillary wall is uniform along its length, the local sieving coefficient will vary with position, mainly because of the progressive increase in plasma protein concentration from the afferent to the efferent end. It has long been recognized that the resulting increase in oncotic pressure along a capillary will tend to slow filtration, which in turn will affect local sieving. Proteins may also have other effects on barrier performance, as will be discussed. The calculation of the average (measurable) sieving coefficient from local solute and volume fluxes (generally not measurable) has been described (e.g., Maddox et al., 1992). Although the local and average sieving coefficients are not identical, factors which affect the former will have a qualitatively similar influence on the latter.

Radius of coarse fibers, r_1, nm	3.5
Radius of fine fibers, r_2, nm	0.5
Volume fraction of coarse fibers, ϕ_1	0.046
Volume fraction of fine fibers, ϕ_2	0.054
Total volume fraction of solids (fibers), ϕ	0.10

Table 1-2: Parameters for 2-fiber model of GBM nanostructure.

The relationship between the overall sieving coefficient at any position along a capillary (Θ) and those of the individual layers can be approximated as

$$\Theta \cong \Theta_{en}\Theta_{bm}\Theta_{ep} \qquad \textbf{[1-4]}$$

For example, Θ_{bm} is the concentration at the downstream edge of the GBM divided by that at the upstream edge, with both concentrations evaluated just inside the GBM. To the extent that $\Theta_i \rightarrow 1$ for layer i, that layer will not contribute to the observed selectivity of the barrier. It is important to note, though, that the product in Eq. [1-4] implies that a 10% change in any individual Θ_i will affect the overall Θ by the same 10%, whether layer i is highly selective (e.g., $\Theta_i = 0.001$) or not (e.g., $\Theta_i = 0.9$). This contrasts with the situation for water flow, where the additive series-resistance relationship (Eq. [1-1]) implies that if layer i contributes a negligible fraction of the overall resistance (i.e., if $1/k_i << 1/k$), then a 10% change in k_i will have no noticeable effect on k. Thus, the layers combine to influence macromolecule selectivity in a fundamentally different way than they combine to influence water filtration. To obtain a more precise relationship between the overall Θ and those of the individual layers, additional factors must be included in Eq. [1-4] to account for the effects of soluble proteins (e.g., albumin) on the equilibrium partitioning of macromolecules, as discussed in Chapter 3.

Another important distinction between water filtration and macromolecule sieving is that the individual Θ_i's affect one another, whereas the individual k_i's could be computed independently. Moreover, the Θ_i's depend in general on the filtrate velocity, whereas the k_i's could be approximated as constants. (Constancy of k assumes, of course, that the applied pressures are not so large as to alter the structure of the capillary wall). The interdependence of the layer sieving coefficients and the effects of filtrate velocity are illustrated next by a somewhat simplified model for transport in the GBM.

As in the application of Darcy's law (Eq. [1-2]), the GBM will be regarded as an isotropic medium, such as an array of randomly oriented fibers. In such a material the local flux (**N**) of an uncharged macromolecule may be expressed as

$$\mathbf{N} = -K_d D_\infty \nabla C + K_c \mathbf{v} C \qquad \textbf{[1-5]}$$

where D_∞ is the solute diffusivity in free solution, **v** is the local fluid velocity vector, C is the solute concentration, and K_d and K_c are hindrance factors for diffusion and convection, respectively. The local solute concentration is based here on total volume (water plus solids), as is usually done in describing equilibrium partitioning or transport in gels. Just as Eq. [1-2] relates the local fluid velocity to the pressure gradient, Eq. [1-5] relates the local solute flux to the concentration gradient and the fluid velocity.

The diffusivity and hindrance factors in Eq. [1-5] all depend on molecular size. In general, steric and hydrodynamic interactions between a macromolecular solute and the fixed polymeric fibers of a membrane or gel will cause K_d and K_c to be less than unity, with both decreasing as r_s increases. The experimental estimation of these hindrance factors in GBM is discussed later. Another property of a fibrous membrane or gel that influences transport and depends on r_s is the equilibrium partition coefficient (Φ). The partition coefficient is a thermodynamic quantity that describes the tendency of steric and/or electrostatic interactions to exclude macromolecules from the material. As with the hindrance factors, it is typically less than unity and decreases with increasing r_s. As defined here, if the GBM were in equilibrium with plasma, then $C = \Phi C_p$, where C_p is the plasma concentration. Steric exclusion from the GBM is important, but it appears that electrostatic interactions are not (Bolton et al. 1998). Although the partition coefficient does not appear in Eq. [1-5], it enters the analysis when concentrations within the GBM are related to those in plasma or the other structures.

Assume for the moment that the GBM extends from $z = 0$ to $z = L$, that the solute concentration depends only on z and that the solute flux and fluid velocity (magnitudes N and v, respectively) are each constant. This "one-dimensional" model, involving just z, corresponds to a hypothetical GBM with fully accessible surfaces (i.e., $\varepsilon_f = \varepsilon_s = 1$). As shown in Deen et al. (2001), only a slight modification of the results is needed to describe the more realistic situation where the surfaces are largely blocked by cells. In the one-dimensional model the solute concentration profile in the GBM can be derived analytically for any specified values of Θ_{en} and Θ_{ep}. This allows the sieving coefficient in the GBM to be evaluated. The result is

$$\Theta_{bm} = \frac{\Phi K_c}{\Theta_{ep}\left(1 - e^{-Pe}\right) + \Phi K_c e^{-Pe}} \qquad \textbf{[1-6]}$$

where Pe is the Péclet number,

$$Pe = \frac{(\Phi K_c) v L}{(\Phi K_d) D_\infty} \qquad \textbf{[1-7]}$$

Notice in Eq. [1-6] that the sieving coefficient in the GBM depends on that for the epithelium (filtration slits). Notice also the effect of v, which is in the numerator of Pe (Eq. [1-7]). The physical significance of the Péclet number is that it measures the importance of convection relative to diffusion; convection tends to dominate for large Pe and diffusion for small Pe. Equation [1-7] has been written with the common factor Φ in the numerator and denominator to emphasize that, because only the products ΦK_c and ΦK_d appear there and in Eq. [1-6], those two lumped quantities are sufficient to describe the intrinsic size-selectivity of a membrane such as the GBM. That is, Φ, K_c, and K_d need not be known separately. Although the simplified model employed here assumes that Φ for a tracer (e.g., Ficoll) has the same value at both sides of the GBM, a more detailed theory

indicates that it depends on the local concentration of albumin and other abundant proteins (see Chapter 3). Accordingly, it is expected to differ at the two sides of the GBM, as discussed later.

The dependence of Θ_{bm} on Θ_{ep} predicted by Eq. [1-6] is illustrated by the curve in Fig. 1-4. In these calculations Pe and ΦK_c were held constant at values representative of a macromolecule with $r_s = 35$ Å in rat GBM. It is seen that Θ_{bm} is predicted to range from values above unity for a highly selective filtration slit ($\Theta_{ep} \rightarrow 0$) to values below unity for a nonselective one ($\Theta_{ep} = 1$). The behavior for highly selective slits reflects concentration polarization within the GBM, as noted in Edwards et al. (1999). That is, a concentration increase in the direction of flow arises to provide a diffusional driving force in the other direction. The opposing contributions of diffusion and convection in the GBM reduce N to what can be accommodated by the slit, thereby maintaining the steady state. Inspection of Eq. [1-6] reveals that the upper limit of the polarization effect in the GBM is $\Theta_{bm} \rightarrow \exp(Pe)$ for $\Theta_{ep} \rightarrow 0$. It is seen also that GBM polarization disappears exactly (i.e., $\Theta_{bm} = 1$) if $\Theta_{ep} = \Phi K_c$, for any Pe. Only for $\Theta_{ep} > \Phi K_c$ is the slit permeable enough to allow the basement membrane to enhance the overall selectivity (i.e., $\Theta_{bm} < 1$), rather than degrade it. A final noteworthy aspect of Eq. [1-6] is that it shows that $\Theta_{bm} \rightarrow 1$ as $Pe \rightarrow 0$, for any positive values of Θ_{ep} and ΦK_c. This is an example of a well-known phenomenon in ultrafiltration, which is the tendency for filtrate and retentate concentrations to equilibrate as diffusion becomes more important. In this instance, the equilibration is just across the GBM.

The simplified, one-dimensional analysis just discussed illustrates an important, general point, which is that the individual sieving coefficients depend on one another and on the relevant Péclet number(s). Although the Péclet number discussed was that for the GBM, analogous Péclet numbers for the fenestrae and filtration slits can be expected to influence Θ_{en} and Θ_{ep}, respectively. Such effects have been discussed in models of the slit diaphragm (Drummond and Deen 1995; Edwards et al. 1999). A consequence of the dependence of the sieving coefficient on the Péclet numbers is that great care must be taken in extrapolating results from one experimental situation to another. For example, one cannot expect a sieving coefficient measured for GBM in vitro to equal that in vivo, even if the isolated GBM preparation is perfect. The thickness of a filter made by

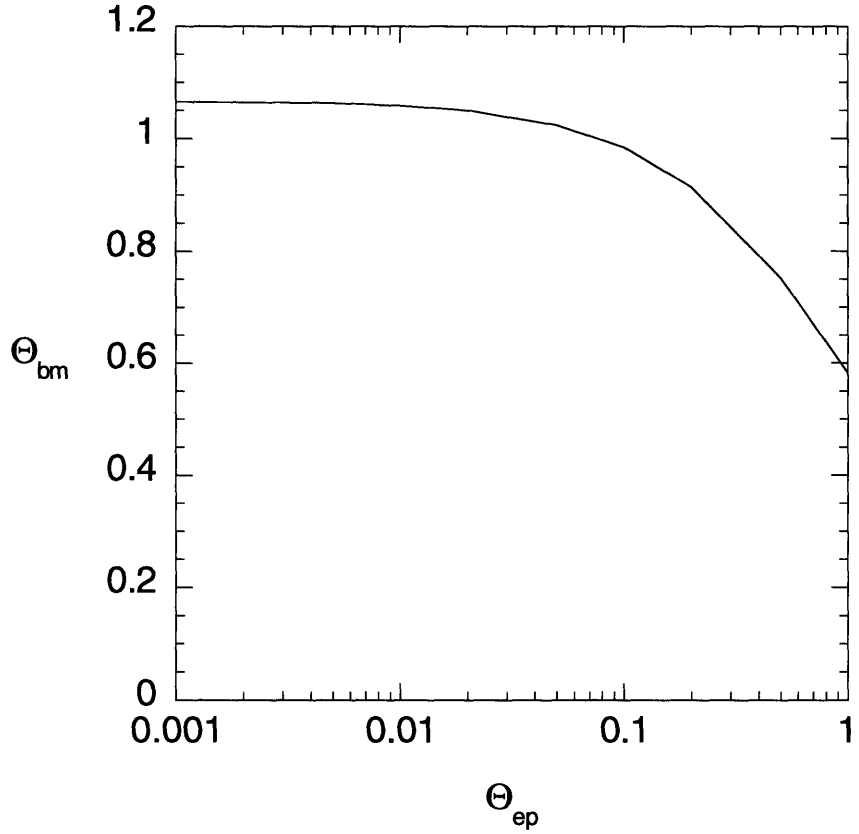

Figure 1-4: Dependence of the GBM sieving coefficient (Θ_{bm}) on that in the epithelial filtration slit (Θ_{ep}), for a molecule with $r_s = 35$ Å. The predictions are based on Eq. [1-6], with $Pe = 0.065$.

consolidating GBM fragments will greatly exceed that of a single layer of GBM and the filtrate velocity is unlikely to equal that in vivo; both of these differences will affect *Pe* (Eq. [1-7]). Moreover, the modifying effect of the epithelial sieving coefficient will be absent.

1.4.2 Experimental assessment of GBM and cellular contributions. As mentioned earlier, measurements of water filtration rates across filters prepared from isolated GBM have permitted the evaluation of its Darcy permeability. Sieving experiments using similar isolated GBM preparations have been valuable in assessing its selectivity to macromolecules, including proteins, neutral and charged derivatives of dextran, and neutral and charged derivatives of Ficoll (Bolton et al. 1998; Cochrane et al. 1997; Cochrane and Robinson 1995; Daniels 1994; Daniels et al. 1992; Edwards et al. 1997b; Walton et al. 1992). Ficoll has been preferred in the more recent studies, because it diffuses as an ideal, neutral sphere (Bohrer et al. 1984; Davidson and Deen 1988) and because it can be used also in fractional clearance studies in vivo [e.g., (Blouch et al. 1997; Oliver et al. 1992; Remuzzi et al. 1993)]. An example of sieving data obtained in isolated rat GBM with uncharged Ficoll is shown in Fig. 1-5. The data are those of Bolton et al. (1998), as replotted in slightly modified form (see Chapter 3). As shown by the lower set of symbols, which are results for protein-free solutions, there was a gradual decline in sieving coefficient with increasing molecular size, from about 0.6 at r_s = 20 Å to about 0.03 at r_s = 50 Å. Not shown in Fig. 1-5 are results obtained for Ficoll sulfate, which were indistinguishable from those for Ficoll (Bolton et al. 1998).

The sieving results for Ficoll and Ficoll sulfate in protein-free solutions were analyzed by Lazzara and Deen (2001) (Chapter 3) to estimate values of ΦK_d and ΦK_c for GBM. The data were fitted using a sieving relationship similar to Eq. [1-6] (but with $\Theta_s = 1$) and assumed expressions of the form

$$\Phi K_d = \exp(-Ar_s) \qquad \textbf{[1-8]}$$

$$\Phi K_c = \exp(-Br_s) \qquad \textbf{[1-9]}$$

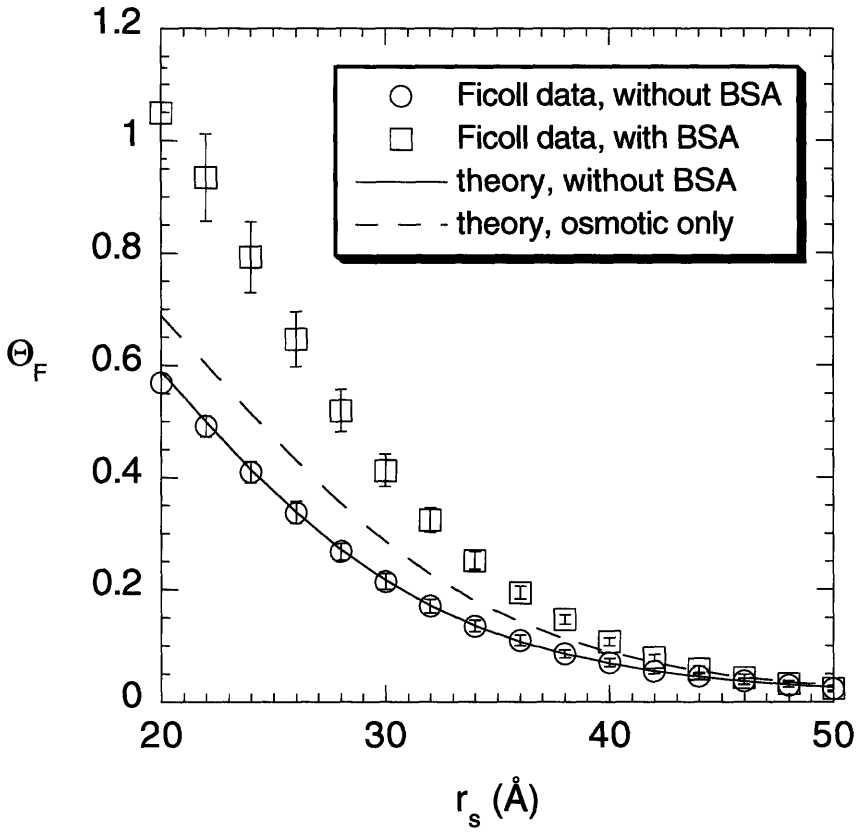

Figure 1-5: Sieving coefficient of Ficoll (Θ_F) as a function of Stokes-Einstein radius (r_s) for isolated rat GBM. The symbols with error bars represent the data of Bolton et al. (1998). Theoretical curves are shown for a solution without BSA and for a BSA solution with osmotic effects. From Chapter 3 and Lazzara and Deen (2001).

The values of the empirical constants A and B were very similar for Ficoll and Ficoll sulfate, with averages of $A = 0.130$ Å^{-1} and $B = 0.072$ Å^{-1} for the two sets of data. Equations [1-8] and [1-9] have no theoretical basis, except for the expectation that both quantities should be near unity for small r_s, and should decline to zero for very large molecules. Nonetheless, as shown by the lower curve in Fig. 1-5, excellent fits to the data for $20 \leq r_s \leq 50$ Å were obtained with just the two adjustable parameters. Empirical expressions similar to Eqs. [1-8] and [1-9] were also employed previously (Bolton et al. 1998; Edwards et al. 1999).

The use of Eqs. [1-8] and [1-9] to make inferences about the glomerular capillary wall assumes, of course, that the isolated GBM was not functionally different from that in vivo. The possibility that GBM is altered during the isolation process has been examined using a variety of methods. Immunofluorescent microscopy of consolidated GBM filters demonstrated the presence of type IV collagen, laminin, and the core protein of heparan sulfate proteoglycan (Daniels et al. 1992), the main components of GBM. The sulfated side chains of GBM proteoglycans are also present in GBM isolated using N-lauryl sarcosine to lyse cells (Daniels 1994), the procedure employed to obtain the data from which Eqs. [1-8] and [1-9] were derived (Bolton et al. 1998). The permeability of GBM filters was not changed when a milder detergent, Triton X-100, which has been shown to preserve heparan sulfate proteoglycan, was used to lyse glomerular cells (Daniels 1994). That isolated GBM is relatively intact is suggested also by electron microscopy studies: the spatial distribution of cationic ferritin has been found to be similar to that in vivo (Kanwar and Venkatachalam 1992).

A technical advance due to Daniels and co-workers that has permitted the measurement of diffusional permeabilities for macromolecules is the use of confocal microscopy to monitor the movement of fluorescent tracers across segments of isolated glomerular capillaries (Daniels et al. 1993; Edwards et al. 1997b). Experiments have been performed with intact glomeruli, freshly isolated from rats, and with glomeruli in which the cells have been removed by detergent lysis, leaving only GBM. Thus, it has been possible to compare the diffusional permeability of intact

capillary walls (p) with that of bare GBM (p_{bm}). Diffusional permeabilities of series barriers obey a resistance formula like Eq. [1-1], so that

$$\frac{1}{p} = \frac{1}{p_{en}} + \frac{1}{p_{bm}} + \frac{1}{p_{ep}} = \frac{1}{p_{bm}} + \frac{1}{p_{cell}} \qquad \textbf{[1-10]}$$

The two cellular contributions, which cannot be distinguished using this approach, have been lumped together in the second equality as p_{cell}. Edwards et al. (1997b) measured p and p_{bm} for four narrow fractions of Ficoll (r_s = 30-62 Å), and found that p_{bm} for each molecular size was an order of magnitude larger than p. It was calculated that the GBM contributes only 13-26% of the diffusional resistance of the intact capillary wall (depending on r_s). The finding that $p_{cell} << p_{bm}$ for Ficoll is qualitatively similar to earlier results for dextran (Daniels et al. 1993).

The experimental estimates of the GBM hindrance factors for Ficoll are plotted in Fig. 1-6. The results for ΦK_d and ΦK_c derived from sieving data (Eqs. [1-8] and [1-9]) are compared with values of ΦK_d calculated from p_{bm}. The relationship between the diffusional permeability and diffusional hindrance factor is $p_{bm} = \Phi K_d D_o / L$, where L (the GBM thickness) was taken to be 200 nm. The agreement between the two independent estimates of ΦK_d is remarkably good, given the different experimental preparations and the several assumptions required in making this comparison. The finding that $\Phi K_c >> \Phi K_d$ for Ficoll is qualitatively consistent with data for globular proteins and Ficoll in agarose gels (Johnson et al. 1996; Johnston and Deen 1999, 2002).

Using v = 4 μm/s as a typical average filtrate velocity for the rat (corresponding roughly to single nephron glomerular filtration rate of 40 nl/min), Pe calculated from Eqs. [1-7]-[1-9] ranges from 0.016 at r_s = 20 Å to 0.22 at r_s = 50 Å. These small values of Pe indicate that diffusion within the GBM is relatively rapid in vivo (compared to convection), even for relatively large molecules. A consequence of this is that concentration polarization within the GBM will tend to be minimal, even if the filtration slits are highly selective barriers. This tends to mitigate objections that are sometimes made to a glomerular capillary "design" in which the limiting barrier is the one farthest

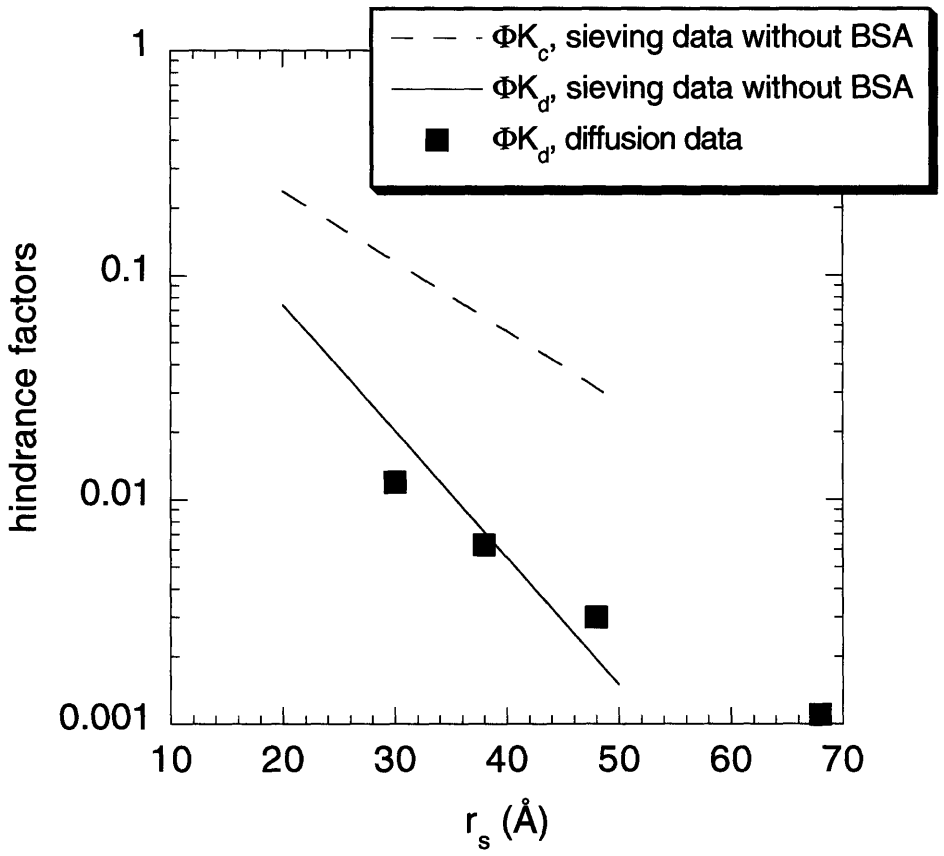

Figure 1-6: Diffusive (ΦK_d) and convective (ΦK_c) hindrance factors for Ficoll in GBM, as a function of Stokes-Einstein radius (r_s). The filled squares are values of ΦK_d calculated from the confocal microscopy data of Edwards et al. (1997), and the lines are the estimates from sieving data in isolated GBM without BSA (Eqs. [1-8] and [1-9]).

downstream. Although diffusion in the GBM is rapid relative to convection, it is still much slower than diffusion in water. This is indicated by the small values of ΦK_d in Fig. 1-6. For example, ΦK_d = 0.01 (the value for r_s = 35 Å) means that the diffusional permeability of the GBM is only 1% of that of a film of water of equivalent thickness.

Not considered in Fig. 1-6 are the possible effects of GBM compressibility on macromolecule partition coefficients and diffusive or convective hindrance factors. In particular, the sieving data used were obtained at an applied pressure of ΔP = 60 mmHg (Bolton et al. 1998), whereas the diffusion experiments (Edwards et al. 1997b) corresponded to ΔP = 0. The hydraulic and/or Darcy permeabilities of filters made from isolated GBM have been found to decrease with increases in applied pressure (ΔP) (Daniels et al. 1992; Edwards et al. 1997a; Robinson and Walton 1989; Walton et al. 1992). Because $f(\phi)$ in Eq. [1-4] decreases with increasing ϕ, one would expect κ to decrease if compression of the GBM forces out water and thereby increases the volume fraction of solids. Based on theories for fiber matrices, increases in ϕ are expected to result also in decreases in Φ (see Chapter 2) and K_d (Johnson et al. 1996; Phillips 2000). Experimental results for proteins and Ficoll in agarose suggest that K_c would decrease as well (Johnson et al. 1996; Johnston and Deen 1999, 2002; Phillips 2000). Attempts have been made to model the effects of pressure on ΦK_d and ΦK_c (Edwards et al. 1997a; Edwards et al. 1999), but these efforts are confounded by the lack of an adequate theory for K_c in fibrous materials and by the probable effects of BSA on the values of Φ for Ficoll (see Chapters 2 and 3). The effects of BSA are an issue because BSA has been present in some sieving experiments with isolated GBM, but not others.

The interpretation of p_{cell} depends, of course, on the relative contributions of the endothelium and epithelium to the diffusional resistance of the intact capillary wall. Assuming that the cellular resistance resides in the slit diaphragm, and modeling that structure as a row of parallel cylinders (as in the "ladder" of Fig. 1-3), it was found that the diffusion results could be explained by a cylinder spacing that followed a lognormal distribution, with small areas (~0.2%) devoid of cylinders (Edwards et al. 1997b). That representation of the cellular barrier was incorporated into

later simulations of macromolecule filtration in vivo (Edwards et al. 1999). The one significant difference was that in healthy subjects, at least, there was no evidence for "shunts" created by small areas of the slit diaphragm devoid of cylinders.

As already stated, it was found that sieving curves measured in isolated GBM for Ficoll and its anionic derivative, Ficoll sulfate, were indistinguishable. Only when the ionic strength of the solutions was reduced below physiological levels, thereby amplifying the effects of electrostatic interactions, was Θ_{bm} for Ficoll sulfate less than that of neutral Ficoll (Bolton et al. 1998). This finding of little or no charge-selectivity is generally consistent with other studies of isolated GBM. That is, Bray and Robinson (1984) found only small differences in sieving curves for dextran and dextran sulfate and Bertolatus and Klinzman (1991) noted only small differences in the filtration rates of native (anionic) and cationized BSA. Procedures used in those laboratories to neutralize GBM charge, including methylation of carboxyl groups (Bertolatus and Klinzman 1991) and reductions in pH from 7.4 to 5.7 (the isolectric point of GBM) (Robinson and Walton 1987) had little effect on the sieving of BSA. Likewise, Daniels (1994) found that treating the GBM with heparatinase to remove heparan sulfate proteoglycan, adding protamine to neutralize GBM polyanions, or reducing the experimental pH to the isoelectric point of the GBM or BSA, had little or no effect on the sieving coefficient of BSA. Thus, to the extent that the glomerular barrier is charge-selective, it is the cellular layers, and not the GBM, which appear to be responsible. The charge-selectivity of the intact glomerular capillary wall is discussed below.

1.4.3 Charge-selectivity. Research in the 1970s and 1980s led to the view that the glomerular capillary wall discriminates among macromolecules on the basis of their net charge, as well as their size (Maddox et al. 1992). The pattern seen was that, for a given r_s and molecular conformation, anionic polymers passed through the capillary wall less readily than did neutral polymers, which in turn passed less readily than cationic polymers. Differences due to molecular charge tended to be diminished in proteinuric disorders. The inference was that fixed negative charges in one or more parts of the capillary wall normally make entry into and passage through the barrier less favorable for polyanions (such as albumin) than for neutral molecules of similar size

and configuration. Much of the evidence for charge-selectivity was based on comparisons between the fractional clearances in rats of dextran (uncharged) and dextran sulfate (anionic) [e.g., (Chang et al. 1975)]. Other influential studies employed native (neutral) and anionic horseradish peroxidase (nHRP and aHRP, respectively) [e.g., (Rennke et al. 1978)]. Technical concerns have been raised in recent years concerning both sets of test molecules, motivating a reexamination of the concept of charge-selectivity. Indeed, arguments against glomerular charge-selectivity are the main theme of a review by Comper and Glasgow (1995). What follows is a summary of certain key issues and a review of the most recent findings.

At least two factors may complicate the interpretation of fractional clearance data for dextran sulfate (DS). First, it has been shown that DS binds to plasma proteins (Guasch et al. 1993; Mayer et al. 1993). This binding was studied extensively by Guasch et al. (1993), using ultrafiltration and equilibrium dialysis experiments with ^{3}H-DS and/or unlabeled DS added to Krebs buffer solutions or to human serum. For the relatively small sizes of ^{3}H-DS examined, only some 45% of the activity in serum was not protein-bound. Using total radioactivity to determine the plasma concentration of a protein-bound tracer will tend to overestimate the concentration of free tracer and therefore underestimate its urinary clearance. Nonetheless, when corrections were made for protein binding, the fractional clearance of ^{3}H-DS with r_s = 15-18 Å in normal rats (68) or humans (Guasch et al. 1993) was still only 0.5-0.7, much smaller than that for dextran of similar size ((Abrhamson 1987). This charge-selectivity was almost abolished in the nephrotic syndrome, the fractional clearance of ^{3}H-DS increasing from 0.68 in healthy humans to 0.95 in nephrotics (Guasch et al. 1993).

Another concern with the use of dextran sulfate is cellular uptake and intracellular desulfation, as examined in a series of studies by Comper and co-workers (Abrhamson 1987; Burne et al. 1998; Burne et al. 1997; Comper et al. 1994; Tay et al. 1991; Vyas et al. 1996; Vyas et al. 1995). When ^{3}H-DS was added to isolated kidney perfusates or administered i.v. to rats, most of the tritiated polymer in urine was found to be desulfated (Burne et al. 1998; Comper et al. 1994; Vyas et al. 1995). This occurred without a significant change in molecular size (Burne et al. 1998;

Comper et al. 1994). Evidence was found for uptake of ^{3}H-DS, but not uncharged dextran, by glomerular cells (Tay et al. 1991; Vyas et al. 1996), and it was argued that the glomerulus is a primary site for desulfation. Increases in the urinary clearance of intact DS with increasing DS concentration showed the uptake and/or desulfation to be saturable (Burne et al. 1998; Burne et al. 1997; Vyas et al. 1996).

The significance of the cellular processing of DS depends on where the uptake occurs, and the time required for intracellular levels to become constant. The half-time for accumulation of label in the glomeruli of isolated perfused kidneys (IPK) was < 5 min (Tay et al. 1991), indicating that for clearance measurements done over much longer periods, time-dependent accumulation in the glomerulus will be unimportant. This is true for the studies of Mayer et al. (1993) and Guasch et al. (1993), where bolus doses of ^{3}H-DS were followed by constant infusions, and sample collections not begun until after 45-60 min of equilibration. Thus, the rate at which the tracer crossed the glomerular barrier in those studies should have equaled its rate of appearance in urine, as assumed in the fractional clearance methodology. Under such steady state conditions, if the cellular uptake and desulfation were downstream of the barrier (i.e., by epithelial cells from Bowman's space fluid), total tritium in urine (reflecting both intact and desulfated DS) would accurately reflect filtration of anionic DS and no new interpretation would be needed. Other possibilities include uptake by the foot processes from the filtration slits or GBM, and uptake by the endothelial cells from the GBM or plasma. Potentially most significant is endothelial uptake of DS from plasma. If uptake by glomerular endothelial cells were rapid enough to compete with movement through the fenestrae, and if desulfation and release on the contraluminal side of the cells were slow, then entry of DS into the GBM would be slowed by the cellular processing. This would have the effect of reducing the fractional clearance of DS relative to uncharged dextran.

In support of the concept of DS processing in glomerular endothelial cells, Vyas et al. (1995) cited evidence for endothelial endocytosis of sulfated polysaccharides in other organs. Moreover, following an i.v. bolus of ^{3}H-DS in rats, some 78% of the label remaining in plasma was found by affinity chromatography to be desulfated within 2 hr (Comper et al. 1994). However, the

evidence for uptake by glomerular endothelial cells, specifically, tends to be ambiguous. Processing of DS by those cells was not rapid enough to allow detection of an increase in desulfated DS in perfusate collected from the IPK (Comper et al. 1994). The finding that DS isolated from glomerular digests (Tay et al. 1991) or vesicles (Vyas et al. 1995) has a similar size distribution to that in plasma could mean that it is of endothelial origin, as argued, or that size-based fractionation occurs mainly at the level of the epithelium. Likewise, the finding of similar amounts of DS in vesicles isolated from filtering and non-filtering perfused kidneys (Vyas et al. 1995) is consistent with either cellular source. That is, the very small values of *Pe* estimated for the GBM (as discussed above) imply that diffusion is rapid enough that water filtration will not greatly speed access of macromolecules to the epithelial cells.

The criticism of the data with horseradish peroxidase is based on the finding that aHRP is preferentially degraded in the kidney (Osicka and Comper 1995). Accordingly, the use of an enzymatic assay to detect aHRP in kidney tissue and urine leads to a systematic underestimate of its sieving coefficient, relative to that of nHRP. The apparent charge-selectivity was reduced, but not eliminated, when radiolabels were employed (Osicka and Comper 1995, 1998). The ratio of nHRP to aHRP sieving coefficients was reduced to 2-3, as compared to a value of 8-9 in the original report (Rennke et al. 1978).

We turn now to more recent studies by Haraldsson and co-workers, which provide additional evidence in favor of glomerular charge-selectivity. Using the IPK preparation at 8 °C to inhibit tubular activity, Ohlson et al. (2000) found the fractional clearances of albumin and Ficoll of comparable size (r_s = 36 Å) to be 0.0019 and 0.021, respectively. Using the cooled IPK preparation to examine the filtration of somewhat larger proteins (r_s = 40-42 Å), Lindstrom et al. (1998) showed that the fractional clearance of anionic lactate dehydrogenase (LDH) was less than that of a slightly cationic isoform.

In comparing the forms of HRP and LDH with differing charge, variations in molecular shape are not an issue. However, Ficoll is spherical and albumin is modeled more accurately as a prolate spheroid with an axial ratio of about 3.3 ((Al-Malah et al. 1995; Johnson et al. 1995;

Lazzara et al. 2000; Tanford 1961). To what extent would that difference in molecular shape account for the ten-fold difference in sieving coefficients between Ficoll and albumin? The link between membrane partitioning and sieving (e.g., Eq. [1-6]) suggests that a partial answer would be provided by the theoretical effect of molecular shape on Φ in a random fiber matrix such as that used to represent GBM. Applying the excluded volume theory presented in Chapter 2 to the parameter values in Table 1-2, the results were $\Phi = 0.0234$ for BSA and $\Phi = 0.0219$ for Ficoll. This difference is not only very small but is in the wrong direction to contribute to the low sieving coefficient for albumin. Supporting the conclusion that the non-spherical shape of albumin is of minor importance are data for ΦK_d and ΦK_c in agarose gels of varying concentration, which show little difference between the results for Ficoll and various globular proteins, including BSA (Johnson and Deen 1996; Johnston and Deen 2002).

Another recent finding with the cooled IPK is that reductions in the ionic strength of the perfusate decreased the fractional clearances of both aHRP and albumin, without affecting those of Ficoll (Sorensson et al. 1998). Because low ionic strengths amplify electrostatic interactions by reducing Debye screening, this was the taken as evidence for functional, fixed negative charges. However, as with experiments with isolated GBM at reduced ionic strength (Bolton et al. 1998), this shows only that charge was influential at the lower ionic strength. Because charge interactions will tend to be fully suppressed above a certain ionic strength (i.e., when the Debye length is very small relative to the spaces accessible to permeating macromolecules), examining normal and reduced ionic strengths does not exclude the possibility that the charges are fully screened under normal conditions. A more definite conclusion would be reached by showing that an ionic strength above physiological elevates the fractional clearances of aHRP and albumin, making them more like those of a neutral test solute such as Ficoll.

A crucial aspect of the controversy over charge-selectivity is the manner and extent to which the glomerular barrier restricts the passage of albumin. Two very different hypotheses have emerged. The conventional view, recapitulated recently in Ohlson et al. (2000, 2001), is that the sieving coefficient for albumin is normally quite low, on the order of 10^{-4} to 10^{-3}, due in part to

electrostatic interactions between albumin and fixed negative charges in the glomerular capillary wall. An alternative hypothesis proposed in Osicka et al. (1996) is that the sieving coefficient of albumin is unaffected by charge and roughly 100-fold higher; using various drugs (including NH_4Cl) to inhibit tubular protein reabsorption in the IPK at 37 °C, they inferred an albumin sieving coefficient of 0.07. This high sieving coefficient was reconciled with the low concentrations of albumin normally found in proximal tubule fluid by postulating a high-capacity absorption pathway that returns intact albumin from tubular fluid to plasma (Osicka et al. 1996).

A critique of the alternative hypothesis for albumin handling is given in Ohlson et al. (2000), who measured fractional clearances of albumin and Ficoll in IPK preparations at both 8 °C and 37 °C. Using NH_4Cl at 37 °C, they too found a high fractional clearance for albumin (0.02), approaching that for similarly-sized Ficoll under those conditions (0.04). They argued that the apparent loss of barrier selectivity for albumin in the IPK at 37 °C, and especially the loss of charge-selectivity, is the result of irreversible glomerular injury due both to hypoxia-reperfusion and to drugs used to inhibit tubule function. They also criticized the concept of rapid reabsorption of intact albumin, citing inconsistencies with the finding of Maunsbach (1966) that practically all albumin is degraded during reabsorption. Finally, they noted the electron microscopic evidence of Ryan and Karnovsky (1976) that albumin is efficiently excluded from the glomerular capillary wall, and micropuncture measurements by Tojo and Endou (1992) which confirm that albumin concentrations in early proximal tubule fluid are very low. This last study is noteworthy in that a technique was devised to avoid the difficult problem of sample contamination with subcapsular fluid; the sieving coefficient estimated for albumin was 6×10^{-4} (Tojo and Hitoshi 1992). We find all of these arguments persuasive.

To summarize our conclusions from the various experimental studies, the concept that charge-selectivity contributes to the exclusion of albumin and other polyanions from glomerular filtrate remains viable, despite technical concerns. It is certain that dextran sulfate is not as inert a tracer as once believed, and it is likely that earlier studies (e.g., with dextran sulfate and aHRP) overestimated the effects of charge. Indeed, a major lesson has been how difficult it is to design

experiments to test charge-selectivity in vivo. Nonetheless, recent results with the IPK tend to reinforce, rather than negate, the conclusions from earlier fractional clearance studies in vivo.

1.4.4 GBM nanostructure and macromolecule filtration. As with the Darcy permeability, efforts to predict the values of ΦK_d and ΦK_c in the GBM have been based largely on representing it as an array of randomly oriented fibers with fluid-filled interstices. Before considering the GBM specifically, we first survey the various theoretical results which might be used for this purpose. For media containing fibers of uniform size, theories for the partitioning of neutral macromolecules have been developed for dilute (Ogston 1958) or concentrated (Fanti and Glandt 1990b) solutions of rigid spheres, for dilute or concentrated mixtures of rigid solutes of arbitrary shape , and for dilute solutions of random-coil chains (White and Deen 2000). For neutral, rigid solutes, mixtures of fiber sizes are considered in the model presented in Chapter 2. Hydrodynamic models to predict K_d in fiber matrices have been described in Johnson et al. (1996), Clague and Phillips (1997), and Phillips (2000), but there is a paucity of information on K_c. The convective reflection coefficient (σ) for a random fiber matrix is related to K_c as $\sigma = 1 - \Phi K_c$, and it has been assumed that $\sigma = (1 - \Phi)^2$ (Curry and Michel 1980), a relationship derived originally for the osmotic reflection coefficient in cylindrical pores (Anderson and Malone 1974). This prediction for σ (or ΦK_c) has been found to be unreliable for proteins in polyacrylamide gels (Kapur et al. 1997) and for proteins or Ficoll in agarose gels (Johnston and Deen 2002; Johnston et al. 2001). The same is true for an early diffusion model (Ogston et al. 1973), frequently quoted in the literature, which has been reported to greatly overestimate K_d in agarose gels (Johnson et al. 1996). In contrast, the theories for partitioning and the recent theories for diffusion appear to be reasonably accurate (Johnson 1995; Johnson et al. 1996; Johnson and Deen 1996; Phillips 2000).

In an effort to model the sieving results for Ficoll (without BSA) shown in Fig. 1-5, Bolton and Deen (2001) represented the GBM as an array of fibers of uniform radius. They evaluated ΦK_d using the theory of Ogston (1958) for Φ and that of Johnson et al. (1996) for K_d, but chose to employ an empirical expression for ΦK_c similar to Eq. [1-9]. It was found that a fiber-matrix model based on a single population of fibers could accurately predict both the sieving curve for

Ficoll and the value of κ, but only if the volume fraction of fibers was assumed to be unrealistically large. It was concluded that fiber matrix models based on a uniform fiber size do not adequately relate the microstructure of the GBM to its permeability properties. The success of the two-fiber model in describing the Darcy permeability, as discussed above, suggests that a promising direction for future research is the development of analogous hindered transport models.

1.5 Effects of Proteins on the Sieving of Tracers

As already noted, Ficoll and Ficoll sulfate sieving coefficients measured in isolated GBM were found to be indistinguishable, at any given value of r_s (Bolton et al. 1998). However, the same study revealed a pronounced upward shift in the sieving curves of both tracers when BSA was added at a concentration of 4 g/dL. The results for Ficoll, with and without BSA, are shown in Fig. 1-5. Because the hydraulic permeability of the GBM filters was unaffected by BSA, the shift in the sieving curves apparently was not due to an alteration of the intrinsic properties of the GBM (i.e., a result of binding of BSA to the membrane). An increase in Θ would result from the measured reduction in filtrate velocity in the presence of BSA, caused by its osmotic pressure; this is the Péclet number effect discussed in connection with Eq. [1-6]. However, as shown by the theoretical curve in Fig. 1-5 labeled "osmotic only", this was calculated to account for only about one-third of the increase, on average. It was suggested that the remainder of the BSA effect might be due to another physical phenomenon, namely, a tendency of steric interactions with BSA to facilitate entry of the tracers into the membrane (Bolton et al. 1998). That phenomenon had been the subject of several previous theoretical and experimental investigations, which showed that the equilibrium partition coefficient of a macromolecule between a bulk solution and a porous or fibrous material is dependent on its concentration (Anderson and Brannon 1981; Brannon and Anderson 1982; Fanti and Glandt 1990a; Glandt 1981). In essence, steric interactions between molecules in a concentrated solution cause entry into the porous or fibrous material to be more favorable thermodynamically than if the solution were dilute. As shown in Eq. [1-6], increases in Φ will tend

to increase Θ. Thus, the sieving coefficients of Ficoll and BSA in synthetic membranes were found to increase with increasing solute concentration (Mitchell and Deen 1986).

Proteins may also have more specific effects on glomerular permeability. Orosomucoid is a serum protein which is thought to have a role in determining capillary permeability by maintaining and reinforcing the charge barrier (Curry et al. 1989; Haraldsson and Rippe 1987). Haraldsson et al. (1992) and Johnsson and Haraldsson (1993) demonstrated that orosomucoid influences the glomerular barrier by showing that the clearance of albumin in the IPK was four to five times lower when orosomucoid was present.

1.6 Motivation and Thesis Overview

As already mentioned, at the time this work was begun, the effect of solute concentration on colloidal partition coefficients had been demonstrated in a number of theoretical and experimental investigations (Anderson and Brannon 1981; Brannon and Anderson 1982; Fanti and Glandt 1990a; Glandt 1981). A detailed survey of previous models for macromolecular partitioning in pores and fibrous media is presented in Chapter 2. The previously available models, however, only addressed concentration effects for uniform systems of spherical solutes. In many situations of interest, important interactions may exist among unlike solutes, as in the case of the isolated GBM sieving experiments of Bolton et al. (1998) using BSA and Ficoll. In addition, models for the hindered transport of macromolecular solutes through isotropic media, and across the intact glomerular capillary wall, were restricted to dilute solutions. As shown by the data in Fig. 1-5, the effect of plasma protein concentration may significantly augment tracer sieving beyond the ability of the reduced Péclet number effect to describe the change. As will be discussed in further detail in Chapter 3, the effect of protein concentration on tracer partitioning is expected have important effects on solute transport across the intact glomerular barrier as well. There is some experimental evidence from the literature in support of this idea. Ohlson et al. (2001) recently reported Ficoll sieving data in the isoalted perfused kidney (at 8 °C) in the presence of either 1.8 g/dL or 5.0 g/dL

albumin. The fractional clearances over much of the size range examined were significantly elevated at the higher protein concentration, qualitatively consistent with the effects previously described. Thus, the effect of plasma protein concentration on tracer partitioning and sieving has important implications for the interpretation of data from a wide variety of experimental techniques used to measure the permeability properties of the glomerular barrier.

In order to test the hypothesized effect of protein concentration on tracer sieving for studies of glomerular macromolecular permeability, we pursued a combined modeling and experimental approach. The specific objectives of this thesis work were: (1) to develop a partitioning theory for mixtures of rigid, spheroidal macromolecules of arbitrary concentration in porous and random-fiber media; (2) to extend the theoretical description of macromolecular sieving across single-layered membranes and the intact glomerular capillary wall to account for the presence of a second, abundant solute and reanalyze the isolated GBM sieving data of Bolton et al. (1998); and (3) to experimentally demonstrate the effect of solute concentration for dissimilar solutes and to test the applicability of the newly developed partitioning model for random-fiber media.

The development and discussion of a novel model for the partitioning of systems of unlike spheroidal solutes based on excluded volume concepts is presented in Chapter 2. The extension of hindered transport models to include effects of concentrated solutes for single-layer membranes and the intact glomerular capillary wall is presented in Chapter 3. Presented there also is a reanalysis of the isolated GBM sieving data of Bolton et al. (1998) making use of the newly developed models. Experimental measurements of the concentration effect on macromolecular partitioning for dissimilar solutes and synthetic random-fiber media is presented in Chapter 4. A summary of this work and a discussion of future directions are contained in Chapter 5. Chapter 6 contains the various FORTRAN codes used in the modeling portions of this work.

This Chapter contains excerpts (Sections 1.3, 1.4, and 1.5) from a recent review article by Deen, Lazzara, and Myers (2001). Chapters 2 and 3 have already been published and appear in substantially the same form as they appear here in Lazzara et al. (2000) and Lazzara and Deen (2001), respectively. Chapter 4 is pending submission for journal publication.

Chapter 2

Effects of Multisolute Steric Interactions on Membrane Partition Coefficients

2.1 Abstract

A key parameter in membrane and chromatographic separations is the partition coefficient, the equilibrium ratio of the solute concentration in a porous or fibrous material to that in bulk solution. The theoretical effects of solute size on partition coefficients in straight pores or randomly oriented fiber matrices have been investigated previously for very dilute solutions, where solute-solute interactions are negligible, and also for more concentrated solutions consisting of spherical solutes of uniform size. For concentrated solutions it has been found that steric and other repulsive interactions among solutes increase the partition coefficient above the dilute limit. To extend the results for porous or fibrous media to include concentrated mixtures of solutes with different sizes or shapes, we used an excluded volume approach. In this formulation, which describes steric interactions only, partition coefficients were computed by summing all volumes excluded to a solute molecule by virtue of its finite size, the finite size of other solutes, and the presence of fixed obstacles (pore walls or fibers). For a mixture of two spherical solutes, the addition of any second solute at finite concentration increased the partition coefficient of the first solute. That increase was sensitive to the size of the second solute; for a given volume fraction of

the second solute, the smaller its radius, the larger the effect. When the total volume fraction of solutes was fixed, an increase in the amount of a second, smaller solute increased the partition coefficient of the first solute, whereas an increase in the amount of a second, larger solute had the opposite effect. Results were obtained also for oblate or prolate spheroidal solutes and for fibrous media containing fibers of different radii. For constant total fiber volume fraction, an increase in the amount of a second, smaller fiber decreased the partition coefficient of a spherical solute, whereas an increase in the amount of a second, larger fiber had the opposite effect. Overall, the theory suggests that the introduction of heterogeneities, whether as mixtures of solute sizes or mixtures of fiber sizes, may cause partition coefficients to differ markedly from those of uniform systems.

2.2 Introduction

The equilibrium distribution of a solute between a bulk liquid solution and a fibrous or porous material is a critical factor in various membrane and chromatographic separation processes. The ability of solute i to enter the confined phase (membrane or chromatography bead) is described by its partition coefficient,

$$\Phi_i = \overline{C}_i / C_i \qquad \textbf{[2-1]}$$

where $\overline{C}_i$ and C_i are the equilibrium solute concentrations in the confined phase and external solution, respectively. (Overbars are used throughout this chapter to denote quantities evaluated in the confined phase). For porous materials $\overline{C}_i$ is an average over the pore (liquid) volume, whereas for fibrous materials or gels it is based on total volume (including solids). The importance of Φ_i for various types of separations has motivated numerous efforts to predict its value from the size and shape of a solute molecule and the structural characteristics of various materials. As in most previous work, we are concerned here with systems in which the linear dimensions of the solute molecule are much larger than those of the solvent, so that the solute behaves as a particle in a liquid

continuum. The confined phase is represented in one of two ways. A fibrous material or polymeric gel is modeled as a matrix of randomly oriented fibers with fluid-filled interstices (Fig. 2-1 a); the prototypical model for a porous material is a parallel array of uniform cylindrical pores (Fig. 2-1 b).

The steric exclusion of rigid solutes from fibrous or porous materials has been thoroughly investigated for dilute solutions, where solute-solute interactions are negligible. For a spherical solute of radius r_i in a matrix of long, randomly oriented, uniform fibers, the classical result is that of Ogston (1958), which can be written as

$$\Phi_i^{(0)} = \exp\left[-\phi\left(1+\frac{r_i}{R_f}\right)^2\right] \qquad \textbf{[2-2]}$$

where R_f is the fiber radius, and ϕ is the volume fraction of fibers. [The "(0)" is used to denote results for dilute solutions.] The corresponding expression for spherical solutes in circular pores of radius R_p which dates at least to the work of Pappenheimer et al. (1951), is

$$\Phi_i^{(0)} = \left(1-\frac{r_i}{R_p}\right)^2 \qquad \textbf{[2-3]}$$

Both of these expressions illustrate the central feature of steric exclusion: for a given material, Φ_i decreases with increasing r_i. The partitioning theory for dilute solutions has been extended to arbitrary combinations of solute shape and pore cross-section (Giddings et al. 1968; Limbach et al. 1989), and has been developed also for random-coil polymers in pores (Casassa 1967; Davidson and Deen 1987). The effects of membrane-solute electrostatic interactions have been investigated for spheres (Smith and Deen 1983) and random coils (Lin and Deen 1990) in pores, and for spheres in random fiber arrays (Johnson and Deen 1996).

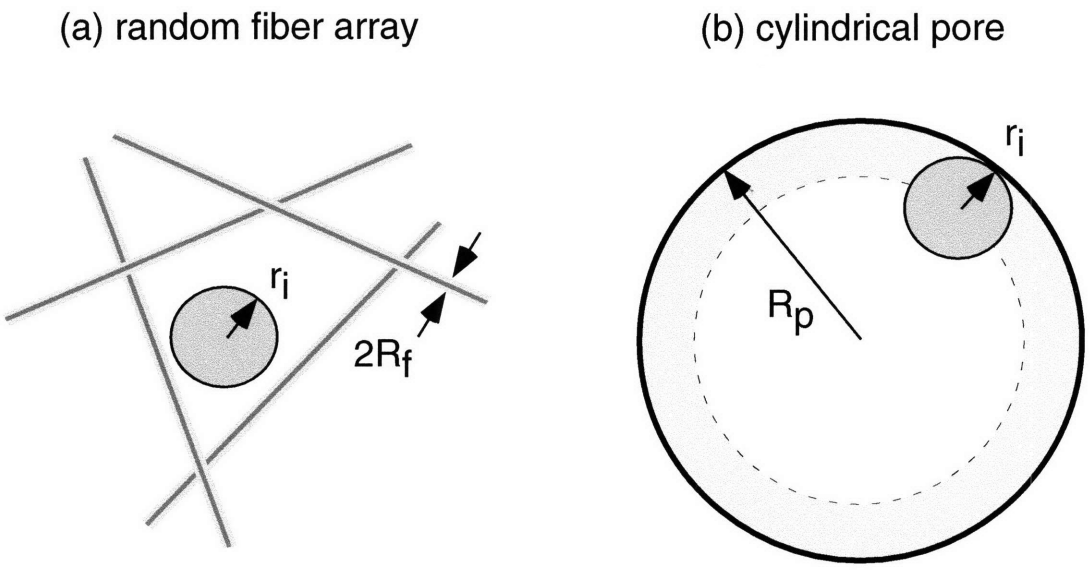

Figure 2-1: Schematic of the partitioning of a spherical molecule of radius r_i in (a) a randomly oriented matrix of fibers of radius R_f and (b) cylindrical pores of radius R_p.

Theoretical and experimental studies that are not restricted to dilute solutions have shown that the partition coefficient depends not just on geometric factors and electrical charge, but also on the solute concentration in bulk solution (C_i). Although it is often neglected in membrane transport models, this effect of solute concentration can be quite significant, especially when Φ_i is small. Concentration effects were examined for uncharged spheres in pores by Anderson and Brannon (1981) and Glandt (1981), who used a statistical mechanical approach. The effects of concentration on the partitioning of spheres in random fiber arrays were investigated using density functional theory (Fanti and Glandt 1990a) and Monte-Carlo simulations (Fanti and Glandt 1990b). Electrostatic effects on the partitioning of concentrated solutions of spherical molecules in pores have also been analyzed (Anderson and Brannon 1981; Mitchell and Deen 1984). In general, repulsive interactions among solutes, whether purely steric or longer range, are predicted to increase Φ above its value for a dilute solution. This trend has been confirmed experimentally (Brannon and Anderson 1982).

Theories which describe the effects of bulk solute concentration on partitioning have been limited to spherical solutes of uniform size. However, in many real systems there may be important interactions among unlike solutes. In the use of ultrafiltration membranes to fractionate blood plasma, for example, there are two classes of abundant proteins, serum albumin and immunoglobulins (Saksena and Zydney 1997). A second example involves the use of polydisperse macromolecules to characterize the permeability properties of kidney capillaries in vivo (Blouch et al. 1997) or in vitro (Bolton et al. 1998). In such experiments tracer molecules of varying size are accompanied by at least one abundant protein. Many other such situations can be imagined that involve mixtures of unlike particles, at least one of which is present at significant concentrations. The objective of the present work was to obtain a theoretical description of the equilibrium partitioning of mixtures of rigid solutes in fibrous or porous materials.

To describe steric interactions among multiple solutes of varying size and shape, we adopted an excluded volume approach. The present analysis is similar to that used previously to describe the partitioning of proteins in phase-separated solutions of polyethylene glycol (Zimmerman and

Trach 1990) and to predict the partition coefficients of spherical proteins in aqueous, phase-separated solutions of cylindrical micelles (Nikas et al. 1992). In the excluded volume formulation the partition coefficient is calculated by adding all volumes excluded to a particle in each phase due to its own size and shape, the presence of other particles, and the presence of fixed structures (fibers or pore walls). This approach is very simple to implement, largely because it avoids the very difficult intermediate problem of computing spatially dependent concentration profiles in the vicinity of a fiber or within the cross-section of a pore. A benefit of its simplicity is that the excluded volume formulation is readily applied not just to unlike spherical particles, but to nonspherical particles and to fibrous materials containing mixtures of two or more fibers of different radii. Thus, it provides a way to examine the effects on partitioning of several kinds of heterogeneity. The results suggest that partition coefficients for mixtures of unlike spherical solutes may differ significantly from those for systems of uniform particles. Likewise, partition coefficients in mixed fibrous materials may be quite different than those for fibers of uniform size.

2.3 Theoretical Development

2.3.1 General considerations. Let $\mathbf{r}$ and $\boldsymbol{\Omega}$ denote the center-of-mass position and orientation, respectively, of a rigid solute molecule. The orientation vector $\boldsymbol{\Omega}$ consists of two spherical angles. Defining $p_i(\mathbf{r},\boldsymbol{\Omega})$ as the probability of successfully fitting a test solute in the confined phase, relative to that in the external solution, the partition coefficient is given by (Giddings et al. 1968)

$$\Phi_i = \frac{\iint p_i(\mathbf{r},\boldsymbol{\Omega})\,d\mathbf{r}\,d\boldsymbol{\Omega}}{\iint d\mathbf{r}\,d\boldsymbol{\Omega}} \qquad \textbf{[2-4]}$$

For fibrous or porous materials the position integrals extend over the entire volume of the confined phase and the pore volume, respectively. With a deformable solute (e.g., a linear polymer), it would

be necessary also to integrate over all possible conformations (Giddings et al. 1968; Lin and Deen 1990). For uncharged spherical solutes there is no effect of particle orientation, and Eq. [2-4] reduces to

$$\Phi_i = \frac{\int p_i(\mathbf{r})d\mathbf{r}}{\int d\mathbf{r}} \qquad \textbf{[2-5]}$$

For dilute solutions of spheres in cylindrical pores of uniform cross-section, $p_i = 0$ in an annular region of thickness r_i next to the pore wall, and $p_i = 1$ elsewhere. Integrating this step function over the pore cross section, Eq. [2-5] leads directly to Eq. [2-3]. The original derivation of Eq. [2-2] was considerably more complicated, in that it was based on calculating the probability of finding a free space of radius $\geq r_i$ within a random array of fibers (Ogston 1958). The integrals in Eq. [2-5] were not evaluated explicitly. As will be seen, the excluded volume approach also bypasses the specification of $p_i(\mathbf{r},\boldsymbol{\Omega})$, and evaluates the integrals in Eqs. [2-4] and [2-5] indirectly.

2.3.2 Fibrous materials. If all intersections of a test particle with fixed structures and/or other particles are random, independent events, the probability of a given number of such intersections can be calculated using a Poisson distribution. (A consequence of the assumed independence of intersections is that fibers and particles with which the test solute interacts are mutually penetrable, as will be discussed later.) As shown in Meyer (1965), the Poisson distribution can be viewed as a limit of the binomial distribution, in which the number of trials in an experiment (n) approaches infinity and the probability of an event occurring in a single trial (p) approaches zero, such that $np = \gamma$ is finite, where γ is the parameter of the Poisson distribution. To evaluate γ for the partitioning problem, it is useful to think in terms of the binomial parameters, n and p. Consider a single spherical particle placed inside an empty box of volume V. If a random fiber matrix is then constructed by placing a series of identical fibers in the box, one at a time, there is a constant probability of intersection p between the particle and any fiber. That probability is the

fractional excluded volume, which is the excluded volume between the particle and a single fiber divided by the volume of the box. The excluded volume for any pair of objects is defined as the volume that is inaccessible to the center of mass of either object, taking into account all possible center-of-mass positions and orientations of the objects. If the excluded volume between objects i and j is denoted as U_{ij}, then $p_{ij} = U_{ij}/V$. For the example of a spherical test solute and a random fiber matrix, the number of trials n is equivalent to the number of fibers added. An analogous experiment can be done by adding other particles to the box. In general, for a test solute of type i and a set of objects of type j,

$$\gamma_{ij} = C_j U_{ij} \qquad \textbf{[2-6]}$$

where C_j is the number concentration of objects of type j. Thus, from the Poisson distribution, the probability of k intersections between test particle i and objects of type j is

$$P_{ij}(k) = \frac{e^{-\gamma_{ij}} \gamma_{ij}{}^{k}}{k!} \qquad \textbf{[2-7]}$$

The probability of successfully placing a solute molecule in a space is the probability that there will be zero intersections with other objects. Setting $k = 0$ in Eq. [2-7], the probability of avoiding objects of type j is

$$P_{ij}(0) = e^{-\gamma_{ij}} \qquad \textbf{[2-8]}$$

Because all test solute intersections are assumed to be independent events, the probability of zero total intersections in either phase (membrane or bulk) can be written as the product of the probabilities of zero intersection with each type of object in that phase. This product accounts for

intersections between the test particle and one or more other types of particles, intersections with one or more types of fibers, and simultaneous intersections with particles and fibers. Similar considerations apply in the bulk solution, except that no fibers are present. Thus, the partition coefficient is given by

$$\Phi_i = \frac{\prod_{j=1}^{m+n} \overline{P}_{ij}(0)}{\prod_{j=1}^{n} P_{ij}(0)} \qquad \textbf{[2-9]}$$

where m and n denote the numbers of fiber and particle types, respectively. There are no integrals to be evaluated in Eq. [2-9], because the sampling of all possible particle positions and orientations is inherent in the calculation of the fractional excluded volumes.

The result for a dilute solution in equilibrium with a random fiber matrix is obtained by ignoring solute-solute interactions and considering only one type of solute-fiber interaction. In this case Eq. [2-9] reduces to

$$\Phi_i^{(0)} = e^{-\overline{\gamma}_{ij}} \qquad \textbf{[2-10]}$$

for solute i and fibers of type j. Neglecting fiber end effects, the excluded volume per fiber equals that of a cylinder of radius $r_i + R_j$. Thus, the expression for $\overline{\gamma}_{ij}$ is

$$\overline{\gamma}_{ij} = \phi\left(1 + \frac{r_i}{R_j}\right)^2 \equiv \phi\alpha_{ij}(s,f) \qquad \textbf{[2-11]}$$

The notation $\alpha_{ij}(x,y)$ indicates the interaction of test particles of type x with objects of type y (s = sphere, f = fiber). Substitution of Eq. [2-11] in Eq. [2-10] yields Eq. [2-2]. Thus, the excluded volume approach provides an independent derivation of the result of Ogston (1958). The validity of Eq. [2-2] was confirmed also by Fanti and Glandt (1990a; 1990b) using two other methods.

2.3.3 Porous materials. The excluded volume formulation must be modified slightly for media containing identical pores, where the calculations are based on a single pore. In this case the test solute can intersect at most one pore wall, and the Poisson distribution is not applicable to the solute-pore interactions. However, the probability of avoiding a solute-pore intersection just equals the partition coefficient for dilute solutions, $\Phi_i^{(0)}$. Replacing the solute-fiber terms in Eq. [2-9] by $\Phi_i^{(0)}$, we obtain

$$\Phi_i = \Phi_i^{(0)} \frac{\prod_{j=1}^{n} \bar{P}_{ij}(0)}{\prod_{j=1}^{n} P_{ij}(0)} \qquad \textbf{[2-12]}$$

Note that for dilute solutions $\bar{P}_{ij}(0) = P_{ij}(0) = 1$ for all j, and $\Phi_i = \Phi_i^{(0)}$. As already mentioned, $\Phi_i^{(0)}$ for spheres in cylindrical pores is given by Eq. [2-3]; similar calculations can be made for other solute shapes and other pore cross-sections.

2.3.4 Evaluation of excluded volumes. The excluded volumes for spherical particles can be calculated from simple geometric considerations. The expression for $\bar{\gamma}_{ij}$ for a spherical particle of radius r_i and fibers of radius R_j has been given already by Eq. [2-11], in terms of ϕ and the geometric parameter $\alpha_{ij}(s,f)$. For spherical molecules of radii r_i and r_j, the excluded volume per molecule of j equals the volume of a sphere of radius $r_i + r_j$. It follows that if the volume fraction of solute j is χ_j, then the fractional excluded volume is

$$\gamma_{ij} = \chi_j \left(1 + \frac{r_i}{r_j}\right)^3 \equiv \chi_j \alpha_{ij}(s,s) \qquad \textbf{[2-13]}$$

For identical spheres we obtain $\alpha_{ij}(s,s) = 8$. Also note that when $\bar{\gamma}_{ij}$ is to be evaluated, the particle volume fraction needed is the value in the confined phase, $\bar{\chi}_i$. For either fibrous or porous materials the partition coefficient is the ratio of internal to external particle volume fractions (as well as the ratio of particle concentrations), so that the internal and external volume fractions of solute i are related as $\bar{\chi}_i = \Phi_i \chi_i$.

In order to implement the excluded volume approach for solutes of arbitrary shape, a general expression for U_{ij} is required. As given in Jansons and Phillips (1990),

$$U_{ij} = V_i + V_j + \frac{1}{4\pi}(S_i M_j + S_j M_i) \qquad \textbf{[2-14]}$$

where V_i is the volume, S_i is the surface area, and M_i is the integral of the local mean curvature over the surface, all for object i. With this expression, partition coefficients for any set of particles can be calculated for an arbitrary fibrous or porous membrane. The excluded volume for sphere-sphere interactions (Eq. [2-13]) is recovered from Eq. [2-14] by noting that the local mean curvature at all points on the surface of a sphere of radius r_i is $1/r_i$. Hence, $M_i = 4\pi r_i$ for a sphere. The corresponding result for sphere-fiber interactions (Eq. [2-11]) is found by recognizing that the local mean curvature on the surface of a cylinder of radius R_j (neglecting the ends) is $1/(2R_j)$.

2.3.5 Systems with two spherical solutes. The simplest multi-solute mixture consists of two types of spherical solutes. For such a solution in contact with a fibrous material containing two types of fibers, Eq. [2-9] reduces to

$$\Phi_1 = \exp\left[-\phi_1 \alpha_{11}(s,f) - \phi_2 \alpha_{12}(s,f) + \alpha_{11}(s,s)(1-\Phi_1)\chi_1 + \alpha_{12}(s,s)(1-\Phi_2)\chi_2\right] \qquad \textbf{[2-15]}$$

For a porous material, the corresponding result from Eq. [2-12] is

$$\Phi_1 = \Phi_1^{(0)} \exp\left[\alpha_{11}(s,s)(1-\Phi_1)\chi_1 + \alpha_{12}(s,s)(1-\Phi_2)\chi_2\right] \qquad \textbf{[2-16]}$$

Note that the cross-sectional shape of the pores affects only $\Phi_1^{(0)}$, which for cylindrical pores is given by Eq. [2-3]. Equations [2-15] and [2-16] are each accompanied by complementary expressions for the partition coefficient of the second solute, Φ_2. To evaluate the partition coefficients, each set of two equations was solved simultaneously for Φ_1 and Φ_2 by Newton-Raphson iteration, using the dilute solution values as initial guesses.

2.3.6 Nonspherical solutes. The theory can be applied to nonspherical solutes by using the appropriate expressions for V_i, S_i, and M_i in evaluating U_{ij} and γ_{ij}. The necessary information for prolate and oblate spheroids (and certain other shapes) is provided by Jansons and Phillips (1990). A prolate (rod-like) spheroid i is characterized by the three semiaxes r_i, r_i, and $\eta_i r_i$, where $\eta_i > 1$; for an oblate (disk-like) spheroid, $\eta_i < 1$. To illustrate the approach, we will consider mixtures of two solutes, only one of which is nonspherical. The development for two nonspherical solutes is very similar. Because we will be considering mixtures of spherical and nonspherical solutes, we will need (in addition to Eqs. [2-11] and [2-13]) expressions for the excluded volume between two nonspherical objects as well as the excluded volume between a sphere and a nonspherical object. The expression for γ_{ij} between prolate spheroid i and a set of prolate spheroids j is

$$\gamma_{ij} = \chi_j\left[1 + \frac{\eta_i}{\eta_j}\left(\frac{r_i}{r_j}\right)^3 + \frac{3}{4}\left(\frac{r_i}{r_j}\right)^2 \frac{f(\eta_i)g(\eta_j)}{\eta_j} + \frac{3}{4}\left(\frac{r_i}{r_j}\right)\frac{f(\eta_j)g(\eta_i)}{\eta_j}\right] \equiv \chi_j \alpha_{ij}(p,p) \qquad \textbf{[2-17]}$$

where the functions $f(\eta_i)$ and $g(\eta_i)$ are defined as

$$f(\eta_i) \equiv 1 + \eta_i^2\left(\eta_i^2 - 1\right)^{-1/2} \cos^{-1}\left(\eta_i^{-1}\right) \qquad \textbf{[2-18]}$$

$$g(\eta_i) \equiv \eta_i + \left(\eta_i^2 - 1\right)^{-1/2} \cosh^{-1}(\eta_i) \qquad \textbf{[2-19]}$$

The expression for γ_{ij} between a prolate spheroid i and a set of spheres j is

$$\gamma_{ij} = \chi_j\left[1 + \eta_i\left(\frac{r_i}{r_j}\right)^3 + \frac{3}{2}\left(\frac{r_i}{r_j}\right)^2 f(\eta_i) + \frac{3}{2}\left(\frac{r_i}{r_j}\right)g(\eta_i)\right] \equiv \chi_j \alpha_{ij}(p,s) \qquad \textbf{[2-20]}$$

For a sphere i and a set of prolate spheroids j, it is found that

$$\gamma_{ij} = \chi_j\left[1 + \frac{1}{\eta_j}\left(\frac{r_i}{r_j}\right)^3 + \frac{3}{2}\left(\frac{r_i}{r_j}\right)^2 \frac{g(\eta_j)}{\eta_j} + \frac{3}{2}\left(\frac{r_i}{r_j}\right)\frac{f(\eta_j)}{\eta_j}\right] \equiv \chi_j \alpha_{ij}(s,p) \qquad \textbf{[2-21]}$$

Finally, the expression for $\bar{\gamma}_{ij}$ between a prolate spheroid i and a set of fibers j is

$$\gamma_{ij} = \phi_j\left[1 + \frac{1}{2}\left(\frac{r_i}{R_j}\right)^2 f(\eta_i) + \left(\frac{r_i}{R_j}\right)g(\eta_i)\right] \equiv \phi_j \alpha_{ij}(p,f) \qquad \textbf{[2-22]}$$

where we have assumed that $V_j >> V_i$ as before for spherical particles.

The excluded volume expressions for oblate spheroids are very similar to those just given. The expression for γ_{ij} between oblate spheroid i and a set of oblate spheroids j is

$$\gamma_{ij} = \chi_j \left[1 + \frac{\eta_i}{\eta_j}\left(\frac{r_i}{r_j}\right)^3 + \frac{3}{4}\left(\frac{r_i}{r_j}\right)^2 \frac{f'(\eta_i)g'(\eta_j)}{\eta_j} + \frac{3}{4}\left(\frac{\eta_i}{\eta_j}\right)\frac{f'(\eta_j)g'(\eta_i)}{\eta_j} \right] \equiv \chi_j \alpha_{ij}(o,o) \qquad \textbf{[2-23]}$$

where the functions $f'(\eta_i)$ and $g'(\eta_i)$ are defined as

$$f'(\eta_i) \equiv 1 + \eta_i^2 \left(1 - \eta_i^2\right)^{-1/2} \cosh^{-1}\left(\eta_i^{-1}\right) \qquad \textbf{[2-24]}$$

$$g'(\eta_i) \equiv \eta_i + \left(1 - \eta_i^2\right)^{-1/2} \cos^{-1}(\eta_i) \qquad \textbf{[2-25]}$$

The remaining expressions for γ_{ij} needed for oblate spheroids are analogs of Eqs. [2-20]-[2-22] for prolate spheroids. By substituting $f'(\eta_i)$ and $g'(\eta_i)$ for $f(\eta_i)$ and $g(\eta_i)$, respectively, expressions are obtained for $\alpha_{ij}(o,s)$, $\alpha_{ij}(s,o)$, and $\alpha_{ij}(o,f)$.

For a mixture of prolate spheroids (particle 1) and spheres (particle 2) in a material with two types of fibers, the partition coefficients are given by

$$\Phi_1 = \exp\left[-\phi_1\alpha_{11}(p,f) - \phi_2\alpha_{12}(p,f) + \alpha_{11}(p,p)(1-\Phi_1)\chi_1 + \alpha_{12}(p,s)(1-\Phi_2)\chi_2\right] \qquad \textbf{[2-26]}$$

$$\Phi_2 = \exp\left[-\phi_1\alpha_{21}(s,f) - \phi_2\alpha_{22}(s,f) + \alpha_{21}(s,p)(1-\Phi_1)\chi_1 + \alpha_{22}(s,s)(1-\Phi_2)\chi_2\right] \qquad \textbf{[2-27]}$$

2.4 Results and Discussion

2.4.1 Comparisons with previous work. This section begins with a brief description of the methodology used in previous studies to describe the effects of solute concentration on partition coefficients, and then compares previous results with the predictions of the excluded volume formulation.

To describe the partitioning of uniform spheres in fibrous materials, Fanti and Glandt (1990a) used density functional theory to compute the solute density (concentration) profile around a single fiber. The partition coefficient was calculated by using a superposition approximation to average that result over all fibers in the membrane, for all possible configurations of fibers. In calculating the density profile around a single fiber, a nonlocal density approximation was employed, which accounts for the effect of the surrounding environment on the particle density at each point. This nonlocal density approximation relies upon the use of a weighting function, which is itself expressed as a truncated virial expansion in density. A limitation of this approach, which is inherent also in the Ogston derivation and in the excluded volume model, is that all spaces in the fiber matrix are assumed to be accessible. In reality, especially for high number densities of fibers, some of the spaces large enough to accomodate a solute molecule may be prevented from doing so because they are completely surrounded by spaces that are too small.

Fanti and Glandt (1990a) reported results from density functional theory only for fibers of zero thickness. The fibrous medium was characterized by a dimensionless fiber length per unit volume, $l^* = l(2r_i)^2$, where l is the (dimensional) fiber length per unit volume and r_i is the sphere radius. The case of infinitely thin fibers is treated with the excluded volume model by noting that the volume excluded to a particle per unit fiber length is just πr_i^2, so that $\bar{\gamma}_{ij} = \pi r_i^2 l$. Using this result in Eq. [2-15], and also omitting the terms arising from the second solute and fiber types, we obtain

$$\Phi_i = \exp\left[-\pi r_i^2 l + 8(1-\Phi_i)\chi_i\right] \qquad \textbf{[2-28]}$$

The excluded volume predictions for a single size of sphere and infinitely thin fibers were obtained by solving this equation iteratively for Φ_i. Figure 2-2 compares the partition coefficients computed in this manner with those obtained from density functional theory. In all cases Φ_i was predicted to increase as the solute volume fraction (χ_i) increases. The results of the two theories agreed well

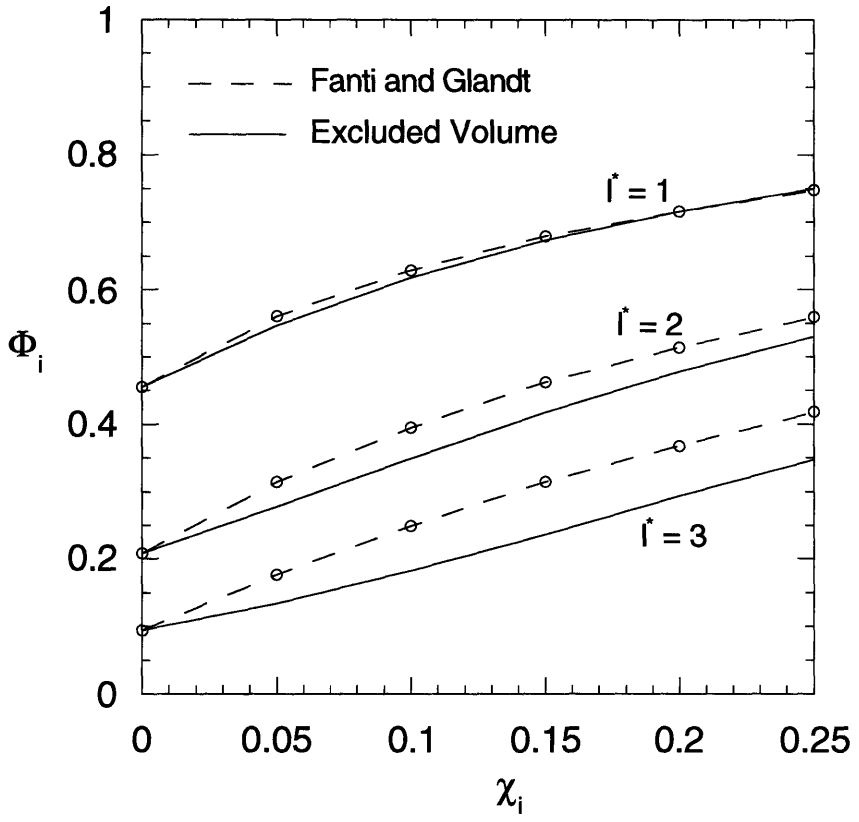

Figure 2-2: Partition coefficient (Φ_i) as a function of solute volume fraction (χ_i) for uniform spherical particles in a fiber matrix composed of infinitely thin fibers. The dimensionless concentration of fibers is l^* (see text). Results from the density functional theory of Fanti and Glandt (1989) are compared with those from Eq. [2-28].

overall, with the excluded volume theory tending to yield somewhat smaller values of Φ_i. The differences between the theories became larger as l^* was increased.

To describe the partitioning of uniform spheres in pores, Anderson and Brannon (1981) used a statistical mechanical formulation to express the local particle concentration inside a pore as a virial expansion in the bulk concentration. The second virial coefficient in that expansion (the order C_i^2 term) involved integrals which were difficult to evaluate numerically. The integrations were facilitated by invoking the Percus-Yevick approximation, which suggests that certain terms cancel one another. In the limit $\Phi_i \to 0$, however, the Percus-Yevick approximation was shown to underestimate the second virial coefficient. Although the comparisons here focus on the results of Anderson and Brannon (1981), similar results were presented by Glandt (1981).

The Anderson and Brannon (1981) model expressed the partition coefficient as a series expansion in powers of the bulk solute concentration,

$$\Phi_i = \Phi_i^{(0)}\left[1 + \alpha_1 C_i + \alpha_2 C_i^2 + ...\right] \qquad \textbf{[2-29]}$$

Curve fits to the computational results were used to develop convenient expressions for the parameter α_1, for both cylindrical and parallel-plate (slit) pores. Anderson and Brannon observed that, independent of the pore geometry, α_1 and $\Phi_i^{(0)}$ were related to good approximation by

$$\frac{\alpha_1}{8v_i} = 1 - 0.99\Phi_i^{(0)} - 1.06\left(\Phi_i^{(0)}\right)^2 + 1.05\left(\Phi_i^{(0)}\right)^3 \qquad \textbf{[2-30]}$$

where v_i is the volume of a single particle. Results for α_2 were provided as a plot of α_2/v_i^2 versus $\Phi_i^{(0)}$. Figure 2-3 compares partition coefficients for cylindrical pores computed from Eq. [2-29] with those obtained from the excluded volume approach (Eq. [2-12]). As with fibrous materials, in all cases Φ_i was predicted to increase as χ_i increases. In general, the two theories were in excellent

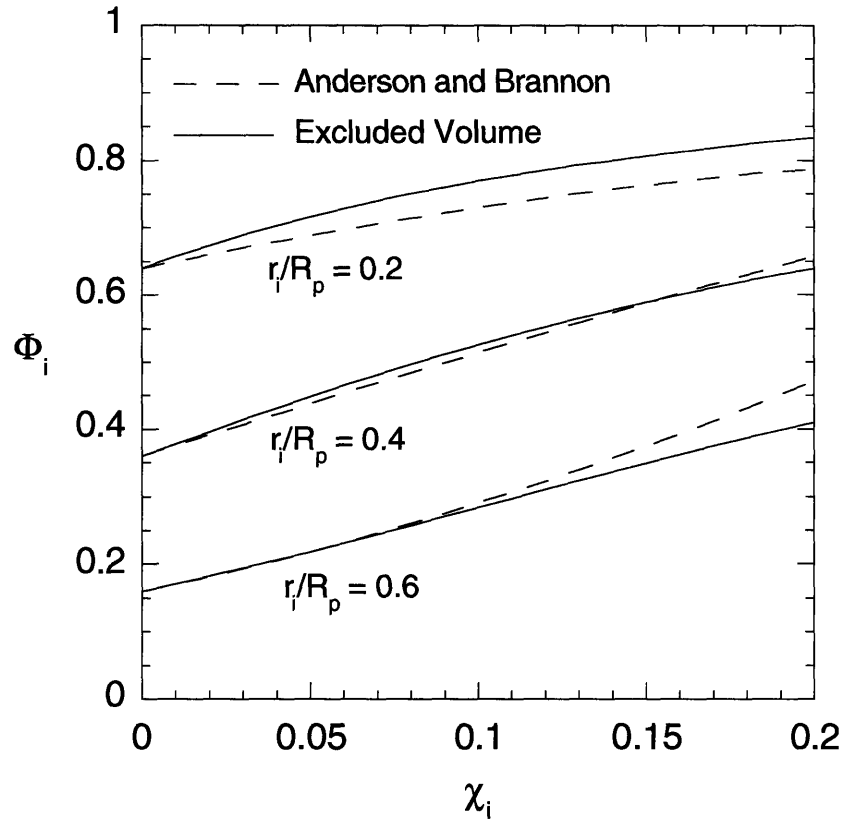

Figure 2-3: Partition coefficient (Φ_i) as a function of solute volume fraction (χ_i) for uniform spherical particles in cylindrical pores. Results obtained either from Eq. [2-29] [the Anderson and Brannon (1981) theory] or from the excluded volume theory are shown for three ratios of solute radius to pore radius (r_i/R_p).

agreement. Including the α_2 term, as done in generating the curves for the Anderson and Brannon theory in Fig. 2-3, did not cause the partitioning behavior to deviate significantly from that predicted using only the first virial coefficient.

The excluded volume approach has its own set of approximations. A central assumption is that all pairwise steric interactions are independent. A consequence of this in applications to fibrous media is that this method, like the Ogston theory, permits fiber overlap. Thus, the true fiber volume fraction, ϕ_0, is less than the nominal value used in the theory, ϕ. The value of ϕ_0 can be calculated by recognizing that a point-size test solute will have a partition coefficient equal to $\Phi_i = 1 - \phi_0$, and noting that for $r_i \rightarrow 0$, Eq. [2-2] predicts that $\Phi_i = \exp(-\phi)$. Equating these two expressions for Φ_i gives $\phi_0 = 1\text{-}\exp(-\phi)$. Accordingly, $\phi \rightarrow \phi_0$ only for small values of ϕ. Moreover, when using the excluded volume approach to describe solute concentration effects in any system, there is a similar ambiguity in the particle volume fraction. Reasoning analogous to that used to describe the effects of fiber overlap leads to the conclusion that the true solute volume fraction, χ_0, and the nominal value, χ, are related by $\chi_0 = 1\text{-}\exp(-\chi)$.

In summary, each of the methods discussed above involves certain approximations, and it is not readily apparent which will provide more accurate results for a given situation. However, the fact that the results of the various methods are in reasonably good agreement, in situations where direct comparisons are possible, lends credence to each approach. The excluded volume method stands out in the sense that it is much simpler to implement than the other two approaches. Accordingly, all results presented hereafter are based on the excluded volume theory.

2.4.2 Fibrous media. We begin a more general discussion of randomly oriented fibrous media with the most basic system, in which the fibers are of uniform radius and the solutes are spheres of uniform size. The dependence of Φ_i on r_i/R_f, ϕ, and χ_i is shown in Fig. 2-4. As one would expect, the partition coefficient decreased as the solute radius was increased relative to that of a fiber (larger r_i/R_f), or as the fiber concentration was increased (larger ϕ); such trends are predicted by the Ogston theory for dilute solutions (Eq. [2-2]). The effect of increasing the volume fraction

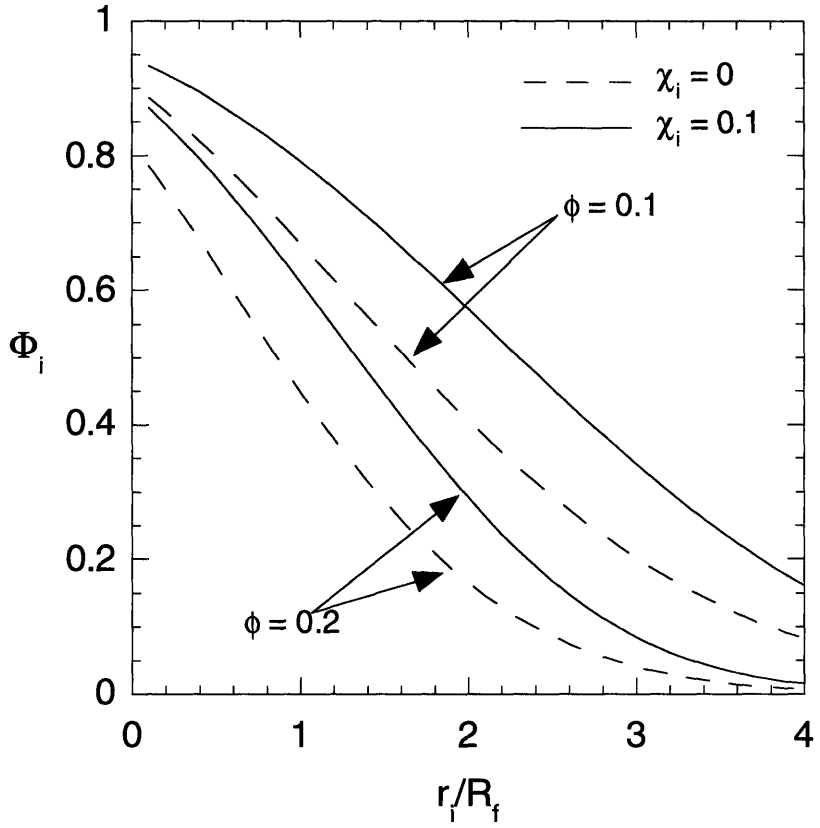

Figure 2-4: Partition coefficient for uniform spherical solutes in a fiber matrix, as a function of the ratio of solute radius to fiber radius (r_i/R_f) and the volume fraction of fibers (ϕ). Results are shown for infinite dilution ($\chi_i = 0$) and finite concentration ($\chi_i = 0.1$).

of solute in the bulk solution was to increase Φ_i, as already illustrated in Fig. 2-2 for infinitely thin fibers.

The effects of solute shape on partitioning in fibrous media are illustrated in Fig. 2-5, in which results are presented for solutions of uniform oblate or prolate spheroids. Here Φ_i is plotted as a function of the axial ratio parameter (η_i) for various values of r_i/R_f and χ_i. Each curve shows a monotonic decrease in Φ_i with increasing η_i. Oblate spheroids ($\eta_i < 1$) are shorter along one principal axis than spherical particles, which reduces their volume (if r_i is fixed). Combined with the change in shape, the reduced volume increases the probability of being able to fit an oblate spheroid into a fibrous network. Hence, Φ_i for oblate spheroids exceeds that for spheres ($\eta_i = 1$). The opposite effect occurs for prolate spheroids ($\eta_i > 1$), where there is an increase in volume relative to that of a sphere of equivalent r_i. As shown, larger values of r_i/R_f were found both to reduce Φ_i and to make the effects of particle shape more pronounced. As with spherical particles, there was always an increase in Φ_i with increasing χ_i.

An unexpected aspect of the results in Fig. 2-5 was that for $\chi_i \neq 0$ the partition coefficient increased rapidly towards unity as $\eta_i \rightarrow 0$, whereas for $\chi_i = 0$ it leveled off. For sufficiently small η_i, there was a noticeable difference even between the results for very small particle concentrations (e.g., $\chi_i = 10^{-3}$) and $\chi_i = 0$. This singular behavior is explained as follows. For any fixed volume fraction of particles (as in any one curve in Fig. 2-5), the number of particles in the bulk must increase as η_i becomes smaller. In general, distributing a given volume among many particles increases the excluded volume associated with those particles. This general effect was noted by Nikas et al. (1992), who found that, for a fixed volume fraction of micelles, smaller spherical micelles excluded proteins more effectively than larger cylindrical micelles. Since the partition coefficient is generally less than unity, the increased particle number causes a larger increase in the excluded volume in the bulk solution than in the confined space. That disproportionate increase in the bulk excluded volume tends to increase Φ_i. Consequently, the effects of solute concentration are greatly amplified as $\eta_i \rightarrow 0$, for any fixed, nonzero value of χ_i. A similar effect was already observed for like spherical particles as r_i decreased in Fig. 2-4, and will be seen again for mixtures

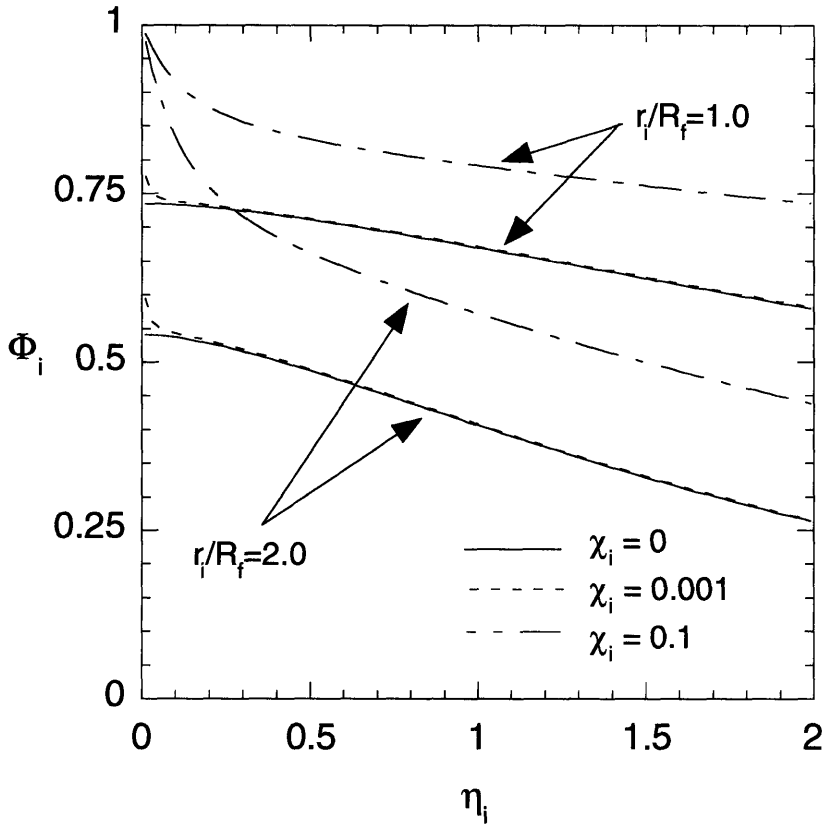

Figure 2-5: Partition coefficient for uniform spheroidal solutes in a fiber matrix, as a function of the axial ratio of the solute, η_i. Oblate spheroids have $\eta_i < 1$; spheres have $\eta_i = 1$; prolate spheroids have $\eta_i > 1$. Results are shown for two ratios of characteristic solute size to fiber radius (r_i / R_f), both for infinite dilution and for finite concentration. In all cases $\phi = 0.1$.

of spherical particles in the discussion which follows. Overall, these results suggest that caution is needed in applying the infinite dilution approximation (i.e., $\chi_i = 0$) to systems where particle dimensions are very small. Another consideration in modeling the behavior of small solutes is that the continuum approximation applied to the solvent will break down when the solute dimensions approach those of the solvent molecules.

The system becomes more complicated when two or more types of solutes are present. Consider first a situation where spherical solute 1 is present at tracer levels and spherical solute 2 is abundant. In this case the partitioning of solute 2 will be affected only by interactions with like molecules, so that Φ_2 will behave as shown in Fig. 2-4. For solute 1, on the other hand, the interactions with like solutes are negligible, but those with solutes of type 2 will affect its partition coefficient. The predicted behavior of Φ_1 is shown in Fig. 2-6. As one would expect from the results already discussed, there was a monotonic increase in Φ_1 with increasing χ_2. More noteworthy is the finding that the magnitude of this increase was strongly dependent on the ratio of solute radii (r_2/r_1). Specifically, the sensitivity of Φ_1 to χ_2 increased as r_2/r_1 was reduced. This may be understood by recognizing that, for equivalent values of χ_2, a smaller r_2 requires a larger number of such particles in the bulk solution. It is the excluded volume due to the type 2 particles, of course, which creates the dependence of Φ_1 on χ_2 in this system.

When two types of particles are present at finite concentration, each experiences steric interactions with solutes of its own type and with solutes of the other type. The effects of these interactions are illustrated in Fig. 2-7, in which Φ_1 is plotted as a function of χ_2 for several values of r_2/r_1. In these calculations the total particle volume fraction in the bulk solution, $\chi_t = \chi_1 + \chi_2$, was held constant. Thus, when the two particle sizes were taken to be identical ($r_2/r_1 = 1$), Φ_1 was unaffected by variations in χ_2. For dissimilar particles, however, Φ_1 was quite sensitive to χ_2. For $r_2/r_1 < 1$, Φ_1 increased with increasing χ_2, whereas for $r_2/r_1 > 1$ it decreased. As with the effects of r_2/r_1 in Fig. 2-4, underlying this trend is the fact that a greater excluded volume results when one distributes a given volume among a larger number of objects. Thus, for $r_2/r_1 < 1$ and χ_t fixed, increasing χ_2 assigns more of the given particle volume to the smaller (type 2) particles, thereby

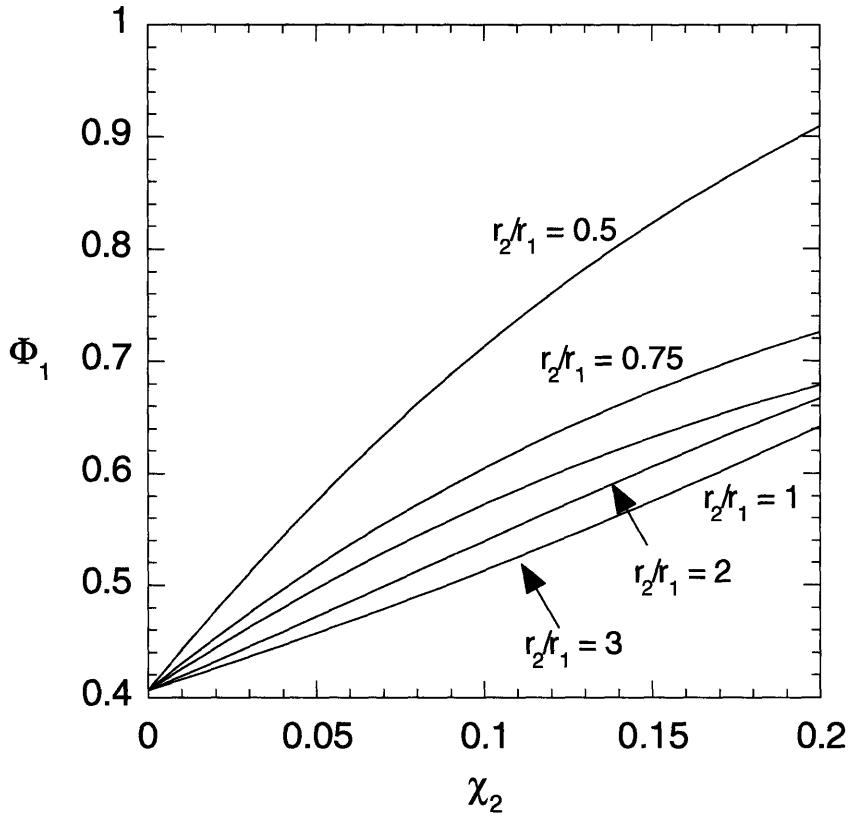

Figure 2-6: The partition coefficient of a tracer (Φ_1) as a function of the volume fraction of an abundant solute (χ_2), for a mixture of two spherical solutes in equilibrium with a random fiber matrix. Results are shown for various values of the ratio of solute radii (r_2/r_1). In each case $\phi =$ 0.1 and $r_1/R_f = 2$.

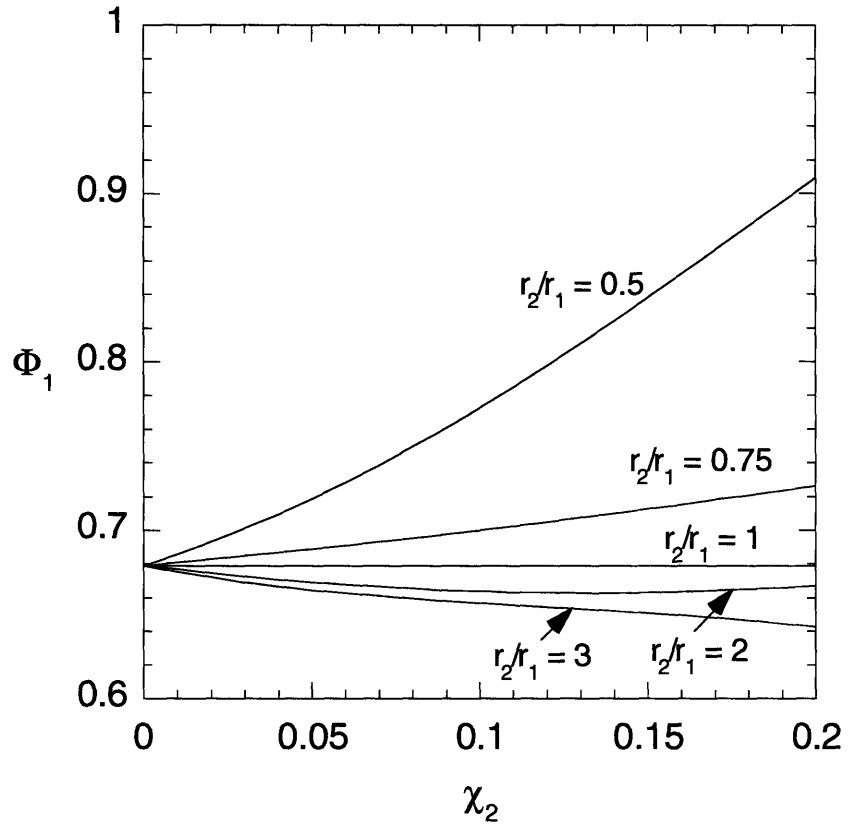

Figure 2-7: The partition coefficient of one solute (Φ_1) as a function of the volume fraction of the other solute (χ_2), for a mixture of two spherical solutes in equilibrium with a random fiber matrix. Both solutes were assumed to be present at finite concentration, such that their total volume fraction was fixed at $\chi_t = \chi_1 + \chi_2 = 0.1$. In each case $\phi = 0.1$ and $r_1/R_f = 2$.

elevating the excluded volume in the bulk solution and increasing Φ_1. For $r_2/r_1 > 1$, increasing χ_2 has the opposite effect.

The results just discussed focused on the effects of nonuniform particle sizes. Analogous effects of heterogeneity are observed in fiber matrix systems in which there are at least two sizes of fiber. Consider a system in which there is only one type of (spherical) solute, but fibers of radii R_1 and R_2. Values of Φ_i for this case are plotted in Fig. 2-8 as a function of ϕ_2, for various choices of R_2/R_1. Here the total fiber volume fraction, $\phi_t = \phi_1 + \phi_2$, was held constant. It was found that Φ_i increased with increasing ϕ_2 for $R_2/R_1 > 1$, remained constant for $R_2/R_1 = 1$, and decreased for $R_2/R_1 < 1$. In this situation, increasing the number of small fibers (i.e., increasing ϕ_2 for $R_2/R_1 < 1$) augmented the excluded volume in the confined phase, and thereby reduced Φ_i. The opposite effect occurred when the number of small fibers was reduced.

Results for systems with two particle sizes and two fiber sizes can be computed if desired from Eq. [2-15], but will not be presented. Some additional findings for fibrous media are presented later, in connection with certain experimental systems, after the behavior of porous materials is discussed briefly.

2.4.3 Porous media. The results presented next are for materials modeled as assemblies of straight, circular pores of uniform radius, R_p. Because the partition coefficient for a single solute in such a system has been presented already in Fig. 2-3, we focus here on the effects of interactions among two types of spherical solutes with different sizes. Fig. 2-9 depicts results for a system in which solute 1 is a tracer and solute 2 is abundant. In most respects, the dependence of Φ_1 on χ_2 and r_2/r_1 was very similar to that found for fibrous media (Fig. 2-6). The only qualitative distinction is that the curve for $r_2/r_1 = 3$ does not fall completely below the curves for smaller values of r_2/r_1. This increase in Φ_1 with increasing r_2/r_1 seems to contradict the reasoning already presented for the observed trends in systems of mixed particles, but it can be understood in terms of a competing effect. As r_2/r_1 increases and the concentration effect diminishes, Φ_2 also falls. This simultaneous decrease in the ability of the second particle to occupy pore volume tends to increase Φ_1, thereby counteracting the diminishing concentration effect. This competing effect due to

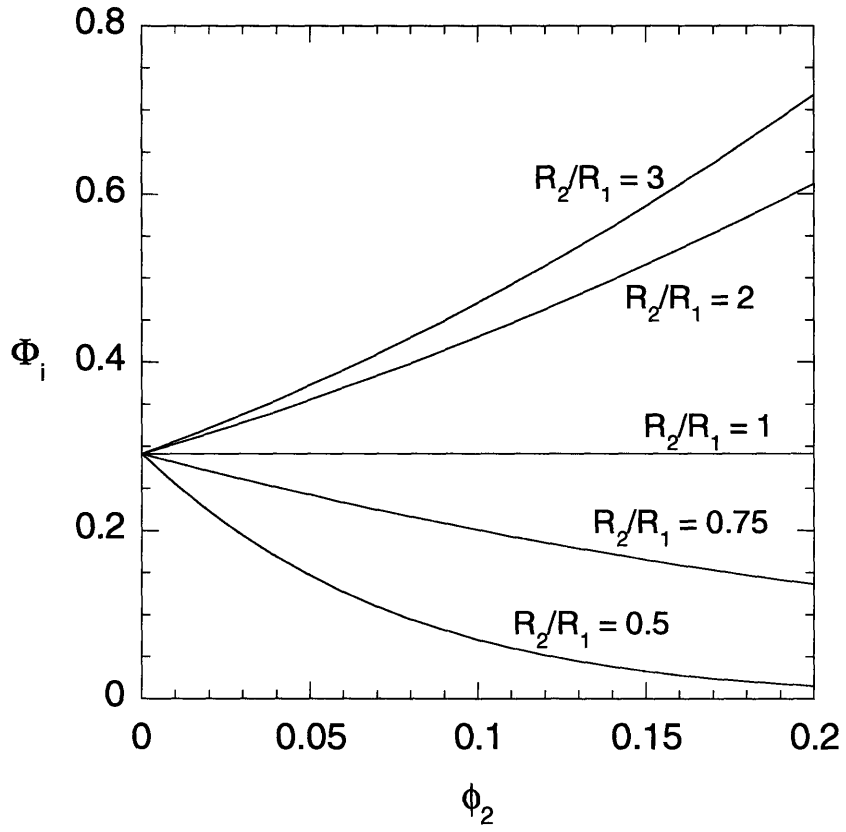

Figure 2-8: The partition coefficient of a spherical solute in a fibrous material containing two types of fibers with different radii. The partition coefficient is plotted as a function of the volume fraction of one fiber (ϕ_2), with the total volume fraction of fibers fixed at $\phi_t = \phi_1 + \phi_2 = 0.2$. Results are shown for various values of the ratio of fiber radii (R_2/R_1). In each case $\chi_i = 0.1$ and $r_i / R_1 = 2$.

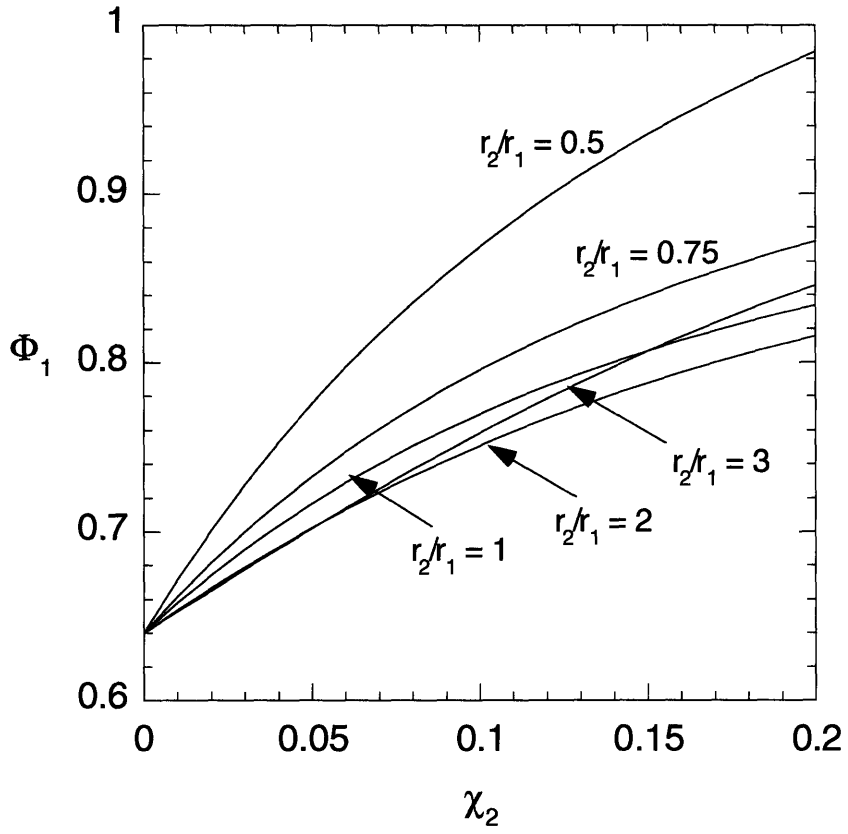

Figure 2-9: The partition coefficient of a tracer (Φ_1) as a function of the volume fraction of an abundant solute (χ_2), for a mixture of two spherical solutes in equilibrium with cylindrical pores of radius R_p. Results are shown for various values of the ratio of solute radii (r_2/r_1). In each case $r_1/R_p = 0.2$.

decreasing Φ_2 also occurs in fiber matrix systems, but is not readily apparent with the parameter values chosen for Figs. 2-6 and 2-7.

Partitioning results for pores with two concentrated solutes are shown in Fig. 2-10. Again, the results were qualitatively similar to those for fibrous media (Fig. 2-7), the main distinction being the non-monotonic behavior observed for $r_2/r_1 = 3$. The basis for that non-monotonic behavior is the same as that described for Fig. 2-6.

2.4.4 Some experimental implications. Agarose gels have been used in a number of experimental investigations of partitioning and diffusive or convective transport of macromolecules (Dubin and Principi 1989; Johnson et al. 1995, 1996; Johnston and Deen 1999; Kong et al. 1997). The α-helical polysaccharide chains of agarose bundle together to form larger, relatively rigid fibers, which in turn are physically crosslinked in an apparently random pattern (Arnott et al. 1974). Agarose gels have been modeled often as randomly oriented arrays of fibers of uniform size, although results from small angle x-ray scattering (SAXS) indicate a bimodal distribution of fiber radii (Djabourov et al. 1989). Specifically, the SAXS results suggest that 42% of the fiber volume is accounted for by fibers with a radius of 1.5 nm and the remaining 58% by fibers with a radius of 4.5 nm. This corresponds to a model where, by number, 87% of the fibers have a radius of 1.5 nm and 13% have a radius of 4.5 nm; this yields a number-average radius of 1.9 nm. Theoretical results are available to describe the effects of such a bimodal distribution on water flow (Darcy permeability) (Clague and Phillips 1997), but there have not been analogous results for equilibrium partitioning. Figure 2-11 compares partition coefficients calculated using the number-average radius ("one fiber") and the bimodal distribution ("two fibers"), for various sizes of spherical solute. The total volume fraction of fibers was held constant at 0.08, which is at the high end of typical experimental values for agarose. It is seen that for any given combination of solute size and solute volume fraction, Φ_i for the bimodal distribution was greater than that for the uniform fiber model. The partition coefficients were higher in the bimodal representation because the fibers with a radius much larger than the average value, although fewer in number, had a more important effect than the more abundant small fibers. The differences between the two models were typically only

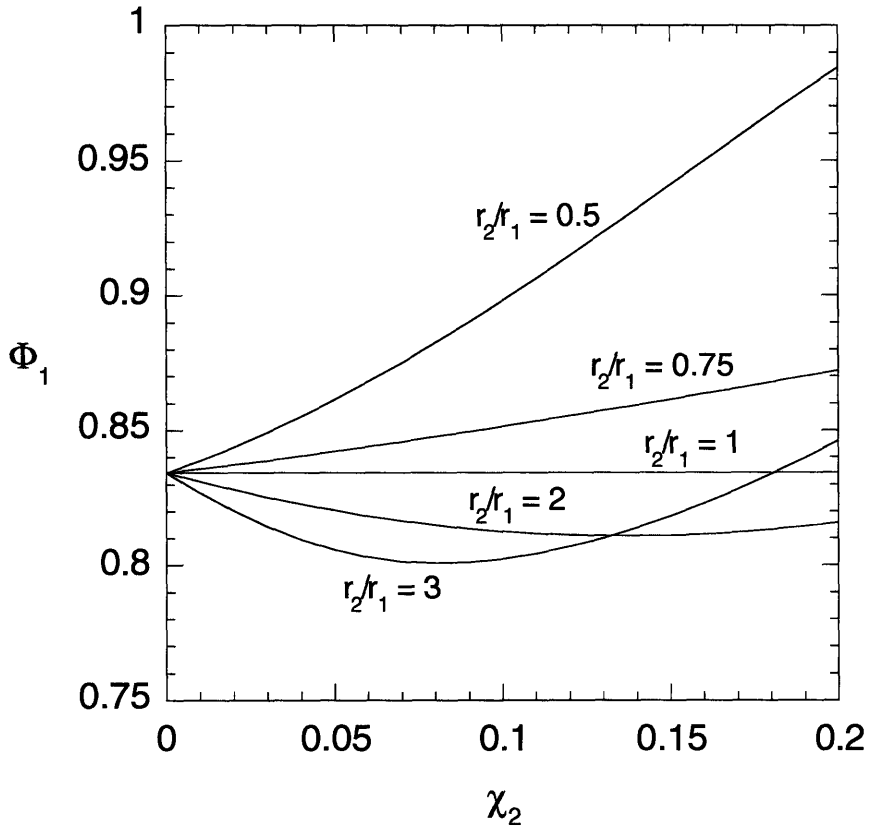

Figure 2-10: The partition coefficient of one solute (Φ_1) as a function of the volume fraction of the other solute (χ_2), for a mixture of two spherical solutes in equilibrium with cylindrical pores of radius R_p. Both solutes were assumed to be present at finite concentration, such that their total volume fraction was fixed at $\chi_t = \chi_1 + \chi_2 = 0.2$. In all cases $r_1 / R_p = 0.2$.

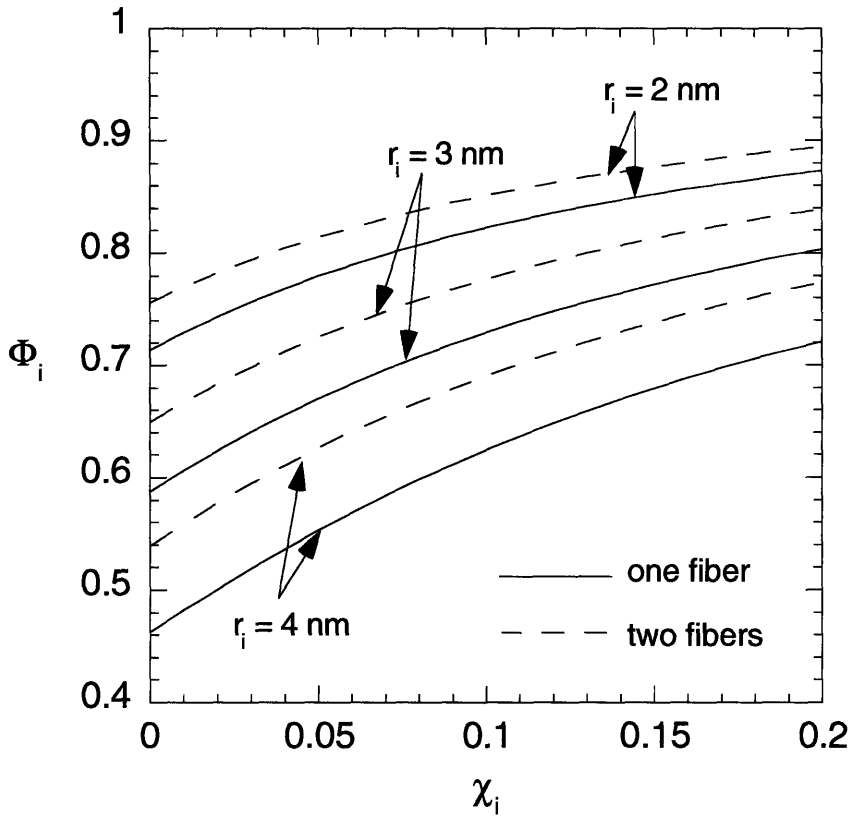

Figure 2-11: Partition coefficients predicted for spherical particles in agarose, in which the agarose gel was represented as a random fiber array having either uniform fibers ("one fiber,"R_f = 1.9 nm) or a bimodal distribution of fiber radii ("two fibers," see text). Results are shown for ϕ_t = 0.08 and solute radii ranging from 2 to 4 nm.

about 10%, however. This is consistent with the observation that, for dilute solutions of spherical or nearly spherical macromolecules, partitioning predictions with the single fiber model for agarose have generally been quite accurate (Johnson et al. 1995, 1996; Johnson and Deen 1996). The predicted effects of fiber heterogeneity on partitioning are proportionately similar to the predicted effects on the Darcy permeability of agarose (Clague and Phillips 1997). Note that the opposite trend was shown in Fig. 11 of Lazzara et al. (2000). The model predictions for the bimodal distribution shown there were made by setting the individual fiber volume fractions equal to the product of the total fiber volume fraction and the corresponding fraction of fibers based on number, rather than volume. The present calculations reflect a more accurate physical description of the gel.

Nonspherical solutes, including globular proteins, are often treated as spheres to simplify partitioning or transport calculations for fibrous or porous media. The radius of an equivalent sphere is usually calculated from bulk solution diffusivity data, using the Stokes-Einstein equation. Although the bulk-phase diffusivity of the model solute is thereby guaranteed to be correct, the equivalent-sphere approach may not yield accurate partition coefficients, as is well known for dilute solutions (Giddings et al. 1968). As an example of the effects of solute shape in more concentrated solutions, we focus on a situation resembling that studied by Bolton et al. (1998), in which the transport of Ficoll through isolated glomerular basement membrane was studied in the presence or absence of bovine serum albumin (BSA). Ficoll, a crosslinked polysaccharide that appears to behave as a neutral sphere, was present in tracer amounts, whereas BSA (when present) was relatively concentrated. In the results to be described, the confined phase was modeled as a fibrous medium of uniform radius, and particle 1 (e.g., Ficoll) was assumed to be a spherical tracer with r_1 = 2.0 or 4.0 nm. Particle 2 is BSA, which was represented either as a sphere or as a prolate spheroid. The Stokes-Einstein radius of BSA is 3.6 nm (Johnson et al. 1995), and reported values of its axial ratio (η_2) range from 3.3 to 4.9 (Oncley et al. 1947; Tanford 1961). The absolute dimensions of a given prolate spheroid were computed from the Stokes-Einstein radius and axial ratio using diffusivity relationships given in Happel and Brenner (1983). Results for Φ_1 as a function of χ_2 are shown in Fig. 2-12 for η_2 = 1.0, 3.3, or 4.9. For all sizes of tracer considered,

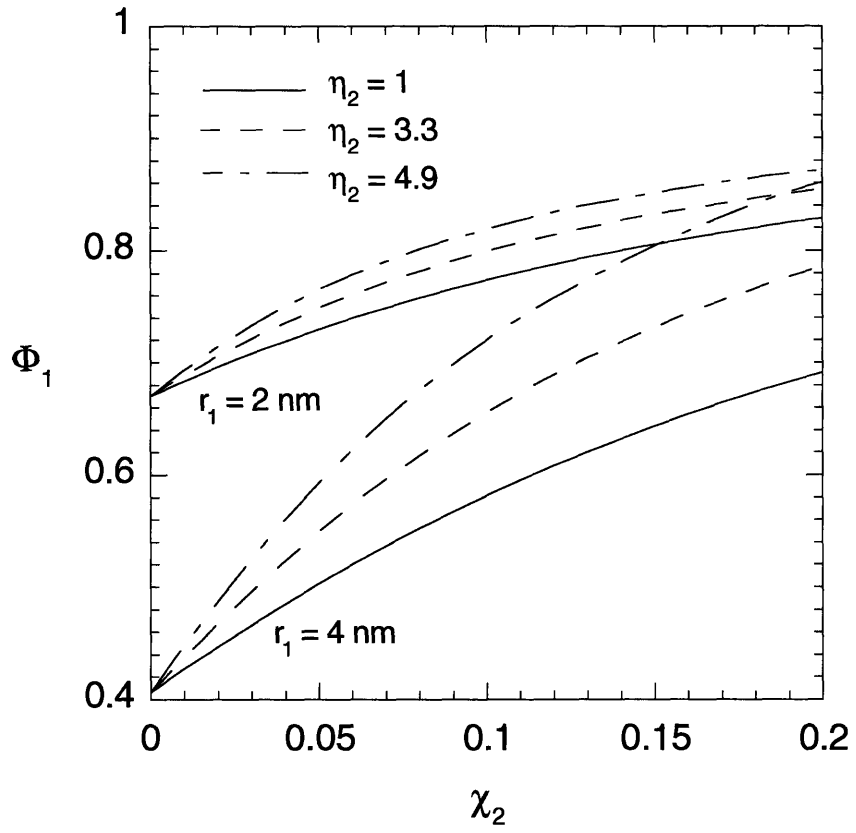

Figure 2-12: Predicted effect of BSA on the partitioning of a spherical tracer in a random fiber matrix. BSA was represented either as a sphere ($\eta_2 = 1$) or as a prolate spheroid ($\eta_2 = 3.3$ or 4.9), with a Stokes-Einstein radius of 3.6 nm in each case. The major and minor semi-axes of the prolate spheroids were 7.0 and 2.1 nm, respectively, for $\eta_2 = 3.3$, and 8.4 and 1.7 nm, respectively, for $\eta_2 = 4.9$. Results are shown for tracer radii of 2 and 4 nm, with $R_f = 2$ nm and $\phi = 0.10$.

increasing the assumed axial ratio of BSA increased the partition coefficient of the tracer and made it more sensitive to the concentration of BSA. For any given tracer, the effects of the assumed axial ratio vanished as $\chi_2 \to 0$, because the BSA-tracer interactions became negligible in that limit. For the particular conditions considered in Fig. 2-12, the errors in modeling BSA as a sphere are seen to be relatively small for $r_1 = 2$ nm, but more significant for $r_1 = 4$ nm. Although the curves were omitted for clarity, the sensitivity to the assumed axial ratio was even greater for $r_1 = 6$ nm.

2.5 Conclusions

The excluded volume formulation provides a computationally simple method for estimating partition coefficients for dilute or concentrated solutes in equilibrium with fibrous or porous media, provided that steric interactions are dominant. Whereas previous models for rigid solutes addressed concentration effects only for spheres of uniform size, the excluded volume theory allows for the presence of multiple solute sizes and/or shapes. The excluded volume results reduce exactly to certain well-known expressions for the partitioning of dilute solutions of spheres, and they are in reasonable agreement with previous results for the partitioning of concentrated solutions of uniform spheres. In addition to facilitating calculations for multiple solute sizes and/or shapes, the simplicity of the excluded volume formulation permits the incorporation of multiple fiber radii in models of fibrous media. Overall, the theory suggests that the introduction of heterogeneities, whether as mixtures of solute sizes or mixtures of fiber sizes, may cause partition coefficients to differ markedly from those of uniform systems.

Chapter 3

Effects of Plasma Proteins on the Sieving of Macromolecular Tracers in Glomerular Basement Membrane

3.1 Abstract

It was found previously that the sieving coefficients of Ficoll and Ficoll sulfate across isolated glomerular basement membrane (GBM) were greatly elevated when BSA was present at physiological levels, and it was suggested that most of this increase might have been the result of steric interactions between BSA and the tracers (Bolton et al. 1998). To test this hypothesis, we extended the theory for the sieving of macromolecular tracers to account for the presence of a second, abundant solute. Increasing the concentration of an abundant solute is predicted to increase the equilibrium partition coefficient of a tracer in a porous or fibrous membrane, thereby increasing the sieving coefficient. The magnitude of this partitioning effect depends on solute size and membrane structure. The osmotic reduction in filtrate velocity caused by an abundant, mostly retained solute will also tend to elevate the tracer sieving coefficient. The osmotic effect alone explained only about one third of the observed increase in the sieving coefficients of Ficoll and Ficoll sulfate, whereas the effect of BSA on tracer partitioning was sufficient to account for the remainder. At physiological concentrations, predictions for tracer sieving in the presence of BSA

were found to be insensitive to the assumed shape of the protein (sphere or prolate spheroid). For protein mixtures, the theoretical effect of 6 g/dL BSA on the partitioning of spherical tracers was indistinguishable from that of 3 g/dL BSA and 3 g/dL IgG. This suggests that for partitioning and sieving studies in vitro, a good experimental model for plasma is a BSA solution with a mass concentration matching that of total plasma protein. The effect of plasma proteins on tracer partitioning is expected to influence sieving not only in isolated GBM, but also in intact glomerular capillaries in vivo.

3.2 Introduction

In a study designed to test the effects of molecular charge on the barrier properties of glomerular basement membrane (GBM), the sieving of polydisperse Ficoll and Ficoll sulfate was examined in vitro using filters prepared from isolated rat GBM (Bolton et al. 1998). Sieving coefficients (Θ, the ratio of filtrate to retentate concentration) were determined for Stokes-Einstein molecular radii (r_s) ranging from 20 to 50 Å. The principal finding was that the values of Θ for any given size of Ficoll and Ficoll sulfate were indistinguishable when buffer solutions of physiological ionic strength were employed. This indicates that the GBM is only a size-selective barrier, and does not exhibit charge selectivity. Although the experiments failed to detect an effect of molecular charge, there was a very pronounced upward shift in the sieving curves (plots of Θ vs. r_s) of either tracer when BSA was present in the retentate at a concentration of 4 g/dL. Because the hydraulic permeability of the GBM filters was unaffected by BSA, the shift in the sieving curves apparently was not due to an alteration of the intrinsic properties of the GBM (i.e., a result of binding of BSA to the membrane). One alternative explanation for the increase in Θ is the reduction in filtrate velocity (or volume flux) caused by the osmotic pressure of BSA. A well-known finding in ultrafiltration is that small filtrate velocities promote diffusional equilibration between the filtrate and retentate, causing Θ to approach unity even for large solutes if the velocity is small enough. Thus, slow rates of filtration diminish the apparent size-selectivity. However, calculations based on the

measured filtrate velocities with and without BSA revealed that this could explain only about one third of the increase in Θ. It was suggested that most of the BSA effect might be due to a second physical phenomenon, namely, a tendency of steric interactions with BSA to facilitate entry of the tracers into the membrane. It is this second phenomenon, known for some time in the membrane science literature but not widely recognized in microvascular physiology, which was examined in more detail in the present work.

Several theoretical and experimental investigations have shown that the equilibrium partitioning of a macromolecule between a bulk solution and a porous or fibrous material is dependent on its concentration. In essence, steric interactions between molecules in a concentrated solution cause entry into the porous or fibrous material to be more favorable thermodynamically than if the solution were dilute. The net effect is that the partition coefficient (Φ, the concentration in the membrane divided by that in the external solution, at equilibrium) increases with the external concentration. For uniform pores of various shapes and for solutions containing a single type of rigid, spherical solute, this effect was predicted by Anderson and Brannon (1981) and by Glandt (1981) using statistical mechanical arguments. Fanti and Glandt (1990) used density functional theory to obtain similar results for spheres partitioning in randomly oriented arrays of fibers. More recently, Lazzara et al. (2000) (Chapter 2) used an excluded volume formulation to extend the results for rigid solutes to arbitrary mixtures of spheres or spheroids, and White and Deen (2001) used Monte Carlo methods to predict the partitioning of concentrated solutions of flexible polymer chains. Experimentally, increases in Φ with increasing solute concentration have been demonstrated, for example, by Brannon and Anderson (1982) for both dextran and BSA in controlled pore glass, and by White and Deen (2001) for dextran in agarose gels. Additionally, the sieving coefficients of Ficoll and BSA in synthetic membranes were found to increase with increasing solute concentration, consistent with theoretical predictions for porous media (Mitchell and Deen 1986).

Most of the work just cited involved concentrated solutions of single solutes, whereas what is of primary interest here is the effect of an abundant solute (e.g., BSA) on the partitioning of a

dissimilar tracer (e.g., Ficoll). The partitioning of a spherical tracer molecule between a solution and a fiber matrix is depicted in Fig. 3-1. When only the tracer is present, as in the top panel, solute-solute interactions are negligible and steric exclusion of the tracer by the fibers causes Φ to be less than unity. This is the situation considered in the classical analysis by Ogston (1958). The balance is altered when a second solute is added at high concentration, as in the bottom panel. When very little of the abundant solute is able to enter the membrane, it will tend to exclude the tracer from the solution, partially canceling the effects of the fibers. Accordingly, while Φ for the tracer is still less than unity, it is larger than for a very dilute solution.

Bolton et al. (1998) were unable to satisfactorily model the effect of BSA on Ficoll or Ficoll sulfate partitioning or sieving because the theories for concentrated solutions that were available at that time were limited to single solutes. The results of Chapter 2, which may be applied to any number of spheroidal solutes, make it possible to further analyze the data and test whether the predicted effect of BSA on partitioning is sufficient to explain its influence on Ficoll and Ficoll sulfate sieving in GBM. That was the objective of the work reported here.

This chapter is organized as follows. The next section begins with a discussion of the relationship between the sieving coefficient and partition coefficient, including the effects of filtrate velocity and the novel behavior caused by the presence of an abundant solute. The key partitioning relationships from Chapter 2 are then summarized, to complete the description of the theory. After some general results are presented to illustrate the effects of solute concentration and filtrate velocity on sieving coefficients, a comparison is made between the theoretical predictions and the data for the GBM. We conclude with predictions of the effects of mixed solutions of proteins (e.g., serum albumin and globulins) and with a discussion of the physiological significance of this phenomenon. As will be explained, abundant, poorly filtered proteins such as albumin are likely to influence the sieving behavior of test macromolecules in vivo in much the same way that they influence their sieving in isolated GBM.

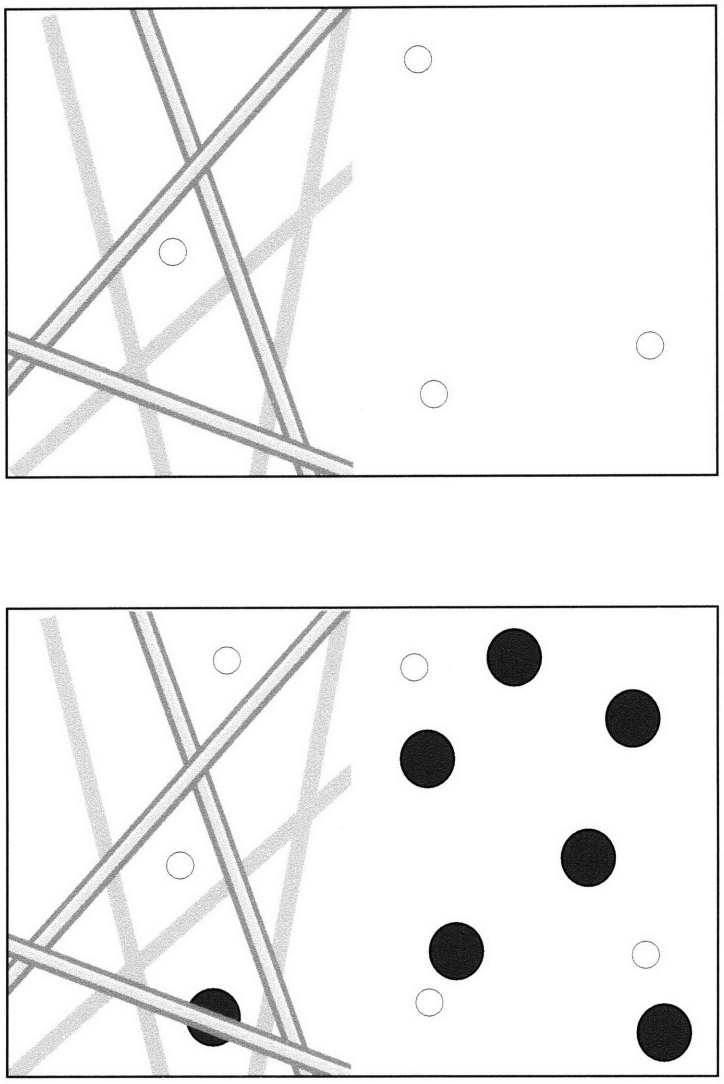

Figure 3-1: Schematic of the partitioning of a spherical tracer (open circles) into a randomly oriented matrix of fibers. In the top panel, only tracer is present and its partitioning is determined by steric interactions with the fibers only. In the bottom panel, tracer interactions with the abundant solute (filled circles) tend to exclude tracer molecules preferentially from the bulk solution and increase the partition coefficient of the tracer.

3.3 Model Development

3.3.1 Relationship between sieving and partitioning. In an isotropic medium, such as an array of randomly oriented fibers, the flux (**N**) of a macromolecular solute may be expressed as

$$\mathbf{N} = -K_d D_\infty \nabla C + K_c \mathbf{v} C \qquad \textbf{[3-1]}$$

where D_∞ is the solute diffusivity in free solution, **v** is the fluid velocity vector, C is the solute concentration, and K_d and K_c are hindrance factors for diffusion and convection, respectively. In general, steric and hydrodynamic interactions between a macromolecular solute and the fixed polymeric fibers of a membrane or gel will cause K_d and K_c to be less than unity, although K_c may exceed unity for small solutes. This has been demonstrated, for example, for Ficoll and globular proteins in agarose gels (Johnson et al. 1996; Johnston and Deen 1999). Consider a membrane extending from $x = 0$ to $x = L$ that is in contact with solutions of concentration C_0 and C_L, respectively. For steady transport in the x direction, integration of Eq. [3-1] reveals that the solute flux is related to the external concentrations and filtrate velocity by

$$N = K_c v \left(\frac{C_0 \Phi_0 - C_L \Phi_L e^{-\mathrm{Pe}}}{1 - e^{-\mathrm{Pe}}} \right) \qquad \textbf{[3-2]}$$

where Φ_0 and Φ_L are the equilibrium partition coefficients at the upstream and downstream surfaces, respectively, and Pe is the membrane Péclet number. The partition coefficient is the concentration just inside the GBM, divided by that in the adjacent external solution. The Péclet number is

$$\mathrm{Pe} = \frac{K_c v L}{K_d D_\infty} \qquad \textbf{[3-3]}$$

An implicit assumption in Eq. [3-2] is that there is an approximate thermodynamic equilibrium between the membrane and the external solutions at $x = 0$ and $x = L$. In ultrafiltration, the filtrate concentration is determined by the ratio of the solute and volume fluxes (i.e., $C_L = N/v$), and the membrane sieving coefficient is defined as $\Theta = C_L/C_0$. These substitutions allow Eq. [3-2] to be rearranged as

$$\Theta = \frac{\Phi_0 K_c}{1-(1-\Phi_L K_c)e^{-\mathrm{Pe}}} \qquad \textbf{[3-4]}$$

Similar expressions for the sieving coefficient have been employed in many studies of ultrafiltration across synthetic or biological membranes. The one novel feature of Eq. [3-4] is the distinction between the upstream and downstream partition coefficients. Whereas with dilute solutions $\Phi_0 = \Phi_L$, an abundant solute in the retentate will tend to make $\Phi_0 > \Phi_L$ for the tracer.

The effects of filtrate velocity are described by the term in Eq. [3-4] that contains Pe. With high filtrate velocities and/or thick membranes, such that Pe >> 1, we obtain

$$\lim_{\mathrm{Pe}\to\infty} \Theta = \Phi_0 K_c \qquad \textbf{[3-5]}$$

In this limit the sieving coefficient depends on the upstream partition coefficient and convective hindrance factor, and is insensitive to filtrate velocity. This standard result is often expressed in terms of a reflection coefficient (σ), where $\Phi_0 K_c = 1 - \sigma$. Because $\Phi_0 K_c < 1$, we expect that $\Theta < 1$ for any macromolecular tracer if the filtrate velocity is large enough. The limit for low filtrate velocities and/or thin membranes is

$$\lim_{\mathrm{Pe}\to 0} \Theta = \frac{\Phi_0}{\Phi_L} \qquad \textbf{[3-6]}$$

In contrast to the usual result of Θ 1 for Pe 0, the sieving coefficient is determined now by the ratio of the partition coefficients. Because a large, abundant solute will tend to make $\Phi_0 > \Phi_L$, the sieving coefficient of an uncharged tracer could exceed unity. Although perhaps counterintuitive, this prediction has a firm physical basis. In general, Eqs. [3-4] - [3-6] indicate that an abundant solute will increase the sieving coefficient of a tracer at all values of Pe, by increasing Φ_0. The extent of the increase will depend also on K_c and Pe.

3.3.2 Effects of concentration on partitioning. The effects of solute concentrations on partition coefficients were modeled using the excluded volume theory from Chapter 2. In that theory, partition coefficients are calculated by summing the volumes excluded to a solute in the membrane and bulk phases due to the fixed structures of the membrane and to other solute molecules which may be present. Long-range intermolecular forces are ignored, limiting this method to media where steric considerations dominate and the effects of electric charge are negligible. As indicated earlier, this appears to be a valid approximation for GBM. The model generates a coupled set of nonlinear algebraic equations for the partition coefficients, one for each solute present. The most complicated situation to be considered here is a three-solute system of Ficoll, serum albumin, and IgG partitioning into a fibrous membrane composed of two distinct types of fibers. We will treat Ficoll and IgG as spherical molecules and BSA as a prolate spheroid. In the equations that follow, the solute indices 1, 2, and 3 refer to Ficoll, serum albumin, and IgG, respectively; there are also indices 1 and 2 for the two types of fibers. Using the notation from Chapter 2, the expressions for the partition coefficients in such a system are

$$\begin{aligned}\Phi_1 = \exp[&-\phi_1\alpha_{11}(s,f)-\phi_2\alpha_{12}(s,f)+\alpha_{11}(s,s)(1-\Phi_1)\chi_1 \\ &+\alpha_{12}(s,p)(1-\Phi_2)\chi_2+\alpha_{13}(s,s)(1-\Phi_3)\chi_3]\end{aligned} \qquad \textbf{[3-7a]}$$

$$\begin{aligned}\Phi_2 = \exp[&-\phi_1\alpha_{21}(p,f)-\phi_2\alpha_{22}(p,f)+\alpha_{21}(p,s)(1-\Phi_1)\chi_1 \\ &+\alpha_{22}(p,p)(1-\Phi_2)\chi_2+\alpha_{23}(p,s)(1-\Phi_3)\chi_3]\end{aligned} \qquad \textbf{[3-7b]}$$

$$\Phi_3 = \exp[-\phi_1\alpha_{31}(s,f) - \phi_2\alpha_{32}(s,f) + \alpha_{31}(s,s)(1-\Phi_1)\chi_1 + \alpha_{32}(s,p)(1-\Phi_2)\chi_2 + \alpha_{33}(s,s)(1-\Phi_3)\chi_3] \quad \textbf{[3-7c]}$$

where ϕ_i denotes the volume fraction of fibers of type i in the membrane and χ_j denotes the volume fraction of solutes of type j in the bulk solution. The quantities $\alpha_{ij}(x,y)$ are dimensionless geometric parameters which are used to describe the interaction of a test solute i of shape x with a set of objects j of shape y (s = sphere, p = prolate spheroid, f = fiber). For example, $\alpha_{11}(s,s)$ describes the steric interaction between two spheres of type 1. For spheres of radius r_i and r_j, the excluded volume parameter is

$$\alpha_{ij}(s,s) = \left(1 + \frac{r_i}{r_j}\right)^3 \quad \textbf{[3-8]}$$

Expressions for the remaining $\alpha_{ij}(x,y)$ parameters, some of which are quite lengthy, can be found in Chapter 2. Once those parameters were specified, Eqs. [3-7a] – [3-7c] were solved using Newton-Raphson iteration, using the dilute solution values for the partition coefficients as initial guesses.

All other systems considered here may be viewed as special cases of Eqs. [3-7a] – [3-7c], obtained by setting certain terms equal to zero. Thus, the dilute solution values of the partition coefficients were found by setting $\chi_j = 0$ for all j. Results for just two solutes (Ficoll and albumin) were computed by setting $\chi_3 = 0$ and dropping Eq. [3-7c]. Calculations for membranes with just one type of fiber were done by setting $\phi_2 = 0$. Among the results that may be recovered in this manner is the partitioning expression of Ogston (1958) for dilute solutions of spheres in random arrays of a single type of fiber; it corresponds to Eq. [3-7a] with $\phi_2 = 0$ and all $\chi_j = 0$.

3.4 Results and Discussion

3.4.1 General trends. Examples of the theoretical increase in the partition coefficient of a spherical tracer due to BSA are shown in Fig. 3-2. The tracer partition coefficient is denoted as Φ_T and the volume fraction of BSA in bulk solution is χ_{BSA}. These results were computed for a hypothetical fiber array with a volume fraction of $\phi = 0.2$ and a fiber radius of $R_f = 10$ Å. Those parameter values were selected so that BSA would be largely excluded from the membrane (Φ_{BSA} 0.01 for dilute solutions), as is true for GBM; otherwise, the choices are arbitrary. As discussed previously (Chapter 2), BSA was represented as a prolate spheroid with an axial ratio of $\eta = 3.3$ (major and minor semiaxes of 70 and 21 Å, respectively). With this assumed shape, the mass concentration that corresponds to $\chi_{BSA} = 0.1$ is 8.6 g/dL. Results are shown for tracers with r_s = 20, 30, 40, and 50 Å. It is seen that Φ_T increases with increasing χ_{BSA} in each case. The greatest percentage variations in Φ_T were obtained for the largest molecule, where the dilute-solution partition coefficient (Φ_T for $\chi_{BSA} = 0$) was smallest. These results demonstrate that the effect of an abundant solute on the partition coefficient of a tracer can be quite large.

Figure 3-3 shows the predicted effects of BSA on the sieving coefficient of a spherical tracer with $r_s = 30$ Å, for the same fiber matrix as in Fig. 3-2. As shown in Eq. [3-4], which was applied here to both the tracer and BSA, the sieving coefficient depends on K_c and Pe, as well as the partition coefficients. Because there is not yet a reliable theory for predicting the convective hindrance factor in a random fiber matrix (Johnston and Deen 2002), $K_c = 0.75$ was used as a representative value, both for the tracer and for BSA. Since $r_s = 36$ Å for BSA, its K_c in the same fiber matrix would probably be smaller than that of a 30 Å sphere. Additionally, one would expect that Pe for BSA would be larger than that of a 30 Å sphere, in part because of the reduced value of D_∞, and perhaps also because of larger values of the ratio K_c/K_d. Eq. [3-4] indicates that using too large a K_c and/or too small a Pe for BSA would increase its predicted sieving coefficient. In other words, the filtrate concentration of BSA was probably overestimated. Because anything that tends to reduce the transmembrane concentration difference for BSA also tends to minimize its effect on

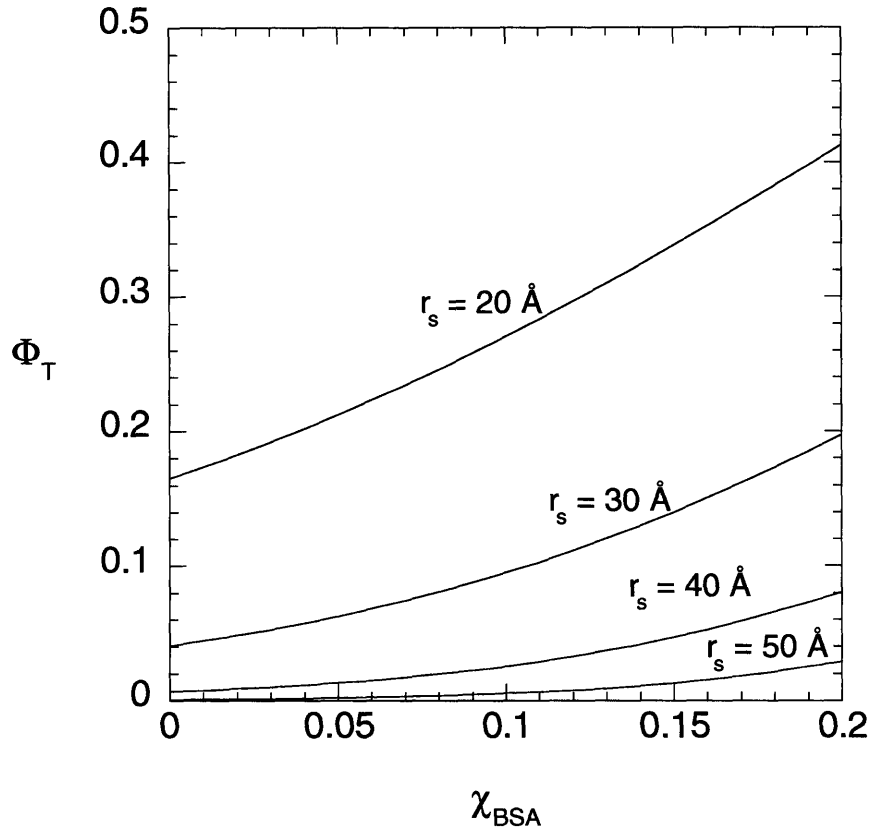

Figure 3-2: Partition coefficient of a spherical tracer (Φ_T) as a function of BSA volume fraction (χ_{BSA}). Results are shown for various tracer Stokes-Einstein radii (r_s). The volume fraction of fibers was $\phi = 0.2$, the fiber radius was $R_f = 10$ Å, and BSA was treated as a prolate spheroid with axial ratio $\eta = 3.3$.

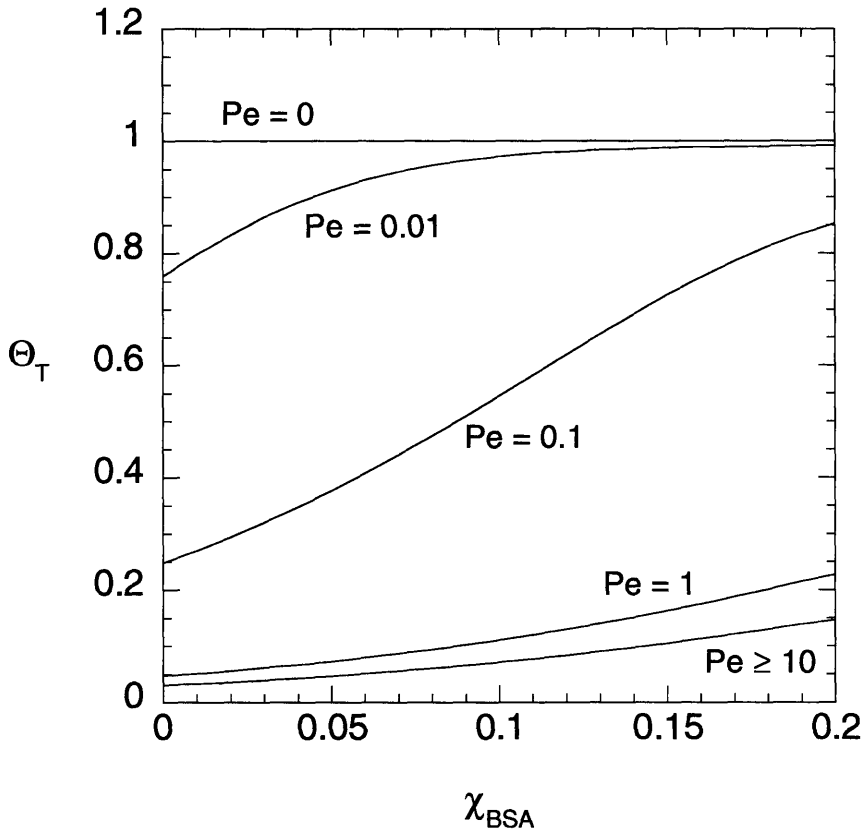

Figure 3-3: Sieving coefficient of a spherical tracer (Θ_T) as a function of BSA volume fraction (χ_{BSA}) and membrane Péclet number (Pe). Results are shown for r_s = 30 Å and K_c = 0.75, with other conditions as in Fig. 3-2.

tracer sieving, the effects shown in Fig. 3-3 should be viewed as conservative estimates. Results were computed for a wide range of Pe values and BSA concentrations in the retentate. As seen in Fig. 3-3, the sieving coefficient of the tracer (Θ_T) is predicted to be elevated as the BSA concentration is increased, for any fixed value of Pe > 0. Note that increasing the BSA concentration would also tend to decrease Pe, because of the osmotic pressure opposing filtration. Thus, the usual effect of adding BSA would be to move toward the higher curves in Fig. 3-3, making Θ_T even more sensitive to the BSA concentration. In contrast to the situation discussed in connection with Eq. [3-6], Θ_T in Fig. 3-3 does not exceed unity even for Pe = 0 and large concentrations of BSA. The reason is that, with identical assumed values of K_c for the tracer and BSA, and with their roughly comparable molecular sizes, $\Theta_{BSA} \rightarrow 1$ as Pe $\rightarrow 0$, much as $\Theta_T \rightarrow 1$. As the BSA concentration in the filtrate approaches that in the retentate, the tracer partition coefficients at the two membrane surfaces become equal. With $\Phi_L \rightarrow \Phi_0$, Eq. [3-6] indicates that $\Theta_T \rightarrow 1$, consistent with the behavior in Fig. 3-3 for Pe $\rightarrow 0$. For Θ_T to exceed unity at small Pe, BSA (or another abundant protein) would have to be excluded from the membrane much more efficiently than the tracer.

3.4.2 Sieving in isolated GBM. In order to predict the effects of BSA on Ficoll and Ficoll sulfate sieving in isolated GBM, values were needed for the convective and diffusive hindrance factors for the range of molecular sizes studied by Bolton et al. (1998). Because it was not possible to measure K_c and K_d independently under those experimental conditions, and because there is not yet a reliable theory for predicting hindrance factors in a material as complex as GBM, we elected to estimate the necessary quantities by fitting the Ficoll and Ficoll sulfate sieving curves measured in the absence of BSA. With protein-free solutions, the partition coefficients at the two sides of the membrane are equal; that is, $\Phi_0 = \Phi_L = \Phi$. Equations [3-3] and [3-4] indicate that knowledge of the products ΦK_c and ΦK_d is sufficient to find the Péclet number and sieving coefficient. Both of these products are expected to decline from values of near unity for very small molecules to nearly zero for large molecules. Accordingly, the empirical forms chosen for the fitting were

$$\Phi K_d = \exp(-ar_s) \qquad \textbf{[3-9a]}$$

$$\Phi K_c = \exp(-br_s) \qquad \textbf{[3-9b]}$$

The constants a and b were evaluated by using Powell's method to minimize the norm of the error between the data and the sieving coefficients predicted using Eq. [3-4]. The resulting values were a = 0.126 Å^{-1} and b = 0.075 Å^{-1} for Ficoll, and a = 0.134 Å^{-1} and b = 0.069 Å^{-1} for Ficoll sulfate. The nearly identical values of a and b computed for Ficoll and Ficoll sulfate reflect the fact that the sieving curves of these neutral and anionic tracers in GBM were indistinguishable. The values of a and b given here for Ficoll differ slightly from those reported by Bolton et al. (1998). The reason is that, in the present work, an effort was made to correct for nonselective "shunts" or "leaks" in the filters made by consolidating cell-free glomeruli. This was done by subtracting from each sieving coefficient the value measured for the largest Ficoll or Ficoll sulfate studied, where r_s = 80 Å. Although this had only a modest effect on the results to be shown for $20 \le r_s \le 50$ Å, the "corrected" sieving coefficients are the ones plotted. Note that the known limiting behavior of ΦK_d and ΦK_c for point-sized solutes in random arrays of fibers can be incorporated into Eqs. [3-9a] and [3-9b] by changing the pre-exponential coefficients from unity to [1 - (5/3)ϕ] and [1 - ϕ], respectively. Using these modified expressions had virtually no effect on the ability to fit the sieving data without BSA or on the predicted sieving curves with BSA. Thus, although the modified forms are more exact for $r_s \to 0$, that had little consequence for the range of molecular sizes studied here.

The central element of the theory used to predict the effects of BSA on Ficoll and Ficoll sulfate sieving was the partitioning model. It has been argued recently that representing GBM as a randomly oriented array of uniform fibers fails to account for its electron microscopic appearance, its measured volume fraction of solids, and its measured hydraulic (or Darcy) permeability (Bolton and Deen 2001). However, assuming it to consist of a mixture of coarse and fine fibers, which correspond roughly to collagen IV and glycosaminoglycan chains, leads to behavior consistent with

all of those properties. Accordingly, we adopted a two-fiber model with parameter values as suggested in Bolton and Deen (2001): the radii of the coarse and fine fibers were taken to be 35 Å and 5 Å, respectively; the corresponding volume fractions were 0.046 and 0.054, for a total solid fraction of 0.10. Also needed for the partitioning calculations are the concentrations of BSA at the upstream and downstream surfaces of the GBM layer studied in vitro. Correcting the retentate value for concentration polarization and using the measured sieving coefficient for BSA (Θ_{BSA} = 0.085) (Bolton et al. 1998), the upstream and downstream concentrations were found to be 6.2 and 0.53 g/dL, respectively. With BSA represented as a prolate spheroid, as described above, the corresponding volume fractions are χ_{BSA} = 0.072 and 0.0061. Determining its concentrations in this manner from experimental data, it was not necessary to specify K_c and K_d for BSA.

Theoretical sieving curves are compared with the GBM data for Ficoll and Ficoll sulfate in Figs. 3-4 and 3-5, respectively. As shown by the lower curves in each plot, the simple expressions adopted for the hindrance factors (Eqs. [3-9a] and [3-9b]) yielded excellent fits to the sieving data obtained in the absence of BSA. Shown also in Figs. 3-4 and 3-5 are the respective sieving curves measured in the presence of BSA, and two predictions for that case. One prediction includes only the osmotic effect of BSA. In those calculations BSA was assumed to reduce Pe (due to the lower filtrate velocity) without affecting the tracer partition coefficients. As shown in both figures, and as noted in Bolton et al. (1998), this purely osmotic effect of BSA accounts for only about 1/3 of the upward shift in the sieving curves. The remaining curves in each plot are based on the complete theory, including both partitioning and osmotic effects. It is seen that the predicted effect of BSA is more than sufficient to account for the upward shifts in the Ficoll and Ficoll sulfate sieving curves. The tendency of the theory to overestimate the effect of BSA, especially for the largest solutes, might be the result of limitations in the representation of the GBM as an array of randomly oriented fibers. Indeed, although glycosaminoglycan chains (and possibly other components) may be relatively disordered, there is evidence from electron microscopy that collagen IV fibers assemble into a branching polygonal network in at least some basement membranes (Yurchenco and Ruben 1987). Thus, it might be more accurate to model GBM as a partially ordered fibrous structure filled

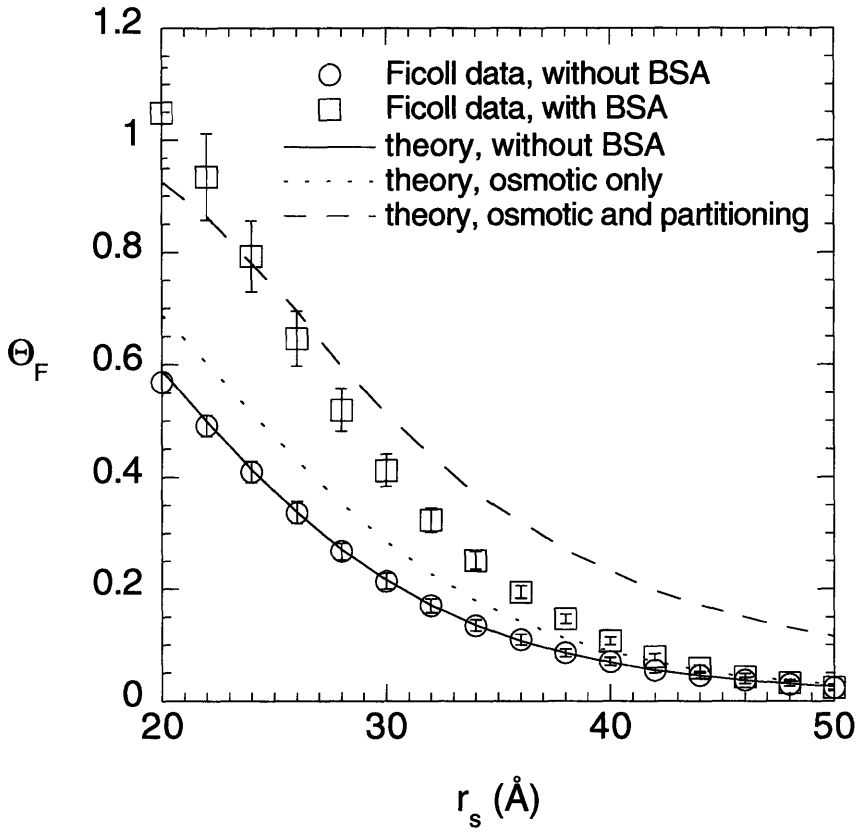

Figure 3-4: Sieving coefficient of Ficoll (Θ_F) as a function of Ficoll radius (r_s) for isolated rat GBM. The symbols with error bars represent the data of Bolton et al. (1998). Theoretical curves are shown for a solution without BSA, for a BSA solution with osmotic effects only, and for the complete theory with osmotic and partitioning effects.

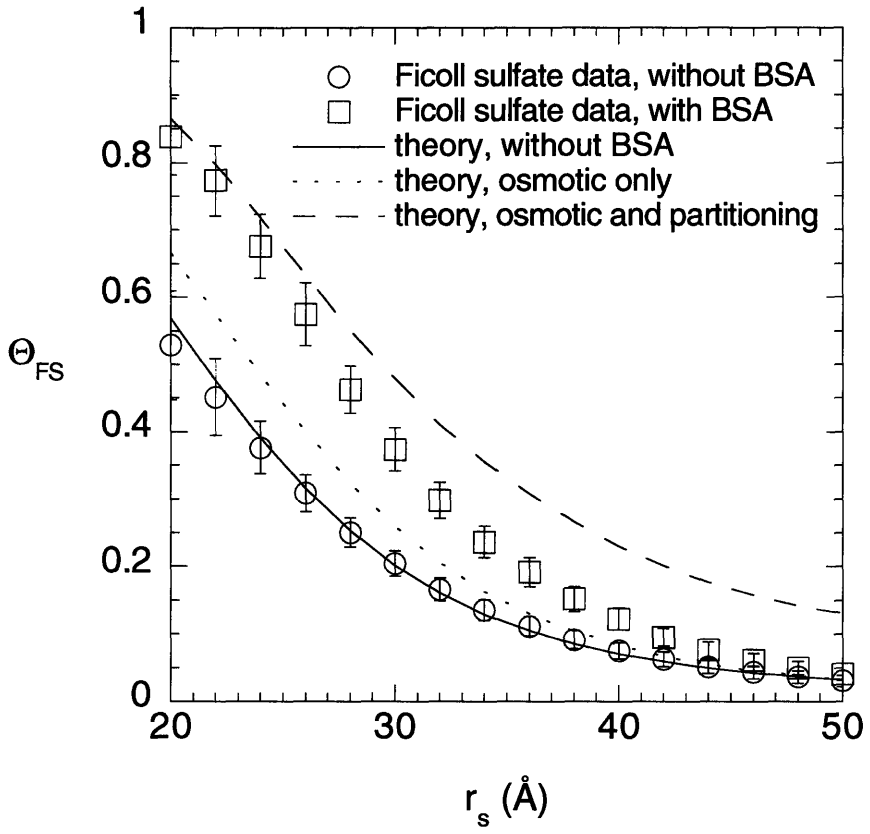

Figure 3-5: Sieving coefficient of Ficoll sulfate (Θ_{FS}) as a function of Ficoll sulfate radius (r_s) for isolated rat GBM. The symbols with error bars represent the data of Bolton et al. (1998). Theoretical curves are shown for a solution without BSA, for a BSA solution with osmotic effects only, and for the complete theory with osmotic and partitioning effects.

with smaller, randomly oriented fibers. Predictions for such mixed structures, however, are beyond the capabilities of current partitioning theories.

3.4.3 Effects of protein size and shape. Although our calculations have focused on BSA, any abundant protein should influence the partition and sieving coefficients of tracer macromolecules. This leads to the question of whether protein size and/or shape are important factors. This was examined in two ways: first, to see if modeling BSA as a sphere would alter the predictions in Figs. 3-4 and 3-5; and second, to see if a mixture of albumin and globulins would behave differently than an albumin solution.

In the preceding calculations BSA was treated as a prolate spheroid with an axial ratio of 3.3 and major and minor semiaxes of 70 and 21 Å. This model appears to be most consistent with its partial specific volume (Al-Malah et al. 1995), intrinsic viscosity (Tanford 1961), and Stokes-Einstein radius (Johnson et al. 1995; Lazzara et al. 2000). However, a much simpler representation is a sphere of radius r_s = 36 Å (the Stokes-Einstein radius of BSA). If the spherical model is adopted, then $\chi_{BSA} = 0.1$ corresponds to a mass concentration of 5.8 g/dL. Repeating the calculations in Figs. 3-4 and 3-5 for a spherical BSA molecule resulted in curves that were virtually indistinguishable from those for the prolate spheroid. Thus, the shape of BSA does not appear to be an important determinant of its effect on the partitioning of tracers in GBM, for the protein concentrations considered here. This is not a general finding, in that molecular shape has been shown to influence the effects of solute concentration on partitioning in other hypothetical situations (see Chapter 2, Section 2.4.4).

To examine the effects of a protein mixture, we simulated partitioning into GBM from a BSA solution or a "plasma" represented as a 1:1 mixture (by mass) of BSA and IgG. Once again, the two-fiber GBM model was employed, and BSA was treated as a prolate spheroid. For simplicity, we did not attempt to model the "Y" shape of IgG, representing IgG instead as a sphere of 52 Å radius (Potschka 1987). The results are shown in Fig. 3-6 as plots of tracer partition coefficient vs. tracer size for various protein solutions. The presence of BSA at 6 g/dL is predicted to roughly double the partition coefficient of a tracer of intermediate size. For the smaller

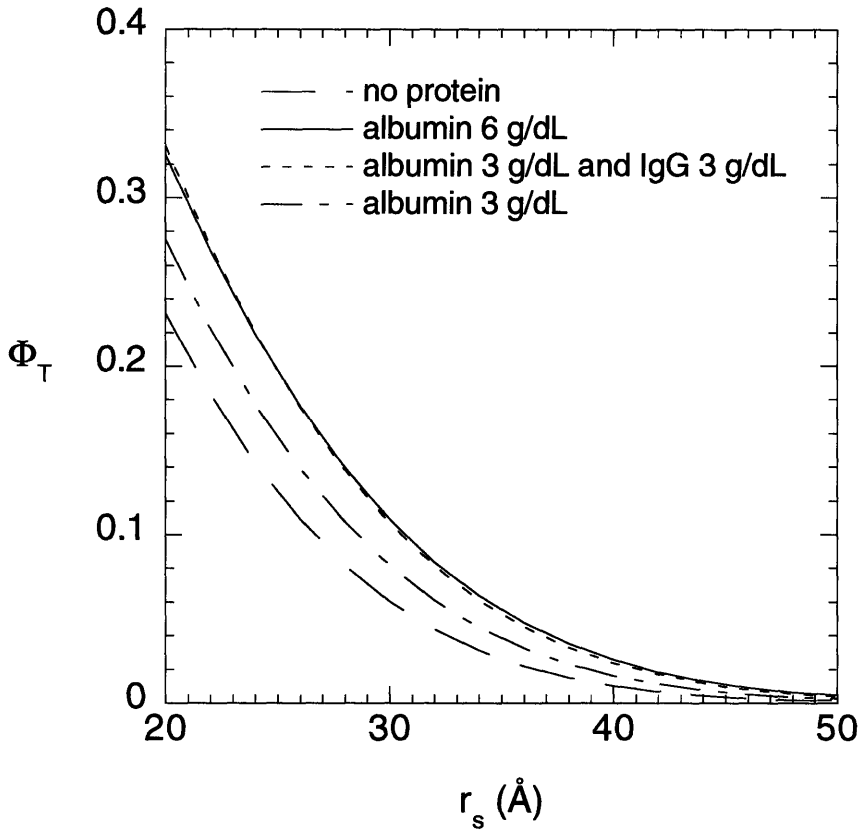

Figure 3-6: Partition coefficient of a spherical tracer (Φ_T) as a function of tracer radius (r_s). Results are shown for a protein-free solution and for solutions containing albumin and/or IgG.

molecules the percentage changes are lower than for the larger molecules. Interestingly, if the total protein consists of 3 g/dL albumin and 3 g/dL IgG, the predicted partition coefficients are barely distinguishable from those for 6 g/dL albumin. This suggests that, from a partitioning viewpoint, a good experimental model for plasma is a BSA solution with a mass concentration that matches that of total plasma protein. (Such a solution is less accurate from an osmotic viewpoint, in that the osmotic pressure of BSA exceeds that of mixed plasma proteins, for a given mass concentration.) If the total protein content is reduced to 3 g/dL (either BSA or an albumin-IgG mixture), the augmentation of the partition coefficient is very nearly half that for 6 g/dL. Thus, the effects of abundant proteins on partitioning in the GBM are predicted to be nearly linear in the protein concentration.

3.4.4 Application to intact capillaries. Attempts to extrapolate these findings to glomerular filtration in vivo are complicated by the fact that the barrier properties of the capillary wall are determined only partly by the GBM. The various factors to be considered will be identified first, and then some conclusions will be reached concerning filtration in intact capillaries. The overall sieving coefficient at any point along a glomerular capillary (Θ, the concentration in Bowman's space relative to plasma) depends on two kinds of quantities. First, there are the individual sieving coefficients for each of the three layers of the capillary wall: Θ_{en} for the endothelial fenestrae, Θ_{bm} for the GBM, and Θ_{ep} for the epithelial filtration slits. As used here, Θ_i is the concentration at the downstream edge of layer i divided by that at the upstream edge. These are "internal" sieving coefficients in the sense that the upstream and downstream concentrations are evaluated just inside the layer under consideration. As exemplified by Eq. [3-4], these sieving coefficients are dynamic quantities that depend on filtrate velocity, as well as on the respective diffusive and convective hindrance factors and thicknesses of the layers. Second, there are equilibrium partition coefficients that describe the step changes in concentration that occur at the phase boundaries. At the boundary between layer i and layer j, we denote the concentration in i divided by that in j as $\Phi_{i/j}$. Of importance, $\Phi_{i/j}$ depends not just on the structural characteristics of layers i and j, such as their pore

sizes or fiber spacings, but also on the concentration of albumin (or other abundant proteins) in the vicinity of the boundary. With these definitions, the overall sieving coefficient is given by

$$\Theta = \Phi_{en/p}\Phi_{bm/en}\Phi_{ep/bm}\Phi_{b/ep}\Theta_{en}\Theta_{bm}\Theta_{ep} \qquad \textbf{[3-10]}$$

where p and b denote plasma and Bowman's space, respectively. Thus, seven quantities are needed to describe the concentration changes that occur across the three layers and at the four boundaries, as one moves from plasma to Bowman's space. If the partition coefficients were not affected by the local protein concentrations within the glomerular capillary wall, then their concentration ratios would cancel (see below) and Eq. [3-10] would simplify to

$$\Theta = \Theta_{en}\Theta_{bm}\Theta_{ep} \qquad \textbf{[3-11]}$$

as used previously (Edwards et al. 1999). Thus, it is the steric effect of proteins on tracer partitioning that requires the four additional terms in the more general expression. In the absence of protein effects, the partition coefficients obey relationships of the form $\Phi_{i/j}\Phi_{j/k} = \Phi_{i/k}$. The cancellation of terms in Eq. [3-10] follows from that and the fact that, without proteins, $\Phi_{b/p} = 1$.

Among the many possibilities that can be imagined, in which proteins might affect any or all of the four partition coefficients in Eq. [3-10], we focus now on two of the more likely scenarios. Both are motivated by the finding of Ryan and Karnovsky (1976) that albumin is almost completely excluded from the GBM. Thus, the common aspect of the two scenarios is the assumption that almost no protein reaches the downstream side of the GBM and the filtration slits, from which it follows that $\Phi_{ep/bm}\Phi_{b/ep} = \Phi_{b/bm} = 1/\Phi_{bm/b}$, where $\Phi_{bm/b}$ is the partition coefficient that would apply if the GBM were in direct contact with Bowman's space (or simply water). Suppose now that albumin passes freely through the endothelial fenestrae, and that the limiting step for it is entry into the GBM. In other words, assume that the fenestrae act only as wide, water-filled channels. This

assumption corresponds to $\Phi_{en/p} = \Theta_{en} = 1$ and $\Phi_{bm/en} = \Phi_{bm/p}$. Thus, for water-filled fenestrae, Eq. [3-10] reduces to

$$\Theta = \frac{\Phi_{bm/p}}{\Phi_{bm/b}} \Theta_{bm} \Theta_{ep} \qquad \textbf{[3-12]}$$

The steric effect of albumin (and other retained proteins) would be to make $\Phi_{bm/p}/\Phi_{bm/b} > 1$. Accordingly, in this scenario the effect of albumin on the overall sieving coefficient will closely resemble its effect on isolated GBM, as already described.

Alternatively, one could assume that the endothelial glycocalyx is the limiting barrier, and that only the upstream sides of the fenestrae are exposed to protein. For this situation, algebraic manipulations like those above reduce Eq. [3-10] to

$$\Theta = \frac{\Phi_{en/p}}{\Phi_{en/b}} \Theta_{en} \Theta_{bm} \Theta_{ep} \qquad \textbf{[3-13]}$$

The first term is similar to Eq. [3-12], except that the partition coefficients are now those for the fenestral glycocalyx. Because the steric effect of abundant proteins on tracer partitioning will be directionally similar for any porous or fibrous material, we expect that $\Phi_{en/p}/\Phi_{en/b} > 1$. Thus, for either of the situations represented by Eqs. [3-12] and [3-13], the effects of abundant proteins on partitioning will be to increase the overall sieving coefficient of a tracer macromolecule.

In obtaining Eqs. [3-12] and [3-13] it was assumed that the limiting barrier for albumin and other abundant proteins was upstream of the GBM. However, qualitatively similar trends are predicted if the limiting barrier is at the level of the slit diaphragm. In other words, no matter what the limiting barrier is for the protein, there will be a tendency for an abundant, poorly filtered protein to augment the sieving coefficient of a tracer. Although the location of the protein barrier does not influence the direction of the effect, it will determine its magnitude. If the effect is mediated by

partitioning in the GBM, it can be estimated from our analysis of sieving data for isolated GBM. If it is mediated by partitioning elsewhere (e.g., between plasma and glycocalyx), then the paucity of information on material properties makes its magnitude more uncertain.

The likelihood that steric interactions with plasma proteins elevate tracer sieving coefficients has an interesting implication for studies of human disease. That is, it suggests that the low plasma protein concentrations characteristic of the nephrotic syndrome will tend to mask some of the glomerular injury revealed by fractional clearance measurements with tracer molecules such as Ficoll. Although the Ficoll (or dextran) sieving coefficients in nephrotic subjects might still be much higher than in healthy individuals, they will not be as high as if plasma proteins levels were normal. In this sense, the true extent of the injury will be partly concealed. Likewise, variations in perfusate protein concentration in studies using the isolated perfused kidney (IPK) (Ohlson et al. 2000, 2001; Osicka et al. 1996) complicate efforts to assess the intrinsic size-selectivity of the barrier. The steric effects we have described would cause apparent (calculated) pore radii to increase with increasing protein concentration, even without any structural change in the capillary wall.

3.4.5 Other effects of proteins. This paper has focused mainly on the idea that steric interactions with plasma proteins tend to elevate the glomerular sieving coefficients of tracers. Such steric effects are entirely physical and non-specific, and will be present to varying degrees with any globular protein and any ultrafiltration membrane. Several other effects of proteins on microvascular permeability have been reported, some of them quite specific. The glycoprotein orosomucoid has been shown to influence the permeability of both glomerular and peripheral capillaries by maintaining charge-selectivity (Curry et al. 1989; Haraldsson and Rippe 1987; Haraldsson et al. 1992; Johnsson and Haraldsson 1993). Studies using frog mesenteric capillaries have revealed effects of albumin itself: omitting albumin from perfusates increased the hydraulic permeability and decreased the reflection coefficients for Ficoll (Mason et al. 1977; Michel 1988; Michel et al. 1985). Specificity was demonstrated by showing that the effect was abolished by chemical modification of arginine residues of albumin (Michel et al. 1985). It was hypothesized

that albumin (and also ferritin) might influence capillary permeability by ordering the fibers of the glycocalyx (Michel 1988). Lowered protein concentrations have been shown to increase the permeability of capillaries in a variety of other vascular beds (Mann 1981; McDonagh 1983; Rippe and Folkow 1977; Watson 1983). In contrast, micropuncture studies in rats have shown that decreases in plasma protein concentration reduce the glomerular ultrafiltration coefficient, the product of hydraulic permeability and surface area for filtration (Baylis et al. 1977; Tucker and Blantz 1981). The underlying mechanism for this remains unknown, but the observation that BSA did not affect the hydraulic permeability of isolated GBM (Bolton et al. 1998) suggests involvement of endothelial cells and/or epithelial foot processes, rather than the GBM.

3.5 Conclusions

The theory presented here suggests that BSA (or other abundant proteins) can markedly increase the sieving coefficients of tracer macromolecules in the GBM, largely as a consequence of steric interactions that favor tracer partitioning into the membrane. The predicted effect of these steric interactions, combined with the osmotic effect of BSA, is large enough to account for the marked elevation of Ficoll sieving coefficients in isolated GBM when BSA is present, reported previously (Bolton et al. 1998). The magnitude of this protein effect is predicted to be less dependent on protein size and shape than it is on the total concentration of protein. It is a factor that should be taken into account in efforts to characterize the intrinsic barrier properties of the glomerular capillary wall.

Chapter 4

Effects of Protein Concentration on the Partitioning of Macromolecular Tracers in Agarose Hydrogels

4.1 Abstract

Measurements of the equilibrium partition coefficients of the protein bovine serum albumin (BSA) and four narrow fractions of Ficoll, a copolymer of sucrose and epichlorohydrin, were made in agarose hydrogels. The measurements were made by equilibrating solutions of known concentration of each macromolecule with a known volume of gel and then applying a material balance. The partition coefficient of each molecule was measured under dilute conditions and under conditions where BSA was present at concentrated levels. All measurements were made for two different agarose solid volume fractions. As expected, the partition coefficients decreased with increasing solid volume fraction and with increasing molecular size. Increasing BSA concentration caused an increase in the partitioning of BSA itself and that of all four sizes of Ficoll. This effect was most significant for the largest molecules. A subset of the measurements repeated at a higher ionic strength demonstrated that any electrostatic interactions between the solutes and the agarose and among solutes were well-screened and that steric interactions were the dominant intermolecular force at the standard ionic strength. The experimental results were compared with predictions

generated from a previously developed excluded volume theory for the partitioning of rigid, spheroidal macromolecules in fibrous media. Using that theory, agarose was treated as a population of randomly oriented uniform cylindrical fibers. BSA was modeled as a prolate spheroid, and Ficoll was treated as a sphere. Comparisons of the theoretical predictions, which are valid for steric interactions only, with the experimental data produced generally good agreement. The experimental results compared best with the theory for the highest solid volume fractions of agarose.

4.2 Introduction

The equilibrium distribution of a macromolecule *i* between a solution and a membrane or other porous phase is described by its partition coefficient,

$$\Phi_i = \overline{C_i} / C_i \qquad \textbf{[4-1]}$$

where $\overline{C_i}$ and C_i are the concentrations of *i* in the porous phase and the adjacent solution, respectively. The partition coefficient is an important determinant of the performance of membrane separations such as ultrafiltration and chromatographic separations such as gel filtration chromatography. The partitioning of macromolecules in certain biological tissues plays a key role in the functioning of a variety of physiological processes in both health and disease. As a result of the importance of solute partitioning in such a wide range of processes, there has been a great deal of effort to elucidate the factors which govern solute partitioning in a variety of media.

Steric and electrostatic interactions between the partitioning solute and the fixed structures of the membrane are important factors in determining the magnitude of the partition coefficient. Theoretical results are available for the steric exclusion of neutral spheres from both random fiber matrices (Ogston 1958) and pores (Pappenheimer et al. 1951). The effects of membrane-solute electrostatic interactions have been investigated theoretically for spheres in random fiber matrices

(Johnson and Deen 1996). Solute-membrane electrostatic interactions for spheres (Smith and Deen 1983) and random coil polymers (Lin and Deen 1990) have been studied for pores as well. In addition to membrane-solute steric and electrostatic interactions, the concentration of the solute itself can have an effect on Φ_i. This effect, although rarely incorporated into models of membrane transport, can be quite significant for a number of systems of interest. The concentration effect has been modeled using a variety of theoretical approaches and demonstrated in several experimental settings. Almost universally, the results of these studies have shown that increasing the concentration of a solute causes an increase in its partition coefficient. Concentration effects were investigated for the partitioning of neutral spheres in random fiber matrices using density functional theory (Fanti and Glandt 1990a) and Monte Carlo simulations (Fanti and Glandt 1990b). White and Deen (2001) developed a theory to describe the effects of polymer concentration on the partitioning of linear polymers in random fiber matrices. The effects of concentration on the partitioning of neutral spheres in pores has been examined as well (Anderson and Brannon 1981; Glandt 1981). A statistical mechanical approach developed by Buck et al. (2001) incorporates the effects of membrane-solute and solute-solute electrostatic interactions in modeling the effect of concentration on the partitioning of spheres in random fiber arrays. Electrostatic effects on the partitioning of concentrated solutions of spherical molecules in pores have also been analyzed (Anderson and Brannon 1981; Mitchell and Deen 1984).

Perhaps the earliest experimental demonstration of the concentration effect was performed by Brannon and Anderson (1982) who showed that the partition coefficients of the proteins BSA and α-lactalbumin in controlled pore glass were each increasing functions of their respective bulk concentrations. White and Deen (2001) found that the partitioning of dextrans in agarose could be augmented by increasing the concentration of dextran in the bulk. Buck et al. (2001) measured concentration effects on BSA and α-lactalbumin partitioning in agarose gels at two different ionic strengths. While they found little effect of concentration at the higher ionic strength, there was a pronounced effect at the lower ionic strength. For BSA, the increased concentration caused an increase in BSA partitioning, whereas increases in α-lactalbumin concentration caused a decrease in

the partitioning of that molecule. The latter finding was apparently the result of attractive solute-solute interactions between α-lactalbumin molecules.

In order to understand the basis for the physical effect of concentraiton, let us first note that the partition coefficient of a given solute can be thought of as the probability of being able to randomly place a single test solute molecule in the membrane phase without it intersecting other objects relative to the same probability in the adjacent bulk solution (see Section 2.3.1). Under dilute conditions, where solute molecules essentially interact only with the membrane fibers and not with eachother, and first considering the case where solutes only experience steric interactions with other objects, Φ_i is less than unity due to the steric exclusion of solute molecules from the membrane phase due to the presence of the fibers. Because Φ_i is less than one, the addition of more solute particles causes a larger increase in the volume excluded to a test solute in the bulk than in the membrane phase. This disproportionate increase in the bulk excluded volume tends to increase Φ_i. In addition to these steric solute-solute effects, electrostatic interactions among similarly charged solutes will further magnify the effect of concentration.

For the most part, work on concentration effects on partitioning has been limited to spherical solutes of uniform size. In many situations, however, there may be important interactions among solutes which are not alike. The fractionation of blood plasma via ultrafiltration, for example, involves at least two classes of abundant proteins, serum albumin and immunoglobulins (Saksena and Zydney 1997). A second example involves the use of polydisperse macromolecular tracers to characterize the macromolecular permeability properties of kidney capillaries *in vivo* (Blouch et al. 1997) and *in vitro* (Bolton et al. 1998). In those experiments tracers of different sizes are accompanied by at least one abundant protein. Many other such situations can be imagined which involve mixtures of unlike particles, at least one of which is present at significant concentrations. While these experimental situations have been used before where concentration effects among unlike solutes presumably existed, the effect of a concentrated solute on the partitioning of a dissimilar molecule has never been directly measured by experiment. In addition to the effects of solute heterogeneity, many membrane materials may be composed of multiple types

of fibers, as opposed to just a single size. To our knowledge, the only theoretical treatment of solute partitioning where the effects of solute and fiber heterogeneity are included is the excluded volume theory from Chapter 2. In that theory, which is valid for steric interactions only, partition coefficients are calculated based on purely geometric arguments by summing up the volume excluded to a test solute in the membrane and in the bulk because of the presence of fibers and other solutes.

We measured the partition coefficients of BSA and four narrow fractions of Ficoll in agarose gels under dilute conditions and under conditions where BSA was present at concentrated levels. Measurements were made for two different solid volume fractions of agarose. The partition coefficients of both BSA and Ficoll increased with increased levels of BSA. Experimental results generally agreed very well with the predictions from the model, the agreement between the two being best for the highest solid volume fraction of agarose.

4.3 Methods

4.3.1 Materials. Agarose type VI (high gelling temperature), bovine serum albumin (fraction V), 5-(4,6-dichlorotriazin-2-yl]amino)fluorescein (DTAF), and 2,000 kDa fluorescein isothiocyanate dextran were purchased from Sigma (St. Louis, MO) and used without further purification. The BSA product chosen (Sigma catalog number A-2153) was the fraction V powder prepared via a modification of the Cohn method (Cohn et al., 1946). According to the manufacturer, this product has a minimum purity of 96% as measured by gel electrophoresis. All lots used in these experiments were at least 99% pure, according to the specification sheets on the individual lots obtained from the vendor. BSA solutions were prepared in PBS at concentrations ranging from 0.4 to 16 g/dL (mass of BSA to volume of buffer). The buffer used here and throughout, unless otherwise noted, was a 0.1 M PBS at pH 7.4. Trace sodium azide was used in all buffers as a bactericide. Four narrow fractions of Ficoll with Stokes radii r_s in the range of ~ 30 to 60 Å were obtained from Amersham-Pharmacia (Uppsala, Sweden) by special order. The Ficolls

were labeled using DTAF following the method of DeBelder and Grannath (1973). After the labelling reaction had been carried out, the Ficoll solutions were eluted through disposable 10 mL EconoPac 10DG desalting columns (Bio-Rad, Hercules, CA) with 1.0 M NaCl to remove bulk quantities of the free DTAF. The resulting mixture was then ultrafiltered with distilled, deionized water in a 200 mL ultrafiltration cell (model 8200, Amicon, Danvers, MA) using a 5 kDa molecular weight cutoff regenerated cellulose membrane (Millipore, Bedford, MA) in order to remove the remaining free DTAF. Successive ultrafiltrations were repeated until there was no detectable free fluorescein, as determined by size-exclusion chromatography. Ficoll samples were then freeze-dried and reserved at -20 °C until use. Ficoll solutions were prepared in PBS and used at a concentration of 0.5 mg/mL in all experiments. The molecular weights and r_s of each of the macromolecules used are summarized in Table 4-1.

4.3.2 Partition coefficient measurements. Agarose gels were prepared by mixing dry agarose powder with buffer at room temperature to create a finely dispersed slurry in glass vials with plastic screw tops. A correlation from Johnson et al. (1995) was used to create gels with a desired ϕ based on initial solid concentration in the slurry. [Henceforth, we shall refer to the value of ϕ as a percent for a given gel, so that a gel with $\phi = 0.04$ shall be referred to as a "4%" gel.] The vials containing the agarose slurry were placed in an oven at 90 °C to dissolve the powder. While heated in the oven, the vials were periodically shaken and rotated to create a homogeneous gel mixture. The gels were kept in the oven for four to six hours (longer times for higher mass concentrations of agarose) until all powder had dissolved and the gel was free of bubbles. Approximately 30 mL of gel was then poured into a disposable polystyrene petri dish. The dish was rotated to distribute the gel evenly along the surface of the dish, and a lid was placed on top of the dish and weighted down to minimize water vapor loss from the hot, solidifying gel. Some water vapor accumulated on the inside of the lid during gel solidification. By collecting and weighing this accumulated liquid for several samples, it was determined that this resulted in a negligible loss of water from the actual gel (i.e., the loss of water did not cause a significant change in the nominal solid volume fraction of the gel). The gels were allowed to solidify at room temperature for at least

solute	MW (Da)	Stokes radius, r_s (Å)
Ficoll, fraction 1	21, 300	29.7
Ficoll, fraction 2	37, 400	37.7
Ficoll, fraction 3	60, 700	46.4
Ficoll, fraction 4	93, 200	58.7
BSA	68, 000	36.0

Table 4-1: Molecular weights (MW) and Stokes radii (r_s) of test macromolecules.

3 hours after pouring and then either used in an experiment immediately or stored at 7 °C until later use.

To begin an experiment, the agarose gel was placed on a clear glass plate with a paper backing on which a 3 mm × 3 mm grid was printed. Using a clean razor blade and the grid as a guide, the gel was cut into pieces which were approximately 3 mm × 3 mm cross-sectionally. Measurements of several gel samples showed that the gels could be cast with a fairly uniform height. The maximum height of the gel measured was 2.3 mm, so that the largest gel "cube" contained in any sample would have dimensions of $3 \times 3 \times 2.3$ mm^3. The method used here for the preparation of the agarose gel cubes is similar to that used by Buck et al. (2001). A single partitioning experiment consisted of adding a known mass of gel and volume of equilibrating solution to an empty 20 mL glass vial; roughly equivalent volumes of gel and equilibrating solution (~5 mL for each) were used for each experiment. Four samples were prepared from each gel casting. For statistical analysis, the number of experiments run for a given condition n was taken as the number of vials prepared. The vials were stored in a dark refrigerator at 7 °C for sufficient time to ensure diffusional equilibration of the samples. Φ_{BSA} was measured using BSA solutions prepared at concentrations of 0.4, 4.0, 8.0, 12.0, and 16.0 g/dL. Φ_i was measured for each of the four narrow fractions using Ficoll solutions prepared at a concentration of 0.5 mg/mL both with and without 8 g/dL BSA added to the buffer.

Once the samples had equilibrated, the bulk solution was separated from the gel by decanting the solution into a separate vial. Φ_i was then calculated by applying a material balance of the form,

$$\Phi_i = \left(\frac{V_l}{V_g}\right)\left[\frac{C_i(0)}{C_i(\infty)} - 1\right] \qquad \textbf{[4-2]}$$

where V_l is the volume of the equilibrating solution, V_g is the volume of the gel, $C_i(0)$ is the concentration of i at the beginning of the equilibration, and $C_i(\infty)$ is the concentration of i at equilibrium. Gel masses were converted to volumes by dividing by gel densities ρ which were measured for the all combinations of ϕ and buffer ionic strength used. ρ was measured by casting gels between two glass plates separated by a plexiglass spacer. After the gels had solidified, circular plugs of known radius were cut from the gel sheet using a metal punch and then weighed. The height of the plugs, which was very uniform because the gels were cast between plates, was measured with a micrometer by placing the gel plugs between two glass microscope slides. The measured ρ values for the three different gel preparations used in these experiments are listed in Table 4-2.

C_{BSA} was assayed by measuring the absorbance of the equilibrated bulk solution and comparing it to a set of standards prepared via the dilution of the initial stock; absorbance measurements were made at 280 nm using a BioSpec 1601 spectrophotometer (Shimadzu, Columbia, MD). C_i for the four Ficolls was assayed by measuring the fluorescence of the equilibrated bulk solution and comparing it to a set of standards prepared via the dilution of the initial stock; fluorescence measurements were made with an excitation wavelength of 488 nm and a detection wavelength of 515 nm using an RF-551 spectrofluorometric analyzer (Shimadzu). For samples where both Ficoll and BSA were present, the background absorbance of the dilute Ficoll at 280 nm was negligible so that C_{BSA} could be reliably measured without interference from the Ficoll. Similarly, the background fluorescence of BSA was low enough that it could be neglected in assaying Ficoll concentrations.

The use of the material balance method employed here requires that the samples be completely equilibrated by the time the bathing solution is separated from the gel. In order to determine the time required for diffusional equilibration to occur, a set of measurements of the apparent partition coefficient as a function of contact time with the equilibrating solution were taken. An extensive set of experiments including some 10 discrete time points was performed for BSA and 4% agarose. Measurements were taken at four different times for BSA and 6% agarose. The

ϕ	buffer ionic strength (M)	ρ (g/cm^3)
0.04	0.1	1.084 ± 0.007
0.04	1.0	1.142 ± 0.012
0.06	0.1	1.095 ± 0.008

Table 4-2: Gel densities (ρ) for all combinations of gel solid volume fraction (ϕ) and buffer used. Values are shown as mean ± s.d., with n = 16 for all conditions.

results of those experiments are plotted in Fig. 4-1. Based on the data for BSA equilibration with 4 and 6% gels, we chose equilibration times of 24 and 48 hr, respectively. A preliminary set of experiments with Ficoll and 4% and 6% gels suggested minimum equilibration times of 48 and 72 hr, respectively. Although the smallest Ficolls should equilibrate approximately as quickly as BSA, all Ficoll samples were equilibrated for the same amount of time for a given ϕ. In addition to the two experimental curves for BSA shown in Fig. 4-1, two theoretical curves are shown for the apparent Φ_{BSA} in 4% and 6% agarose gels. These curves were generated by solving the solute concentration profiles within an agarose cube of dimensions $3 \times 3 \times 2.3$ mm^3 as a function of time $\overline{C}_i(x,y,z,t)$ by employing a finite Fourier transform (FFT) method (Deen 1998), which is similar to the method of separation of variables. In generating the solution for $\overline{C}_i(x,y,z,t)$ we assumed a well-stirred bulk solution of infinite volume. Although the vials were not stirred continuously during equilibration, the well-stirred approximation is not without some basis since the relevant liquid and solid length scales are of the same order of magnitude and macromolecular diffusion within the gel is slower than in the bulk. The assumption of an infinite solution volume simplifies the solution greatly as it uncouples the solid and liquid phase concentration fields. The coupled problem can be solved relatively easily for a one-dimensional case, however the coupled solution in three dimensions is extremely computationally intensive. Comparisons between a coupled and uncoupled solution for a one-dimensional solid, however, suggest that the uncoupled solution should provide a more conservative estimate of equilibration times. The FFT solution was generated by placing the origin of a Cartesian coordinate system at one corner of an agarose cube. The lengths of the agarose prism in the x, y, and z directions were defined as a, b, and c, respectively. The solution for $\overline{C}_i(x,y,z,t)$ is given by

$$\overline{C}_i(x,y,z,t) = \Phi C_i(0)\left[1 - \frac{64}{\pi^3}\sum_{n=1}^{\infty}\sum_{m=1}^{\infty}\sum_{l=1}^{\infty}\frac{\exp\left(-\kappa\pi^2\frac{tD_i}{a^2}\right)}{nml}\sin\left(n\pi\frac{x}{a}\right)\sin\left(m\pi\frac{y}{b}\right)\sin\left(l\pi\frac{z}{c}\right)\right] \qquad \textbf{[4-3]}$$

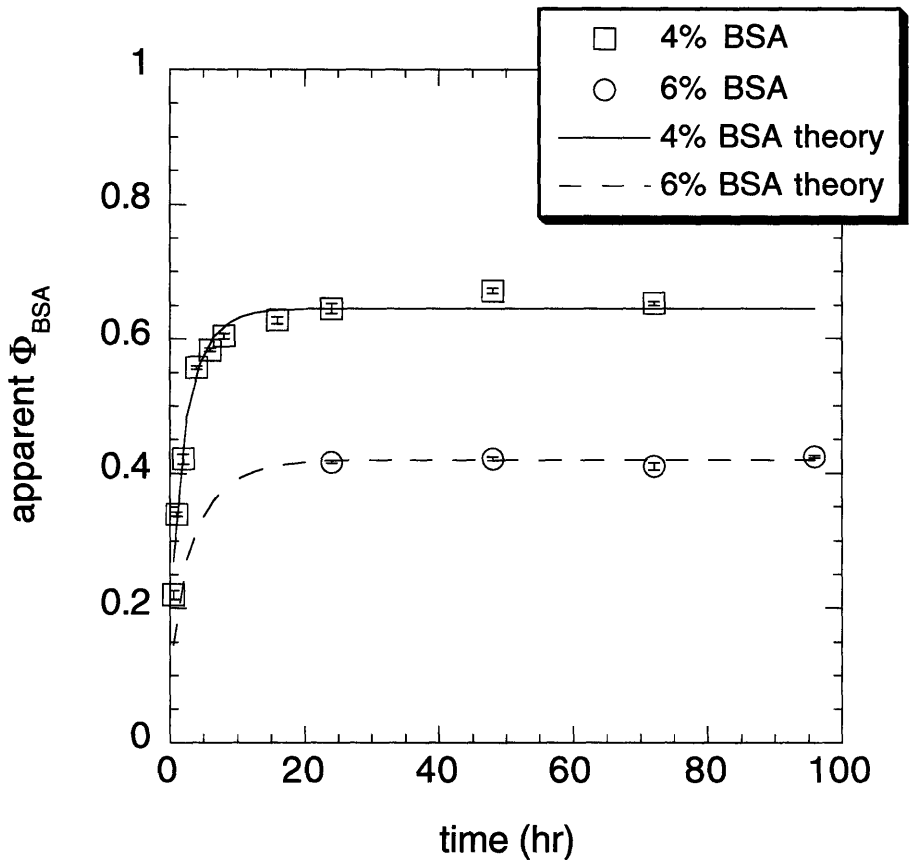

Figure 4-1: Apparent Φ_{BSA} versus time for 4% and 6% agarose gels. Experimental results are shown as mean ± s.e., with $n = 4$ for each point. Theoretical results were generated from the FFT model for an agarose "cube" of dimensions $3 \times 3 \times 2.3$ mm^3.

where D_i is the solute diffusivity within the gel, and κ is

$$\kappa = \left(n^2 + \frac{a^2}{b^2} m^2 + \frac{a^2}{c^2} l^2 \right) \qquad \textbf{[4-4]}$$

Note that $C_i(0)$ is treated as a constant in the FFT calculations because of the assumption of an infinite solution volume. Although not shown in the figure, theoretical equilibration curves were generated for the 58.7 Å Ficoll as well. Values of D_i for BSA and Ficolls in agarose gels at 20 °C measured by fluorescence recovery after photobleaching are available from the studies of Johnson et al. (1996). These values were corrected to 7 °C and used in the FFT model. The values of D_{BSA} used for 4% and 6% gels were 2.20×10^{-7} cm^2/s and 1.40×10^{-7} cm^2/s, respectively. The values of D_i for the 58.7 Å Ficoll in 4% and 6% gels were 0.87×10^{-7} cm^2/s and 0.58×10^{-7} cm^2/s, respectively. In making the calculations, Φ_i was set equal to the experimentally observed value at each condition. This should not affect the computed approach to equilibrium as the characteristic time for diffusion within a medium is influenced only by the macromolecular diffusivity in that medium and the relevant length scales, not by the value of Φ_i. In order to calculate the apparent Φ_i as a function of time from the FFT model, $\overline{C}_i(x,y,z,t)$ was averaged over the volume of an agarose cube via numerical integration at discrete time points. The theoretical predictions for BSA equilibration agree well with the data, despite the assumptions made in the theory. The equilibration times τ used in the experiments and the predictions from theory are reported in Table 4-3. The theoretical values for τ reported are those times when the predicted apparent Φ_i reached 99% of the observed, equilibrated value.

In order to check for the influence of electrostatic interactions on the partitioning measurements, a subset of the 4% agarose experiments were repeated using gels and solutions prepared with a 1.0 M PBS at pH 7.4. Measurements were made with BSA at nominal BSA concentrations of 0.4, 8.0 and 16.0 g/dL, and with the 46.4 Å Ficoll with and without 8 g/dL BSA.

solute	ϕ	τ, experiment (hr)	τ, theory (hr)
BSA	0.04	24	12
	0.06	48	20
Ficoll, r_s = 58.7 Å	0.04	48	31
	0.06	96	47

Table 4-3: Equilibration times (τ) used experimentally and determined theoretically for BSA and 58.7 Å Ficoll with gel solid volume fractions (ϕ) of 0.04 and 0.06.

4.3.3 Other methodological considerations. *4.3.3.1 Agarose gel stability over time.* After a three-hour solidification at room temperature, gels were either used immediately or stored at 7 °C for later use. In order to assess the time for which gels could be stored prior to use in an experiment without drying out or changing in some other way, a series of dilute Φ_{BSA} measurements was made with gels which were stored at 7 °C between one and seven days prior to use in an experiment. The experiments were done using a $C_{BSA}(0) = 0.4$ g/dL and 4% agarose gels, and all samples were equilibrated for 24 hr. Measurements were taken for gels stored for 1, 3, 5, and 7 days, in addition to a data set taken using gel which was used immediately after a 3 hr solidification at room temperature. The measured Φ_{BSA} as a function of gel storage time is plotted in Fig. 4-2. The results suggest that gels can be stored for up to one week without any detectable change in partitioning behavior. For all other experiments reported here, gels were used within four days of casting.

4.3.3.2 Gel swelling. Some hydrogels, such as polyacrylamide, are known to swell or shrink in solution. To determine if the volume of the agarose changed in solution, we measured the change in thickness h of pieces of gel equilibrated with pure buffer or12 g/dL BSA. Gels were cast between glass plates to create a uniform thickness and then cut into rectangular strips. The initial thickness h_i of a gel strip was measured with a micrometer by placing it between glass microslides. Single strips, each weighing approximately 1 g, were then equilibrated with 5 mL of solution. 4% gels were equilibrated for 24 hr, and 6% gels for 48 hr. After equilibration, the gels were removed from solution, blotted dry, and h was measured again between glass microslides. The fractional change in thickness of the gel strips $\Delta h/h_i$ is reported for the various conditions in Table 4-4. The largest $\Delta h/h_i$ was 1% for the 6% gel and 12 g/dL BSA. If gel cubes swell by 1% on all sides, the gel volume would increase by 3%. Combined with the concamitant 3% reduction in solution volume, this swelling would result in a 6% reduction in the calculated Φ_i. This would be slightly offset by a reduction in the actual ϕ due to swelling. Since we we observed $\Delta h/h_i$ values $\leq 1\%$, we concluded that it would be acceptable to calculate the equilibrated gel volume based on the initial mass of gel.

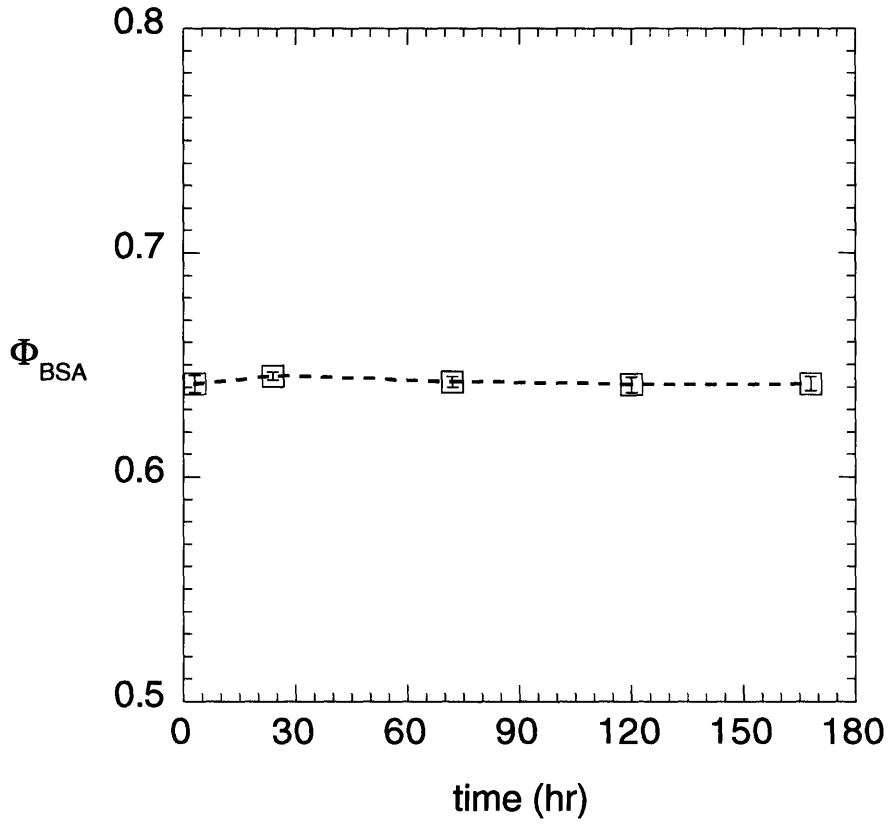

Figure 4-2: BSA partition coefficient (Φ_{BSA}) measured in 4% gels using 0.4 g/dL BSA solutions for gels which were used immediately after a three hr casting or which were first stored at 7 °C between one and seven days. All samples were equilibrated for 24 hr. Data are shown as mean ± s.e., with $n = 4$ for all measurements.

ϕ	equilibrating solution	$\Delta h/h_i$
0.04	pure buffer	0.0009 ± 0.0065
0.04	12 g/dL BSA	0.0037 ± 0.0112
0.06	pure buffer	0.0082 ± 0.0047
0.06	12 g/dL BSA	0.0108 ± 0.0069

Table 4-4: Fractional change in gel thickness ($\Delta h/h_i$) for 4% and 6% agarose equilibrated with pure buffer or 12 g/dL BSA. Values are shown as mean ± s.d., with $n = 6$ for all conditions.

4.3.3.3 Background signals from gel. The use of the mass balance technique assumes that, aside from the protein or Ficoll, there is no source of light absorbing or fluorescing material in the equilibrating solution. To test this assumption, we equilibrated cubes of 4% and 6% agarose with buffer alone and measured the absorbance of the equilibrated solution. 4% gels were equilibrated for 24 hr, and 6% gels for 48 hr. Surprisingly, a significant background signal, ~5% of the typical absorption read in a partitioning experiment, was generated by the agarose when equilibrated with buffer. The level of the background signal roughly doubled going from 4% to 6% gel, which is a good indication that the agarose was the source of the signal. The background signal would only have a significant effect on the calculation of Φ_{BSA} for the dilute samples, for which no dilution is necessary prior to protein assay. The most severe case would be that of dilute BSA and 6% gels, where the background signal would lower the apparent partition coefficient by approximately 20%. Prior to analysis, BSA samples at concentrations of 4 g/dL and higher are diluted by a factor sufficiently high to guarantee that the background signal does not interfere with the measurement. That the source of the background signal was in fact the agarose was further confirmed by casting gels between glass plates instead of in the plastic dishes and by checking the absorbance of buffer after contacting it with all other disposable materials used in the experiments. Short-term equilibration studies on the order of 5 min generated equivalent levels of signal, suggesting that the material generating the signal was present only on the surface of the gels. Additional studies showed that samples of 4% agarose which were pre-soaked in excess buffer for 24 hr at 7 °C and subsequently equilibrated with fresh buffer as in a partitioning experiment did not generate any significant level of background signal. Experiments with 4% and 6% gels which were pre-soaked in this way and then used in a dilute BSA experiment resulted in measured values of Φ_{BSA} which were higher than as measured previously without pre-soaking; in fact, they were within 6% of the values calculated by correcting for the average background signal in a dilute experiment using unwashed gels. This suggests that the diffusible material which generated the background signal does not affect the partitioning of the test molecules within the system. A summary of these Φ_{BSA} results for 4% and 6% washed and unwashed gels can be found in Table 4-5.

ϕ	Φ_{BSA}, unwashed	Φ_{BSA}, corrected	Φ_{BSA}, washed
0.04	0.648 ± 0.002	0.713 ± 0.003	0.675 ± 0.004
0.06	0.419 ± 0.002	0.507 ± 0.003	0.507 ± 0.008

Table 4-5: Comparisons of BSA partition coefficients (Φ_{BSA}) in washed and unwashed agarose gels with solid volume fractions (ϕ) of 0.04 and 0.06. Data are also given for Φ_{BSA} values calculated by correcting for the average background signal measured at each ϕ. Values are shown as mean ± s.e., with $n = 32$ for the unwashed and corrected $\phi = 0.04$ values, $n = 36$ for the unwashed and corrected $\phi = 0.06$ values, and $n = 4$ for the washed $\phi = 0.04$ and 0.06 values.

4.3.3.4 Stability of BSA absorbance as a function of time. Over time and under the appropriate conditions, proteins can denature and/or aglomerate. In order to assess the extent to which the BSA absorbance may change in solution during the course of an equilibration experiment as a result of these or other phenomena, the absorbances of samples of 2 g/dL BSA prepared in PBS were tracked over a seven day period. 5 mL aliquots of BSA were placed in 20 mL glass vials and either (1) placed on an orbital shaker at room temperature, (2) stored at room temperature unshaken, or (3) stored in a refrigerator at 7 °C. Four such samples were prepared for each condition, and the absorbances of the samples and that of a freshly prepared BSA solution were measured at 280 nm using a spectrophotometer at 48 hr intervals for up to seven days. The absorbances of the samples relative to that of a freshly prepared solution are plotted for the three conditions in Fig. 4-3. The data show that the relative absorbances of solutions stored at 25 °C, whether shaken or not, increased steadily with time whereas that of solutions stored at 7 °C did not change. After the second day, the protein solutions which were kept at 25 °C became increasingly turbid by visual inspection; those kept at 7 °C remained clear.

4.3.3.5 BSA oligomerization. BSA is well-known to oligomerize in solution via the formation of disulfide bonds formed between cysteine residues on adjacent BSA monomers (Peters 1985). In order to quantify the amounts of BSA oligomers which may have been present in our samples and to look for the presence of impurities, several samples of BSA were chromatographed on a size exclusion chromatography column packed with Superdex 200 prep grade gel (Amersham-Pharmacia, Uppsala, Sweden). The eluent, 0.1 M PBS at pH 7.4, was supplied by a constant flow rate, high precision pump (P-500, Amersham-Pharmacia) at a rate of 1.5 mL/min. The column was calibrated using the four narrow fractions of Ficoll and a fluorescently labelled 2,000 kDa dextran. Based on the Ficoll and dextran standards, r_s correlated with elution time t as $r_s = \exp(6.05 - 0.046t)$. When running samples of BSA, the column was run in-line with a spectrophotometer (BioSpec 1601, Shimadzu) set to measure absorbance at 280 nm. Samples of 0.4 g/dL BSA were prepared in PBS and chromatographed immediately. A smaller set of samples were stored at 7 °C between 2 and 4 days prior to chromatography. A represntative BSA chromatogram is shown in

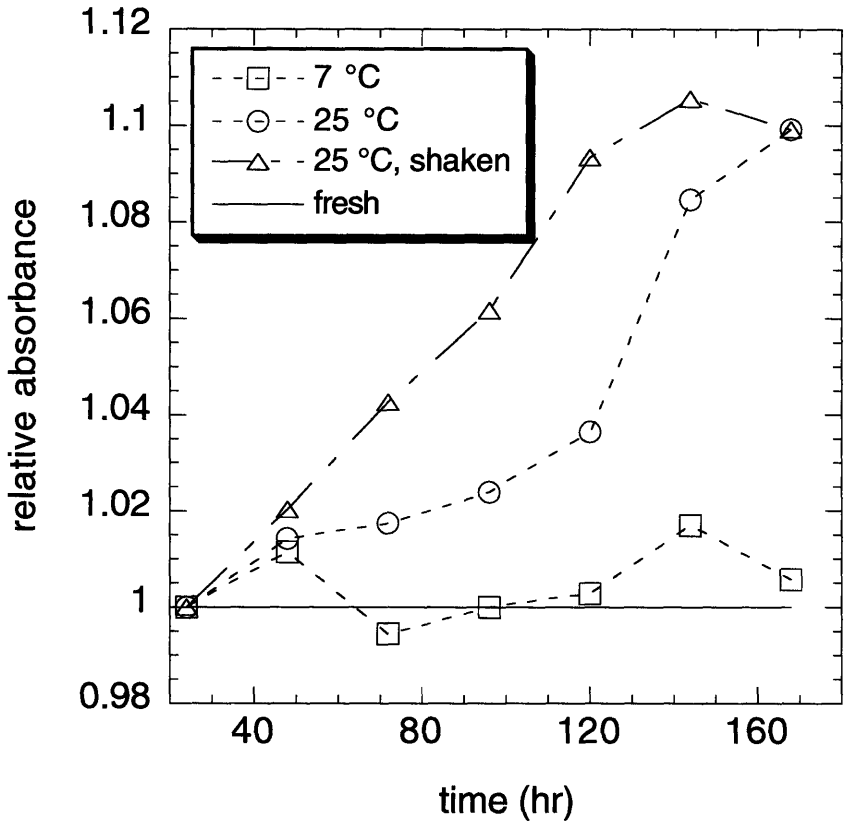

Figure 4-3: Absorbance of 2 g/dL BSA stored between one and seven days relative to the absorbance of a freshly prepared BSA solution. Samples were stored at 7 °C, 25 °C, or 25 °C on an orbital shaker.

Fig. 4-4. Each of the BSA samples had a large, secondary peak which eluted at an r_s = 36 Å, preceded by a small leading peak at r_s = 49 Å. The r_s of the second peak is in close agreement with the rs = 49 Å reported for dimeric by Squire et al. (1968). Low molecular weight impurities were not detected in any sample. To quantify the mass fraction of the dimeric BSA present, we numerically integrated the chromatograms, assigning the local minimum between the two peaks as the cutoff between dimeric and monomeric BSA. Assuming that the absorbance of dimeric BSA is twice that of monomeric BSA, the maximum dimer mass fraction found in any sample was 0.1. This mass fraction of dimer is within the range of values cited previously (Peters 1985). Samples stored for up to four days showed equivalent dimer levels.

4.3.4 Partitioning modeling. The excluded volume theory from Chapter 2 was used to generate predictions for BSA and Ficoll partition coefficients in agarose. In that model, partition coefficients are calculated by summing the volumes excluded to a solute in the membrane and bulk phases due to the fixed structures of the membrane and other solute molecules which may be present. Long-range forces among solutes and between the membrane and solutes are ignored, limiting this method to media where steric interactions dominate and the effects of electric charge are negligible. Although agarose is essentially uncharged, BSA is net negative at physiological pH. Ficoll is uncharged, however the fluorescein conjugate may impart a slight degree of negative charge to those molecules. As will be seen in the results section, the data from the experiments performed at 1.0 M suggest that any electrostatic interactions were effectively screened, so that the assumption of steric interactions only should be valid for the experimental conditions used here.

The application of the excluded volume models to generate predictions for the various Φ_i in agarose requires the specification of a set of physical parameters for the solutes and the gel. While BSA is well-represented hydrodynamically as a sphere of 36 Å radius, its actual structure is more cigar-shaped than spherical (Chapter 2). For this reason, BSA was treated as a prolate spheroid with an axial ratio of 3.3 and major and minor semiaxes of 70 and 21 Å. This model is most consistent with its partial specific volume (Al-Malah et al. 1995), intrinsic viscosity (Tanford 1961), and r_s (Johnson et al. 1995; Lazzara et al. 2000). Ficoll is often used as an ideal tracer in

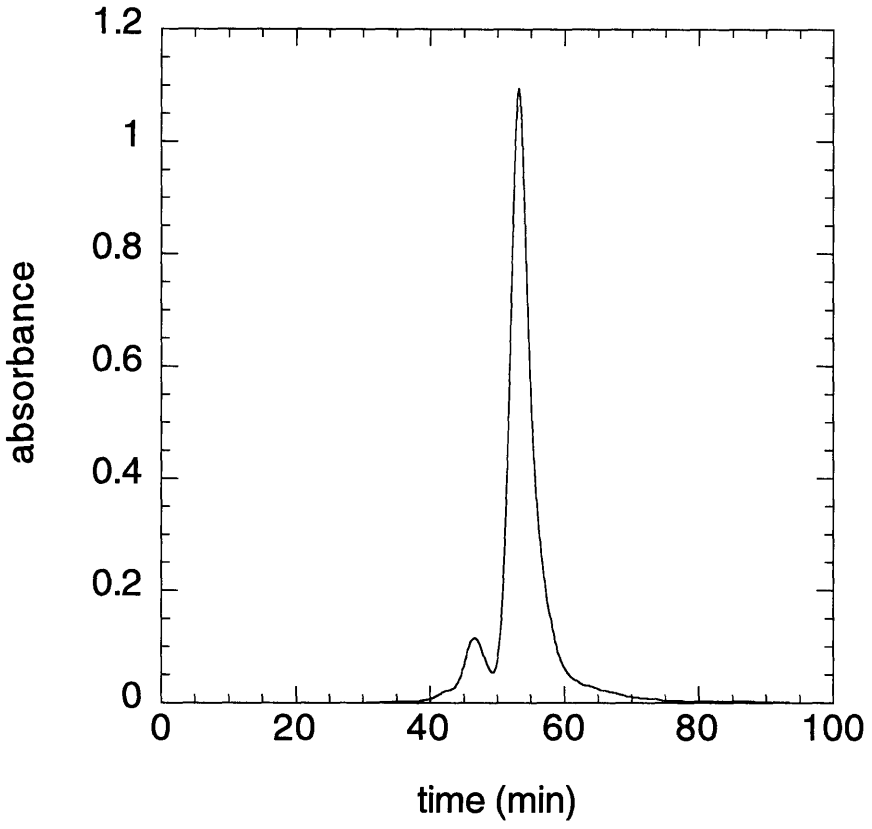

Figure 4-4: Representative size exclusion chromatogram of BSA The second, larger peak corresponds to an r_s = 36 Å, equivalent to the known r_s of monomeric BSA. The smaller leading peak corresponds to an r_s = 49 Å, which is close to a value of r_s = 47 Å for dimeric BSA cited by Squire et al. (1968).

sieving studies because its actual structure is very nearly spherical (Bohrer et al. 1984; Davidson and Deen 1988). Accordingly, the Ficolls were treated as spheres with radii equal to their respective Stokes radii. There is considerable variation in previously reported values of agarose fiber radius r_f. Since the predicted Φ_i is sensitive to the value of the fiber radius, r_f was estimated by fitting the model to the dilute partitioning data shown in Figs. 4-7 and 4-8. Fits were performed by assuming a uniform population of fibers and setting $\chi_1 = \chi_2 = 0$ in Eq. [4-5] and [4-6]. The best-fit values for 4 and 6% gels were 16.0 and 16.8 Å, respectively. Thus, model results are based upon an agarose fiber radius of 16.4 Å. The natural input parameter for modeling solute concentration effects using the excluded volume theory is the bulk solute volume fraction χ_i, rather than the concentration. For the purpose of comparing the experimental results with those from theory, calculations of χ_i were based on the known molecular weights and sizes of each solute.

The model generates a coupled set of nonlinear algebraic equations for the partition coefficients, one for each solute present. A good example of the calculations made here is for the case of a two-solute system, consisting of BSA and Ficoll, partitioning into agarose. In the equations which follow, the solute indices 1 and 2 refer to Ficoll and BSA, respectively; there is a single index 1 for the fibers present in agarose. Using the notation from Chapter 2, the expressions for the partition coefficients are

$$\Phi_1 = \exp\left[-\phi_1\alpha_{11}(s,f) + \alpha_{11}(s,s)(1-\Phi_1)\chi_1 + \alpha_{12}(s,p)(1-\Phi_2)\chi_2\right] \qquad \textbf{[4-5]}$$

$$\Phi_2 = \exp\left[-\phi_1\alpha_{21}(p,f) + \alpha_{21}(p,s)(1-\Phi_1)\chi_1 + \alpha_{22}(p,p)(1-\Phi_2)\chi_2\right] \qquad \textbf{[4-6]}$$

The quantities $\alpha_{ij}(x,y)$ are dimensionless geometric parameters that describe the interaction of a test solute i of shape x with a set of objects j of shape y (s = sphere, p = prolate spheroid, f = fiber). For example, $\alpha_{11}(s,s)$ describes the steric interaction between two spheres of type 1. For spheres of radius r_i and r_j, the excluded volume parameter is

$$\alpha_{ij}(s,s) = \left(1 + \frac{r_i}{r_j}\right)^3 \qquad \textbf{[4-7]}$$

Expressions for the remaining $\alpha_{ij}(x,y)$ parameters can be found in Chapter 2. Once those parameters were specified, Eqs. [4-5] and [4-6] were solved using Newton-Raphson iteration with the dilute solution values for the partition coefficients as initial guesses. Most of the other systems considered here may be viewed as special cases of Eqs. [4-5] and [4-6], obtained by setting certain values equal to zero. The dilute solution values of the partition coefficients were found by setting $\chi_j = 0$ for all j. Results for BSA alone were found by dropping Eq. [4-5] and setting $\chi_1 = 0$. A more complex set of equations, incorporating a third solute, was used to model the effect of BSA dimer on BSA and Ficoll partitioning. Those calculations, where the dimer was treated as a sphere with a radius of 47 Å, suggested that the dimer would have a very small effect on the partitioning of BSA and Ficoll in agarose of either ϕ. For that reason, BSA was treated as pure monomer for all model predictions presented hereafter. For details on the general application of the excluded volume theory to arbitrarily complex systems, see the complete model development section in Chapter 2.

4.4 Results

Experimental and theoretical results for Φ_{BSA} as a function of χ_{BSA} in 4% agarose are shown in Fig. 4-5. The most dilute data shown ($\chi_{BSA} = 0.003$) are the results from the washed gel experiment. All other data were obtained using gels prepared as usual. As expected, Φ_{BSA} increased with increasing χ_{BSA}, the most concentrated result being 30% higher than the value measured under dilute conditions. The model does a fairly good job of predicting increases in Φ_{BSA} with increasing χ_{BSA}, though there is an increasing disparity between model results and experimental data for increasing χ_{BSA}. On average, the theory tended to underpredict the effect of BSA concentration in 4% agarose gels by 6%. As will be shown, the ability of the model to predict experimentally observed increases in Φ_{BSA} was better for 6% gels.

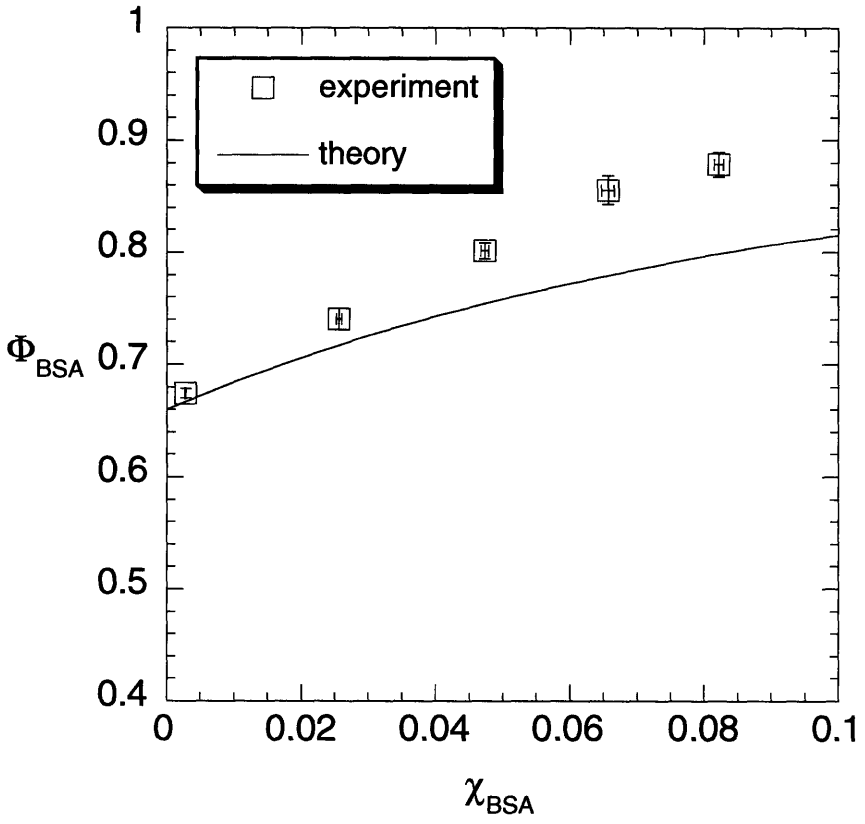

Figure 4-5: Comparison of experimental and theoretical results for BSA partition coefficient (Φ_{BSA}) versus bulk volume fraction of BSA (χ_{BSA}) in 4% agarose gels. The most dilute data point is taken from the experiments using a prewashed gel ($n = 4$). For all other points, $n = 8$, except the most concentrated point for which $n = 12$. Φ_{BSA} and χ_{BSA} values are shown as mean ± s.e.

Experimental and theoretical results for BSA partitioning in 6% gels are shown in Fig. 4-6. Again, Φ_{BSA} increased with increasing χ_{BSA}. For the 6% gels, the agreement between experiment and theory was improved relative to 4% gels. Here, the model predictions agree closely with the experimental data over the entire range of χ_{BSA}. There was a very slight tendency of the theory to overestimate the experimental data, although the agreement between the two is remarkably good. On average, the model overpredicted the experimental data by 3%. The data contained in Figs. 4-5 and 4-6 can also be found listed in Tables 4-6 and 4-7, respectively.

Results for Ficoll partitioning in 4% agarose are shown in Fig. 4-7. As expected, the measured Φ_i for the narrow Ficoll fractions decreased with increasing r_s. The addition of 8 g/dL BSA to the equilibrating solution caused a statistically significant increase in the partitioning of all Ficolls. The greatest augmentation was observed for the 58.7 Å Ficoll, where BSA caused a 40% increase in the partitioning of that tracer. The good fit of the theory to the dilute data, which is expected since r_f was chosen by fitting the model to this data, indicates the validity of the random fiber matrix model for agarose gels. While predicting the correct order of magnitude of the experimentally observed increase in Ficoll partitioning, the theory tended to underestimate the observed increase by an average of 7%.

Results for Ficoll partitioning in 6% agarose are shown in Fig. 4-8. Again, as expected, the measured Φ_i for the narrow Ficoll fractions decreased with increasing r_s. As with 4% gels, the addition of 8 g/dL BSA caused a statistically significant increase in Ficoll partitioning at every r_s. Again, the greatest augmentation in Ficoll partitioning was observed for the 58.7 Å fraction, where BSA caused a 67% increase in the partitioning of that tracer. As with BSA and 6% gel, there was excellent agreement between both the dilute Ficoll measurements and those taken with 8 g/dL BSA in the initial equilibrating solution. The Ficoll data shown in Figs. 4-7 and 4-8 are listed in Tables 4-8 and 4-9, respectively.

Results from the 1.0 M BSA and Ficoll partitioning experiments in 4% are shown in Table 4-10. The close agreement between the Φ_i values for BSA and Ficoll at the two ionic strengths for the most dilute solutions, where solute-agarose interactions predominate, suggests electrostatic

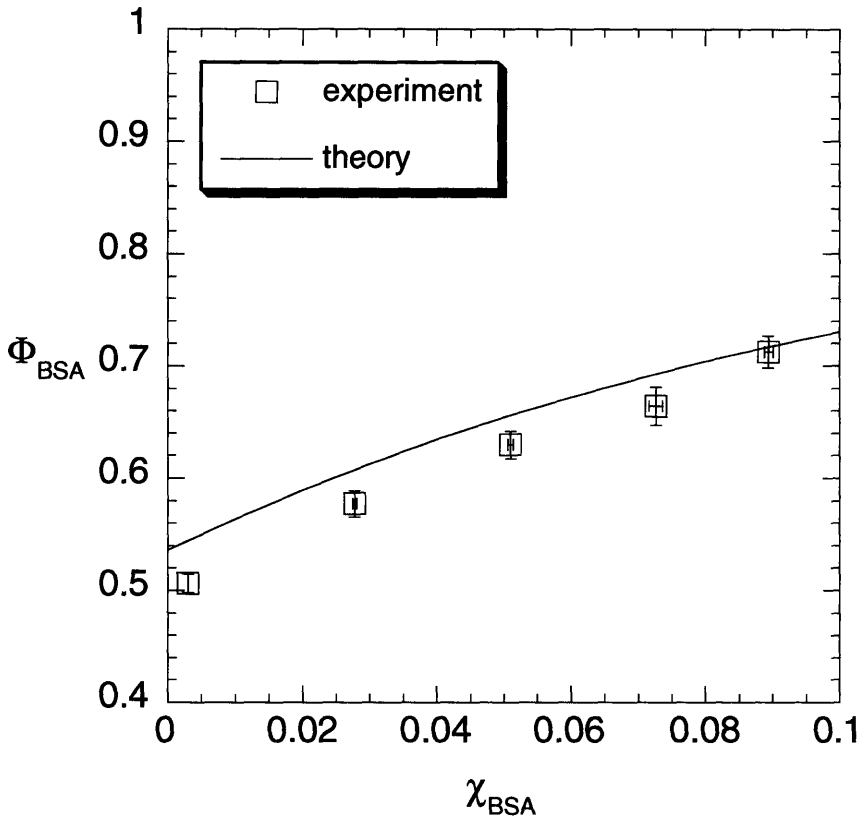

Figure 4-6: Comparison of experimental and theoretical results for BSA partition coefficient (Φ_{BSA}) versus bulk volume fraction of BSA (χ_{BSA}) in 6% agarose gels. The most dilute data point is taken from the experiments using a prewashed gel ($n = 4$). For all other points, $n = 8$. Φ_{BSA} and χ_{BSA} values are shown as mean ± s.e.

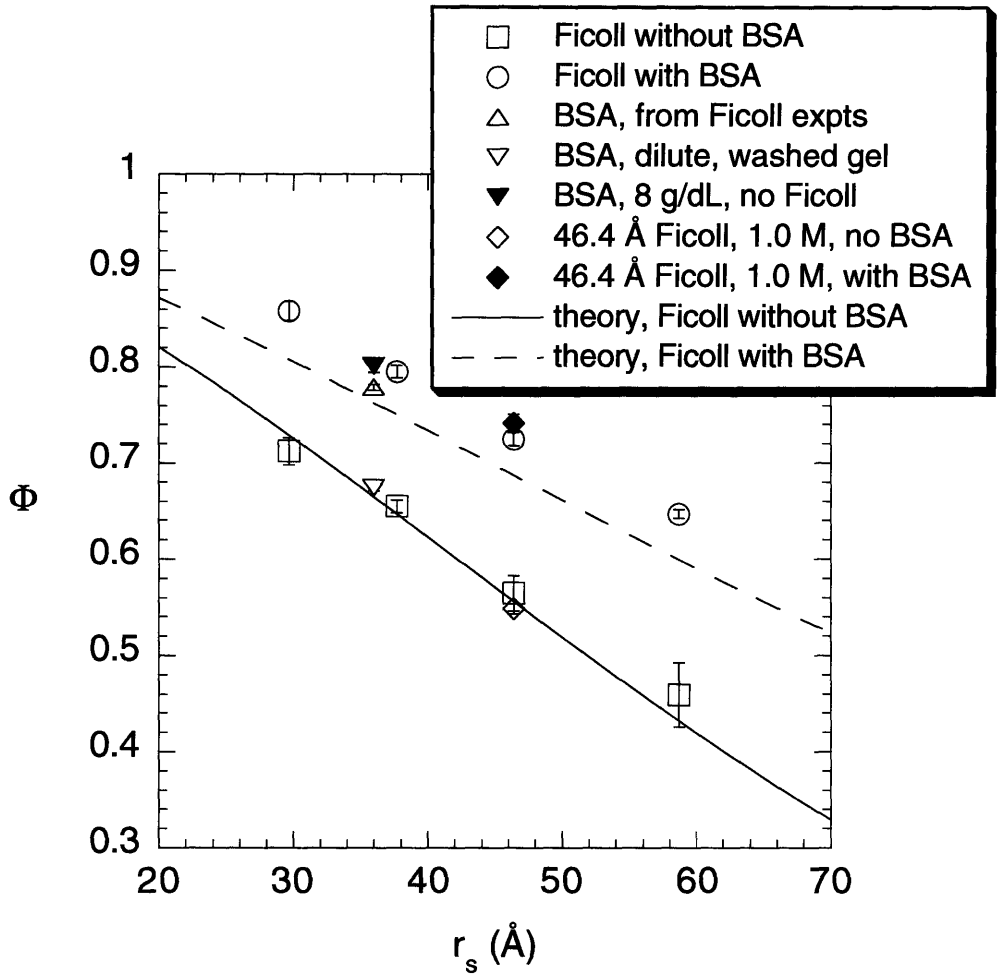

Figure 4-7: Comparison of experimental and theoretical results for partition coefficients (Φ_i) of Ficolls in 4% agarose. Values are shown as mean ± s.e., with $n = 8$ for all Ficoll data, $n = 16$ for BSA points from Ficoll experiments, and $n = 8$ for BSA points from experiments with BSA alone.

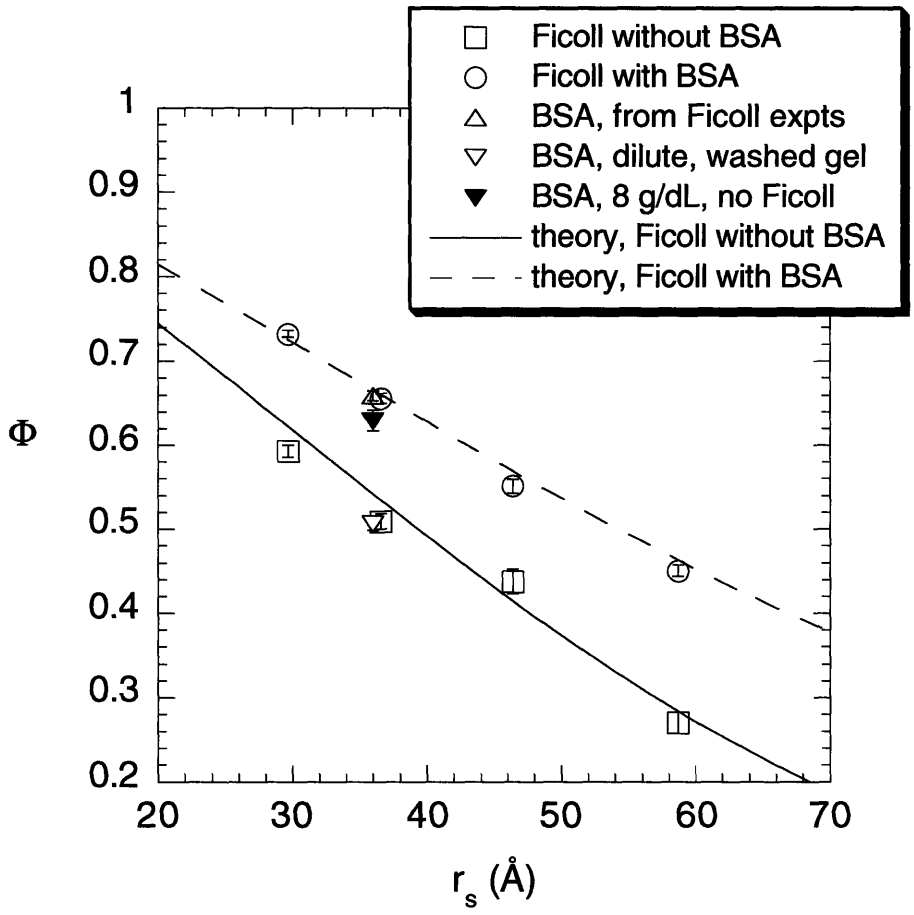

Figure 4-8: Comparison of experimental and theoretical results for partition coefficients (Φ_i) of Ficolls in 6% agarose. Values are shown as mean ± s.e., with $n = 8$ for all Ficoll data, $n = 16$ for BSA points from Ficoll experiments, and $n = 8$ for BSA points from experiments with BSA alone.

$C_{BSA}(0)$ (g/dL)	χ_{BSA}	Φ_{BSA}	n
0.4	0.003 ± 0.00004	0.675 ± 0.004	4
4	0.026 ± 0.0004	0.741 ± 0.010	8
8	0.047 ± 0.0006	0.801 ± 0.007	8
12	0.066 ± 0.0010	0.856 ± 0.013	8
16	0.082 ± 0.0007	0.878 ± 0.011	12

Table 4-6: BSA partition coefficients (Φ_{BSA}) in 4% agarose for nominal BSA concentrations ($C_{BSA}(0)$) from 0.4 to 16.0 g/dL. Values of BSA volume fraction (χ_{BSA}) and $_{BSA}$ are shown as mean ± s.e.

$C_{BSA}(0)$ (g/dL)	χ_{BSA}	Φ_{BSA}	n
0.4	0.003 ± 0.00004	0.507 ± 0.008	4
4	0.028 ± 0.0003	0.577 ± 0.011	8
8	0.051 ± 0.0004	0.630 ± 0.012	8
12	0.073 ± 0.0010	0.664 ± 0.017	8
16	0.089 ± 0.0006	0.713 ± 0.0006	8

Table 4-7: BSA partition coefficients (Φ_{BSA}) in 6% agarose for nominal BSA concentrations ($C_{BSA}(0)$) from 0.4 to 16.0 g/dL. Values of BSA volume fraction (χ_{BSA}) and Φ_{BSA} are shown as mean ± s.e.

r_s (Å)	Φ_i, Ficoll only	Φ_i, with 8 g/dL BSA
29.7	0.712 ± 0.014	0.859 ± 0.010
37.7	0.655 ± 0.007	0.795 ± 0.006
46.4	0.564 ± 0.018	0.725 ± 0.007
58.7	0.459 ± 0.034	0.647 ± 0.005

Table 4-8: Ficoll partition coefficients (Φ_i) in 4% agarose for samples with dilute Ficoll only and with 8 g/dL BSA. Values are shown as mean ± s.e., with n =8 for all conditions.

r_s (Å)	Φ_i, Ficoll only	Φ_i, with 8 g/dL BSA
29.7	0.593 ± 0.007	0.732 ± 0.004
37.7	0.509 ± 0.009	0.656 ± 0.006
46.4	0.437 ± 0.015	0.551 ± 0.008
58.7	0.270 ± 0.013	0.451 ± 0.007

Table 4-9: Ficoll partition coefficients (Φ_i) in 6% agarose for samples with dilute Ficoll only and with 8 g/dL BSA. Values are shown as mean ± s.e., with n =8 for all conditions.

solute i	$C_i(0)$	Φ_i, 0.1 M	n	Φ_i, 1.0 M	n
BSA	0.4	0.648 ± 0.002	32	0.645 ± 0.004	8
BSA	8.0	0.801 ± 0.0006	8	0.795 ± 0.0002	8
BSA	16.0	0.878 ± 0.011	12	0.844 ± 0.011	8
Ficoll, 46.4 Å	0.05	0.564 ± 0.018	8	0.548 ± 0.005	4
Ficoll, 46.4 Å with 8 g/dL BSA	0.05	0.725 ± 0.007	8	0.742 ± 0.009	4

Table 4-10: Comparison of BSA and Ficoll partition coefficients (Φ_i) in 4% agarose at 0.1 and 1.0 M. Values are shown as mean ± s.e.

interactions between the test solutes and agarose do not influence the measurements. At intermediate values of C_{BSA} there is virtually no effect of electrostatic interactions on the value of Φ_{BSA}, while there may be a very slight effect for the most concentrated case of $C_{BSA}(0)$ = 16 g/dL. The difference between the measurements at that concentration was less than 5%, however, and the effect BSA-BSA electrostatic interactions was essentially negligible over the entire range of C_{BSA}. Furthermore, the data for Ficoll partitioning at 1.0 M with 8 g/dL BSA demonstrate the absence of significant electrostatic interactions between BSA and Ficoll at 0.1 M.

Shown also in Figs. 4-7 and 4-8 are the Φ_{BSA} values (r_s = 36 Å) measured for the Ficoll samples which contained 8 g/dL BSA. The BSA partitioning data for $C_{BSA}(0)$ = 0.4 and 8 g/dL shown previously in Figs. 4-5 and 4-6 are also included. For both the dilute and concentrated cases, the measured Φ_{BSA} values fall in line with the Ficoll curves, suggesting that the difference in shape between BSA and Ficoll is not a significant determinant of solute partitioning, at least for the systems used here. This small dependence on solute shape is captured by the excluded volume theory. For example, for 4% gel χ_{BSA} = 0.05, the theory predicts a Φ_{BSA} = 0.750 and a Φ_i for a 36 Å sphere of 0.761. Note also that the close agreement between the Φ_{BSA} values at 8 g/dL for experiments both with and without Ficoll confirms our expectation that the background absorbance of Ficoll had a negligible effect on the measured value of Φ_{BSA}.

4.5 Discussion

While the effect of solute concentration on macromolecular partitioning has been previously demonstrated experimentally for systems containing one type of solute, the effect of the concentration of one solute on the partitioning of a dissimilar macromolecule has not previously been shown. Here, in addition to the effect of protein concentration on protein partitioning, we have demonstrated that elevated levels of protein augment the partitioning of dilute tracers which may also be present in solution. The magnitude of the effect is dependent on the size of the tracer and is greatest for the largest tracer size. In addition to the novelty of the experimental findings, this work also demonstrates the applicability of the excluded volume model developed by Lazzara et al.

(2000) for multi-solute partitioning in fibrous media. That theory, which incorporates effects of solute concentration for spherical and spheroidal solutes as well as effects of fiber heterogeneity, produced predictions which agreed remarkably well with the experimental data. The agreement was best for the largest value of ϕ.

Experimentally, relatively little work has been done to demonstrate the effect of solute concentration on equilibrium partitioning, and until now work has only been done for single-solute systems. One of the earliest demonstrations of the effect was performed by Brannon and Anderson (1982) who showed that the partition coefficients of the proteins BSA and α-lactalbumin in controlled pore glass beads were both increasing functions of their respective bulk concentrations. More recent work by White and Deen (2001) demonstrated an increase in dextran partitioning in agarose gels with increasing dextran concentration. The closest set of experiments to those presented here is contained in a recent paper by Buck et al. (2001) where the partition coefficients of BSA and α-lactalbumin were measured as a function of their respective concentrations in agarose hydrogels with solid volume fractions in the range of 1 to 5%. The experiments were carried out in both 0.15 and 0.01 M KCl to investigate the effects of electrostatic interactions in the system. In addition to the experimental results presented in that paper, Buck et al. (2001) also developed a statistical mechanical model for the partitioning of spherical solutes in random fiber matrices. That model included first-order effects of concentration on solute partitioning as well as effects of charge interactions among solutes and between solutes and membrane fibers. They chose to present their results, both experimental and theoretical, in terms of a virial expansion for solute partitioning of the form

$$\Phi_i = \Phi_i^{(0)} + \alpha\chi_i \qquad \textbf{[4-8]}$$

where $\Phi_i^{(0)}$ is the value of the solute partition coefficient at infinite dilution and α is a parameter describing first order concentration effects on solute partitioning. A comparison between the

experimental and theoretical results for BSA partitioning from the work by Buck et al. (2001) and the present work is presented in Table 4-11. In order to make the closet possible comparisons with the results of Buck et al. (2001), we also reported values of $\Phi_{BSA}^{(0)}$ and α for the present results. For the experiments, we were instrumentally restricted to a lower limit of $C_{BSA}(0) = 0.4$ g/dL. Thus, we computed experimental values of $\Phi_{BSA}^{(0)}$ for 4 and 6% agarose by performing a linear data fit to the first three points in Figs. 4-5 and 4-6. Experimental values of α were generated from the same fits. Theoretical values of $\Phi_{BSA}^{(0)}$ can be readily generated from the model, whereas theoretical values of α were generated via a linear data fit between Φ_{BSA} values generated by the model at χ_{BSA} of 0 and 0.01.

Buck et al. (2001) were able to experimentally detect the influence of electrostatic interactions on both BSA-agarose and BSA-BSA interactions. In 5% gels, they found that $\Phi_{BSA}^{(0)}$ decreased with decreasing ionic strength. This trend is predicted by their theory, but significantly underestimated. In general, however, their experimental and theoretical values of $\Phi_{BSA}^{(0)}$ agree well. What is more relevant to our own work is the extreme difference in the effect of solute concentration they found between 0.01 and 0.15 M ionic strengths. While BSA concentration had very little effect on solute partitioning at 0.15 M, an effect was clearly present at 0.01 M where BSA-BSA repulsive interactions were apparently magnified. Again, this trend was captured by their theory, but significantly underestimated. Looking at the present results, one notices a favorable comparison between the experimentally and theoretically obtained values for both $\Phi_{BSA}^{(0)}$ and α. The extreme discrepancy between the values of α, both theoretical and experimental, found by Buck et al. (2001) and those found in the present work is puzzling. From an electrostatics standpoint, the Buck et al. (2001) experimental results at 0.15 M should be directly comparable to our own since we found no significant change in Φ_{BSA} between 0.1 and 1.0 M. While our results suggest that increases in BSA concentration have a significant effect on BSA partitioning under conditions where steric interactions dominate, the results of Buck et al. (2001) indicate a very weak effect.

Experimentally, this disparity might be explained by differences in protocol. Perhaps the most significant difference is that the experiments of Buck et al. (2001) were run at 25 °C in saline

	ϕ	$\Phi^{(0)}$, experiment	$\Phi^{(0)}$, theory	α, experiment	α, theory
Buck et al. (2001), 0.15 M KCl	0.04	0.58	0.62	0.38	0.22
	0.05	0.46	0.55	0.49	0.24
present results	0.04	0.67	0.65	2.86	2.48
	0.06	0.50	0.52	2.57	2.77

Table 4-11: Comparison of experimental and theoretical infinite dilution partition coefficients ($\Phi^{(0)}$) and α values for BSA from Buck et al. (2001) and the present results.

only, as opposed to buffered saline. Our own preliminary experiments suggested that the absorbances of even buffered BSA solutions stored at 25 °C changed over the course of a few days, whereas the absorbance of BSA in PBS stored at 7 °C did not. We also noticed by visual inspection that BSA solutions stored at 25 °C became turbid after a few days. It is unlikely that bacterial growth was responsible for this turbidity as sodium azide was used in all buffers as a bactericide. Our observations with BSA stored at 25 °C may have been the result of protein denaturation and/or agglomeration. This may have been a factor in the relatively large error bars reported by Buck et al. (2001) for their 0.15 M KCl data. This stands in contrast to their data for BSA partitioning at 0.01 M, however, where the error was much smaller and an effect of concentration was very pronounced. An additional indication of differences in the experimental methodology is their finding that their BSA samples did not equilibrate until 5 or 6 days after beginning an experiment. BSA was the largest solute used in their experiments, and 5% the most concentrated agarose gel. We found that 48 hr was more than sufficient to equilibrate BSA with 6% agarose. While their gels were poured to a height of 3 mm as opposed to the maximum of 2.3 mm for ours, the experiments were run at a higher temperature which will increase the diffusivity of the BSA. The FFT model we created, which compared favorably with our own equilibration data, suggests that 5% agarose cubes with dimensions of $3 \times 3 \times 3$ mm^3 should equilibrate with BSA within 11 hr. For that calculation, we used a value of $D_{BSA} = 3.051 \times 10^{-7}$ cm^2/s, which is the average of the values reported previously, temperature-corrected to 25 °C, for BSA in 4 and 6% gels.

A separate issue is the disparity between the values predicted for α by the theory of Buck et al. (2001) and the excluded volume model from Chapter 2. Here the potential sources of the difference between the two sets of results are less clear. While the excluded volume theory is fairly simple to implement, the statistical mechanical approach used by Buck et al. (2001) is much more complex, making a detailed comparison between the two theoretical approaches and their implementation impractical. In Chapter 2, comparisons were made between the excluded volume model predictions and those of two previously published theories which incorporated solute

concentration effects for uniform, uncharged, spherical solutes. Comparisons were made with the density functional theory results of Fanti and Glandt (1990a) for the case of infinitely thin fibers over a range of fiber densities. Since the excluded volume theory can also be applied to membranes composed of straight pores, the theory was also compared to theoretical results of Anderson and Brannon (1981) who employed a statistical mechanics approach. In that case, comparisons were made between the excluded volume theory and the predictions of Anderson and Brannon (1981) through the second order term. For the cases where direct comparisons could be made between excluded volume and these two other models, the excluded volume results were in quite good agreement with the results from the other two theories. While this favorable comparison does not necessarily guarantee the validity of the results presented in Chapter 2, it does lend them some credence.

As is the case with protein partitioning in agarose, there is relatively little data on Ficoll partitioning in agarose, or any other porous material for that matter. The only data available are those of Laurent (1967) who measured the partitioning of narrow fractions of Ficoll in agarose gel beads of various solid volume fractions by packing a column with the beads and eluting samples of the Ficoll through the columns. This method for measuring partition coefficients is based on the assumption that the macromolecule equilibrates almost instantaneously with the gel beads as it flows through the column (Laurent and Killander 1964). This assumption should be valid for small enough gel beads and slow enough flow rates. A comparison between our dilute Ficoll partitioning data for both 4 and 6% agarose and that of Laurent (1967) is shown in Fig. 4-9. In general the data compare well. Both sets seem to demonstrate a similar dependence of Φ_i on r_s. The 4% data of Laurent et al. (1967) fall slightly above our own, the data for 6% agarose agree almost exactly. This favorable comparison lends further credence to our experimental methodology and results, particularly those for Ficoll.

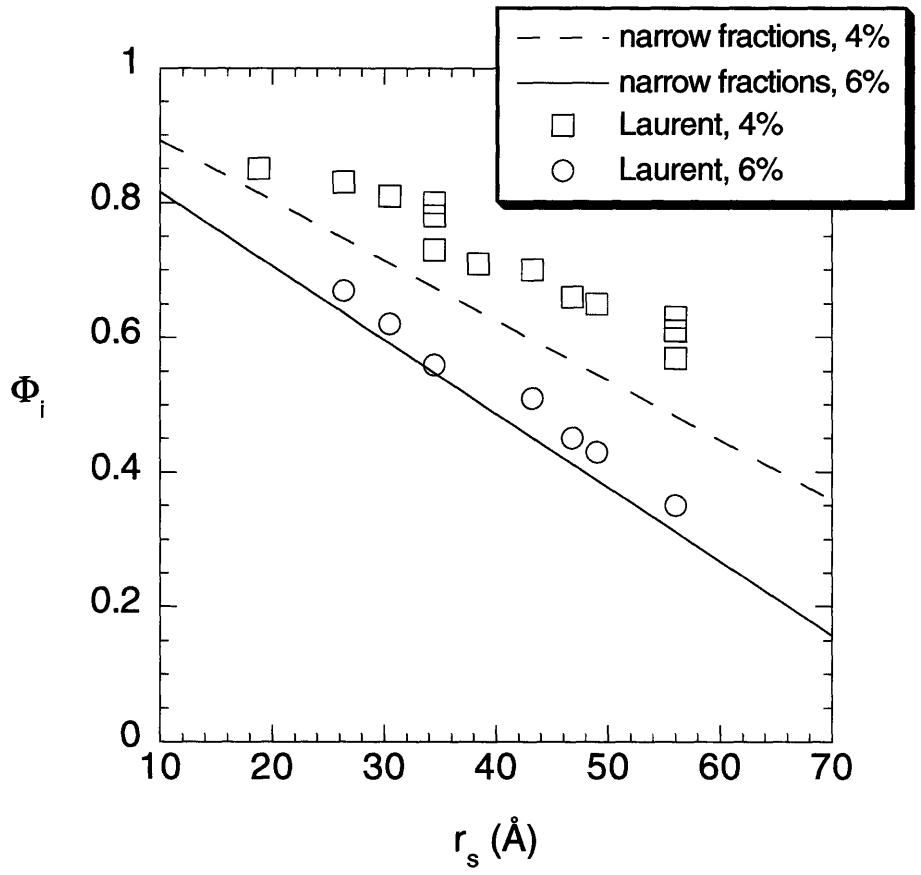

Figure 4-9: Comparison of dilute Ficoll partition coefficients (Φ_i) as a function of Stokes radius (r_s) in 4 and 6% agarose with data obtained by Laurent et al. (1967) using a chromatography method. The lines shown for the present, narrow fraction data are best fits to the four data points obtained at each agarose solid volume fraction.

4.6 Conclusions

We measured the partition coefficients of BSA and four narrow fractions of Ficoll in agarose gels at two different solid volume fractions. The experiments were done under dilute conditions and also with concentrated levels of BSA. The addition of concentrated BSA was found to increase the partition coefficient of BSA itself as well as the partition coefficients of each of the four Ficolls. This effect was most significant for the largest Ficoll. Comparisons were made between the experimental data and predictions made using the excluded volume theory developed in Chapter 2. In general, the predictions agreed well with the experimental data, the agreement being best for the highest solid volume fraction of agarose used. To our knowledge, this is the first experimental demonstration of an effect of solute concentration between dissimilar molecules. This work also demonstrates the applicability of the excluded volume partitioning model for protein and Ficoll partitioning in fibrous media such as agarose hydrogels.

Chapter 5

Summary and Future Work

5.1 Summary

The principal motivation for this work was the experimental observation by Bolton et al. (1998) that physiological concentrations of BSA increased the sieving coefficients of the tracers Ficoll and Ficoll sulfate across isolated GBM. The osmotic reduction in filtrate velocity caused by the concentrated, mostly retained BSA will tend to increase tracer sieving coefficients, but this effect alone explained only about one-third of the observed increase. It was suggested that the majority of the increase was the result of a steric effect of the concentrated protein on the partitioning of the dilute tracers. In order to test this hypothesis, we set out to investigate the effect of solute concentration on solute partitioning and sieving for systems of interest through a combined modeling and experimental effort. The specific objectives of this thesis work were: (1) to develop a partitioning theory for mixtures of rigid, spheroidal macromolecules of arbitrary concentration in porous and random-fiber media; (2) to extend the theoretical description of macromolecular sieving across single-layered membranes and the intact glomerular capillary wall to account for the presence of a second, abundant solute and reanalyze the isolated GBM sieving data of Bolton et al. (1998); and (3) to experimentally demonstrate the effect of solute

concentration for dissimilar solutes and to test the applicability of the newly developed partitioning model for random-fiber media.

At the time this work was begun, the dependence of colloidal partition coefficients on concentration had been demonstrated in a number of experimental and theoretical investigations. For systems where steric interactions predominate, the general trend observed was that the solute partition coefficient increased with increasing concentration (Anderson and Brannon 1981; Brannon and Anderson 1982; Fanti and Glandt 1990). A variety of approaches, including density functional theory and statistical mechanics approaches, had been used to model concentration effects for uniform, uncharged, spherical solutes in both random fiber matrices and straight pores (Anderson and Brannon 1981; Fanti and Glandt 1990). Prior to this work, however, it was not possible to predict the effect of concentration of one solute on the partitioning of a dissimilar solute. In many situations of interest, however, important interactions may exist among unlike solutes, as in the sieving experiments of Bolton et al. (1998). To address the multi-solute partitioning problem, we adopted an excluded volume approach, as described in Chapter 2. In that formulation, which is valid for steric interactions only, partition coefficients were computed by summing all volumes excluded to a solute molecule by virtue of its finite size, the finite size of other solutes, and the presence of fixed obstacles (pore walls or fibers). As shown in Chapter 2, results from the excluded volume theory reduce exactly to certain well-known expressions for the partition coefficients of dilute solutions of spheres (Ogston 1958; Pappenheimer et al. 1951). Results from the excluded volume theory were also found to be in reasonable agreement with previous results for the partitioning of concentrated solutions of uniform spheres (Anderson and Brannon 1981; Fanti and Glandt 1990). In addition to facilitating calculations for multiple solute sizes and/or shapes, the simplicity of the excluded volume formulation permits the incorporation of multiple fiber radii in models of fibrous media. Overall, the theory suggests that the introduction of heterogeneities, whether as mixtures of solute sizes or mixtures of fiber sizes, may cause partition coefficients to differ markedly from those of uniform systems.

Previous models of hindered transport through fibrous or porous media, and across the intact glomerular capillary wall, were limited to dilute solutions (Bolton et al. 1998; Deen 1987; Edwards et al. 1997; Edwards et al. 1999). In Chapter 3, we extended the sieving theory for single-layered membranes to account for the presence of an abundant solute. The new feature of that model was the distinction between the equilibrium partition coefficients at the upstream and downstream surfaces of the membrane. This distinction is necessary because variations in the local concentration of the solute itself, or of some other solute, can cause the partition coefficients to differ from one another. Using the excluded volume method to model tracer partitioning, we returned to the data of Bolton et al. (1998) to see if the combined predicted effects of lowered filtrate velocity and augmented tracer partitioning could explain the increase in tracer sieving observed with the addition of BSA (see Figs. 3-4 and 3-5 of Chapter 3). GBM was modeled as a random fiber matrix composed of two types of fibers, the larger fibers representing collagen IV fibrils and the smaller fibers representing GAG chains. For both Ficoll and Ficoll sulfate, the predicted effect was more than sufficient to account for the upward shift in the sieving curves. The model predictions agreed with the data well at the lower r_s, but tended to overpredict the sieving coefficients at higher r_s. Among the possible explanations for this tendency to overpredict is the potential limitation in the representation of GBM as a random fiber matrix . This and other possibilities are addressed in Section 5.2 in a discussion of future directions for this research.

In addition to models for sieving across single-layered barriers, we also applied the concentration-effect concept to models for macromolecular sieving across the intact glomerular capillary wall (Section 3.4.4). In general, the glomerular sieving coefficient is a product of seven terms, four partition coefficients, representing the solute distribution at each of the four interfaces, and three sieving coefficients, one for each layer of the barrier. Under dilute conditions, the partitioning effects cancel one another, and the total sieving coefficient depends only upon the sieving coefficients for the individual layers. Fairly limited, and somewhat conflicting, information is available on how deeply plasma proteins penetrate into the capillary

wall, so it is difficult to say with certainty where concentration effects are most likely present for the intact barrier. Several investigators have proposed that the endothelial glycocalyx may represent the major glomerular charge barrier. If this is so, then albumin would be restricted primarily to the capillary lumen, and concentration effects would be important mainly at the plasma/glycocalyx interface. More information is needed to further develop this model, as is discussed briefly in Section 5.2.

In order to demonstrate the concentration effect for dissimilar solutes and to test the applicability of the excluded volume theory to random fiber media, we measured the partition coefficients of BSA and four narrow fractions of Ficoll in agarose prepared at two different solid volume fractions, 4 and 6%. The results of this work are contained in Chapter 4. Agarose represents a good choice of material as it is easily manipulated and has been shown to behave as a random fiber matrix in partitioning experiments. The experiments were carried out under dilute conditions and also with concentrated levels of BSA. The addition of concentrated BSA was found to increase the partition coefficients of BSA itself and that of each of the four Ficolls. The magnitude of the effect varied with solute size and was most significant for the largest Ficoll. A subset of the experiments repeated at a higher ionic strength confirmed that electrostatic interactions between the solutes and the agarose or among the solutes were not a factor and that steric interactions were the primary determinant of solute partitioning. Comparisons were made between the experimental data and model predictions generated using the excluded volume theory. Agarose was modeled as a random fiber matrix, BSA was treated as a prolate spheroid, and Ficoll was treated as a sphere. In general, the model predictions agreed well with the experimental data for both BSA and Ficoll. The good agreement between the data and model over a wide range of protein concentrations demonstrates the applicability of the excluded volume theory for modeling concentration effects among dissimilar solutes in random fiber media. To our knowledge, this is the first experimental demonstration of the concentration effect for systems of dissimilar solutes.

In total, the results of this work confirm the hypothesis that physiological concentrations of protein can significantly augment the partitioning and sieving of macromolecular tracers such as Ficoll in studies of the macromolecular selectivity of the glomerular capillary wall. The models created here were sufficient to capture the effect of BSA on the sieving of Ficoll and Ficoll sulfate in the isolated GBM sieving studies of Bolton et al. (1998). The tendency of the model to overestimate the concentration effect for high tracer r_s is likely related to limitations in the representation of GBM as a random fiber matrix. This possibility seems especially likely in light of the good agreement between model predictions and the experimental data for BSA and Ficoll in agarose, which behaves as a random fiber matrix. In addition to studies involving isolated components of the capillary wall, the effect of plasma proteins on partitioning has important implications for the interpretation of data from a wide variety of experimental techniques involving the intact glomerular barrier.

5.2 Future Work

The observation that the model presented in Chapter 3 tended to overpredict the isolated sieving data at high r_s motivates several directions for future work in the area of fiber matrix modeling. The first, and perhaps most likely, explanation for the overprediction at high r_s is that there may be limitations in the representation of GBM as a random fiber matrix. Instead, a more structurally, and functionally, accurate model might include an ordered arrangement for at least some of the fibers. It has been shown, for example, that collagen assembles into polygonal networks in some basement membranes (Yurchenco and Ruben 1987). Were fibers arranged in such a way in the basement membrane, openings of fixed size would exist and molecules above a certain size would be completely excluded from the matrix. In other words, such a regular arrangement of fibers would confer a molecular weight cutoff to the GBM. The excluded volume theory applied here assumes a completely random distribution of fibers and no such molecular weight cutoff is implied. Returning to the thought experiment developed in Section

2.3.2, we see that the excluded volume theory begins with the assumption that the test solute is in the confined space before the fiber matrix is assembled around it. Further, the exponential form of the probability distribution used there ensures that the partition coefficient will always have some finite values greater than zero. Comparing the tracer sieving curves under dilute and concentrated conditions, it is clear that some GBM molecular weight cutoff exists. Given what is known about the regular assembly of collagen in some basement membranes, it seems that it might be more appropriate to model GBM as a partially-ordered fiber matrix in which the larger collagen fibers are arranged in some regular way and the smaller GAG chains are randomly distributed. The development of such a partitioning model for partially-ordered fibrous media is a good candidate for the further development of macromolecular partitioning theories for physiological membranes such as GBM.

Another potential explanation for the tendency of the theory to overpredict the concentrated sieving data at high tracer r_s may lie in the absence of any consideration of percolation effects in partitioning and sieving theories presented in Chapters 2 and 3, respectively. More specifically, the model assumes that if a molecule is able to enter the membrane at all, then its flux across the membrane will be permitted. For media such as random fiber matrices, however, there may not be a sufficient connectivity of spaces which are large enough to permit the passage of the solute. These types of considerations, termed percolation effects, are not considered in any of the models presented here, and, to our knowledge, no percolation theories exist for fiber matrices. The development of such a theory would no doubt present a significant challenge, but it would be a valuable contribution to the effort to model hindered transport through fibrous media.

A final potential explanation for the tendency of the theory to overpredict is the possibility that the amounts of fine and coarse fibers used in the model representation of GBM may be incorrect. As stated in Chapter 3, the fractional amounts of the total GBM solids content assigned to collagen and GAGs were chosen by matching the measured value of the Darcy permeability for the isolated GBM with a value generated by a two-fiber model for water

permeability. Specifying the total solids volume fraction and fiber radii at values taken from the literature, the model suggested that roughly equivalent volumes of collagen IV and GAGs are needed to describe GBM water permeability. While the identities of the primary constituents of GBM are known, virtually no quantitative information on their concentrations is available. Of the limited data available, one study found that heparan sulfate proteoglycan makes up approximately 1% of the dry weight of GBM (Kanwar and Farquhar 1979). Thus, it seems possible that the GBM model we used in Chapter 3 may contain an unrealistically high relative amount of GAG. Interestingly, lowering the relative amount of GAG in the GBM model while maintaining a total solids content of 10% produces model predictions which more closely match the experimental data. More detailed quantitative information on GBM composition would be extremely valuable for the purpose of refining our fiber matrix model of GBM.

As mentioned previously, the role of the endothelial glycocalyx in determining the permeability properties of the glomerular capillary wall is a subject of some debate. From a macromolecular permeability standpoint, the highly sulfated glycocalyx represents a candidate location for the charge barrier which is associated with the capillary wall. This possibility is strengthened by the finding of Bolton et al. (1998) that GBM, although it too has a fixed negative charge content, does not appear to have charge selective properties at physiological ionic strength and pH. Much as with GBM, however, little firm quantitative data is available on the exact composition of the glomerular endothelial gylcocalyx. More detailed information would be invaluable to the development of models for the water and macromolecular resistance properties of this layer and its contribution to the overall permeability properties of the capillary wall.

The slit diaphragm represents another area where more detailed structural information would be valuable. As mentioned in Chapter 1, various structures have been proposed for the slit diaphragm based on findings from electron microscopy studies. These proposed structures remain tentative, but new information on the chemical constituents that form the diaphragm has been emerging recently. The protein nephrin, for example, has received a great deal of attention

(Holthofer et al. 1999; Lenkkeri et al. 1999; Ruotsalainen et al. 1999; Tryggvason 1999). As more information becomes available on the complete set of building blocks which make up the slit diaphragm, it may be possible to develop more refined models for the contribution of this piece of the capillary wall to the permeability properties of the capillary wall.

In addition to the partition coefficient, the coefficients of hindered convection (K_c) and diffusion (K_d) are important parameters for the description of hindered transport through fibrous media. These appeared in the sieving model developed in Chapter 3. While several hydrodynamic models exist for predicting K_d in fiber matrices (Clague and Phillips 1997; Johnson et al. 1996; Phillips 2000), there is a paucity of information on K_c. For lack of an appropriate alternative, a common practice has been to use the result of Anderson and Malone (1974) for pores. In conjunction with the development of models for K_c and K_d in fibrous media, it would be useful to develop experimental techniques for measuring these parameters in fibrous media similar to GBM. White and Deen (2002) developed an agarose-dextran composite hydrogel for use as a synthetic GBM model in water and macromolecular permeability studies. Interestingly, the composite with a 10% total solids content, 80% of which was agarose and 20% of which was dextran, exhibited water permeabilities in the range which has been reported for isolated rat GBM. Studies of hindered diffusion in these gels are currently being conducted in our lab using the fluorescence recovery after photobleaching (FRAP) technique. Planned also are studies of simultaneous hindered convection and diffusion in the composites by inducing flow in the sample during the FRAP measurement.

Chapter 6

Appendix: FORTRAN code

```
!*************************************************************
!
!     Iterative Solver for Partition Coefficients
!     using Newton's Method with Two Spherical Solutes
!     and Two Fibers
!
!     /mlazzara/partmodel/phinewt.f
!
!*************************************************************

      PROGRAM PHISOLVE

      DOUBLE PRECISION K1,K2,chi1,chi2,phi1,phi2
      DOUBLE PRECISION rp1,rp2,rf1,rf2
      DOUBLE PRECISION a11sf,a12sf,a21sf,a22sf
      DOUBLE PRECISION a11ss,a12ss,a21ss,a22ss
      DOUBLE PRECISION delK1,delK2,det,f,g
      DOUBLE PRECISION dfdK1,dfdK2,dgdK1,dgdK2,count

      PARAMETER (rp1 = 36)     ! BSA, Angstrom units
!      PARAMETER (rp2 = 22)    ! tracer
      PARAMETER (rf1 = 16.4)
      PARAMETER (rf2 = 45)
      PARAMETER (chi1 = 0.0)    ! BSA
      PARAMETER (chi2 = 0.0)    ! tracer
      PARAMETER (phi1 = 0.04)
      PARAMETER (phi2 = 0.00)

      open(unit=8,file='data.txt',status='unknown')

      WRITE (*,*) 'spheres'
```

```
      rp2=20            ! Angstrom units

      K1=0
      K2=0

2     a11sf=(1+(rp1/rf1))**2
      a12sf=(1+(rp1/rf2))**2
      a21sf=(1+(rp2/rf1))**2
      a22sf=(1+(rp2/rf2))**2

      a11ss=(1+(rp1/rp1))**3
      a12ss=(1+(rp1/rp2))**3
      a21ss=(1+(rp2/rp1))**3
      a22ss=(1+(rp2/rp2))**3

      f=K1-exp(-phi1*a11sf-phi2*a12sf+a11ss*(1-K1)*chi1
     &+a12ss*(1-K2)*chi2)
      g=K2-exp(-phi1*a21sf-phi2*a22sf+a21ss*(1-K1)*chi1
     &+a22ss*(1-K2)*chi2)

      dfdK1=1+exp(-phi1*a11sf-phi2*a12sf+a11ss*(1-K1)*chi1
     &+a12ss*(1-K2)*chi2)*a11ss*chi1
      dfdK2=exp(-phi1*a11sf-phi2*a12sf+a11ss*(1-K1)*chi1
     &+a12ss*(1-K2)*chi2)*a12ss*chi2

      dgdK1=exp(-phi1*a21sf-phi2*a22sf+a21ss*(1-K1)*chi1
     &+a22ss*(1-K2)*chi2)*a21ss*chi1
      dgdK2=1+exp(-phi1*a21sf-phi2*a22sf+a21ss*(1-K1)*chi1
     &+a22ss*(1-K2)*chi2)*a22ss*chi2

      det=dfdK1*dgdK2-dgdK1*dfdK2

      delK1=(1/det)*(-dgdK2*f+dfdK2*g)
      delK2=(1/det)*(dgdK1*f-dfdK1*g)

      K1=K1+delK1
      K2=K2+delK2

      IF (abs(delK1).GT.0.0001 .AND. abs(delK2).GT.0.0001) THEN
         count=count+1
         GO TO 2
      ENDIF

      WRITE (*,*) rp2,K1

      IF (rp2.LT.50) THEN
        rp2=rp2+2
        GO TO 2
      ENDIF

      STOP
      END
```

```
!*************************************************************
!
!     Iterative Solver for Partition Coefficients
!     using Newton's Method with Two Spherical Solutes
!     and Cylindrical Pores
!
!     /mlazzara/partmodel/phiporenew.f
!
!*************************************************************

      PROGRAM PHISOLVE

      DOUBLE PRECISION K1,K2,chi1,chi2,phi1,phi2
      DOUBLE PRECISION rp1,rp2,R
      DOUBLE PRECISION a11sf,a12sf,a21sf,a22sf
      DOUBLE PRECISION a11ss,a12ss,a21ss,a22ss
      DOUBLE PRECISION delK1,delK2,det,f,g
      DOUBLE PRECISION dfdK1,dfdK2,dgdK1,dgdK2,count
      DOUBLE PRECISION lambda1,lambda2

      PARAMETER (rp1 = 2.0)
      PARAMETER (rp2 = 0.75)
      PARAMETER (rf1 = 10)
      PARAMETER (rf2 = 4.5)
!      PARAMETER (chi1 = 0.0)
!      PARAMETER (chi2 = 0.0)
      PARAMETER (phi1 = 0.2)
      PARAMETER (phi2 = 0)
      PARAMETER (R=10.0)

      open(unit=8,file='data.txt',status='unknown')

      WRITE (*,*) 'spheres'

      chi1=0.2
      chi2=0.0

      K1=0
      K2=0

 2    a11sf=(1+(rp1/rf1))**2
      a12sf=(1+(rp1/rf2))**2
      a21sf=(1+(rp2/rf1))**2
      a22sf=(1+(rp2/rf2))**2

      lambda1=rp1/R
      lambda2=rp2/R

      a11ss=(1+(rp1/rp1))**3
      a12ss=(1+(rp1/rp2))**3
      a21ss=(1+(rp2/rp1))**3
      a22ss=(1+(rp2/rp2))**3

      f=K1-(1-lambda1)**2*exp(a11ss*(1-K1)*chi1
```

```
     &+a12ss*(1-K2)*chi2)
      g=K2-(1-lambda2)**2*exp(a21ss*(1-K1)*chi1
     &+a22ss*(1-K2)*chi2)

      dfdK1=1+(1-lambda1)**2*exp(a11ss*(1-K1)*chi1
     &+a12ss*(1-K2)*chi2)*a11ss*chi1
      dfdK2=(1-lambda1)**2*exp(a11ss*(1-K1)*chi1
     &+a12ss*(1-K2)*chi2)*a12ss*chi2

      dgdK1=(1-lambda2)**2*exp(a21ss*(1-K1)*chi1
     &+a22ss*(1-K2)*chi2)*a21ss*chi1
      dgdK2=1+(1-lambda2)**2*exp(a21ss*(1-K1)*chi1
     &+a22ss*(1-K2)*chi2)*a22ss*chi2

      det=dfdK1*dgdK2-dgdK1*dfdK2

      delK1=(1/det)*(-dgdK2*f+dfdK2*g)
      delK2=(1/det)*(dgdK1*f-dfdK1*g)

      K1=K1+delK1
      K2=K2+delK2

      IF (abs(delK1).GT.0.0001 .AND. abs(delK2).GT.0.0001) THEN
         count=count+1
         GO TO 2
      ENDIF

      WRITE (*,*) chi2,K1,K2

      IF (chi2.LT.0.2) THEN
        chi2=chi2+0.01
        chi1=0.2-chi2
       GO TO 2
      ENDIF

      STOP
      END

!************************************************************
!
!     Iterative Solver for Partition Coefficients
!     using Newton's Method with One Prolate Spheroid,
!     One Sphere, and Two Fibers
!
!     /mlazzara/partmodel/phiprosph.f
!
!************************************************************

      PROGRAM PHISOLVE

      DOUBLE PRECISION K1,K2,chi1,chi2,phi1,phi2
      DOUBLE PRECISION rp1,rp2,rf1,rf2
      DOUBLE PRECISION a11pf,a12pf
      DOUBLE PRECISION a11pp
```

```
      DOUBLE PRECISION delK1,delK2,det,f,g
      DOUBLE PRECISION dfdK1,dfdK2,dgdK1,dgdK2
      DOUBLE PRECISION feta1,geta1
      DOUBLE PRECISION eta1
      DOUBLE PRECISION a12ps,a21sp,a21sf,a22sf,a22ss
      DOUBLE PRECISION d_acosh

      PARAMETER (rp1 = 17.1)     ! in Angstrom units
!      PARAMETER (rp2 = 36)
      PARAMETER (rf1 = 5)
      PARAMETER (rf2 = 35)
      PARAMETER (chi1 = 0.0564)
      PARAMETER (chi2 = 0.0)
      PARAMETER (phi1 = 0.015)
      PARAMETER (phi2 = 0.085)
      PARAMETER (eta1 = 4.9)

      open(unit=8,file='data.txt',status='unknown')

      WRITE (*,*) 'prolate'

      rp2=20              !  Angstrom units

      K1=0
      K2=0

 1    a21sf=(1+(rp2/rf1))**2
      a22sf=(1+(rp2/rf2))**2

      a22ss=8

      feta1=1+(eta1**2)*(eta1**2-1)**(-0.5)*acos(eta1**(-1.0))
      geta1=eta1+(eta1**2-1)**(-0.5)*d_acosh(eta1)

      a11pf=1+(rp1/rf1)*geta1+(0.5)*(rp1/rf1)**2*feta1
      a12pf=1+(rp1/rf2)*geta1+(0.5)*(rp1/rf2)**2*feta1

      a11pp=2+(1.5)*(1/eta1)*feta1*geta1


a12ps=1+eta1*(rp1/rp2)**3+(1.5)*geta1*(rp1/rp2)+(1.5)*feta1
     $*(rp1/rp2)**2.0


a21sp=1+(1/eta1)*(rp2/rp1)**3+(1.5)*(geta1/eta1)*(rp2/rp1)**2
     $+(1.5)*(feta1/eta1)*(rp2/rp1)
!       WRITE (*,*) a21sp*(4.0/3.0)*3.14158*eta1*rp1**3

 2     f=K1-exp(-phi1*a11pf-phi2*a12pf+a11pp*(1-K1)*chi1
     &+a12ps*(1-K2)*chi2)
       g=K2-exp(-phi1*a21sf-phi2*a22sf+a21sp*(1-K1)*chi1
     &+a22ss*(1-K2)*chi2)

       dfdK1=1+exp(-phi1*a11pf-phi2*a12pf+a11pp*(1-K1)
```

```
     &*chi1+a12ps*(1-K2)*chi2)*a11pp*chi1
      dfdK2=exp(-phi1*a11pf-phi2*a12pf+a11pp*(1-K1)
     &*chi1+a12ps*(1-K2)*chi2)*a12ps*chi2

      dgdK1=exp(-phi1*a21sf-phi2*a22sf+a21sp*(1-K1)*chi1
     &+a22ss*(1-K2)*chi2)*a21sp*chi1
      dgdK2=1+exp(-phi1*a21sf-phi2*a22sf+a21sp*(1-K1)*chi1
     &+a22ss*(1-K2)*chi2)*a22ss*chi2

      det=dfdK1*dgdK2-dgdK1*dfdK2

      delK1=(1/det)*(-dgdK2*f+dfdK2*g)
      delK2=(1/det)*(dgdK1*f-dfdK1*g)


      K1=K1+delK1
      K2=K2+delK2

      IF (abs(delK1).GT.0.0001 .AND. abs(delK2).GT.0.0001) THEN
         GO TO 2
      ENDIF

      WRITE (*,*) rp2,K2

      IF (rp2.LT.50) THEN
        rp2=rp2+2
        GO TO 1
      ENDIF

!      WRITE (*,*) log(eta1+(eta1**2-1)**(0.5))
!      WRITE (*,*) d_acosh(eta1)

      STOP
      END

!*************************************************************
!
!    Iterative Solver for Partition Coefficients
!    using Newton's Method with One Oblate Spheroid,
!    One Sphere, and Two Fibers
!
!    /mlazzara/partmodel/phioblsph.f
!
!*************************************************************

      PROGRAM PHISOLVE

      DOUBLE PRECISION K1,K2,chi1,chi2,phi1,phi2
      DOUBLE PRECISION rp1,rp2,rf1,rf2
      DOUBLE PRECISION a11of,a12of
      DOUBLE PRECISION delK1,delK2,det,f,g
      DOUBLE PRECISION dfdK1,dfdK2,dgdK1,dgdK2
      DOUBLE PRECISION eta1
      DOUBLE PRECISION a21sf,a22sf,a22ss
```

```
      DOUBLE PRECISION fpeta1,gpeta1,a11oo,a12os,a21so
      DOUBLE PRECISION d_acosh

      PARAMETER (rp1 = 40)
      PARAMETER (rp2 = 50)
      PARAMETER (rf1 = 20)
      PARAMETER (rf2 = 45)
      PARAMETER (chi1 = 0.1)
      PARAMETER (chi2 = 0.0)
      PARAMETER (phi1 = 0.1)
      PARAMETER (phi2 = 0.0)
!      PARAMETER (eta1 = 1.01)

      open(unit=8,file='data.txt',status='unknown')

      WRITE (*,*) 'oblate'

      eta1=0.01

      K1=0
      K2=0

      a21sf=(1+(rp2/rf1))**2
      a22sf=(1+(rp2/rf2))**2

      a22ss=8

 1    fpeta1=1+(eta1**2)*(1-eta1**2)**(-0.5)*d_acosh(eta1**-1)

      gpeta1=eta1+(1-eta1**2)**(-0.5)*acos(eta1)

      a11of=1+(rp1/rf1)*gpeta1+(0.5)*(rp1/rf1)**2*fpeta1
      a12of=1+(rp1/rf2)*gpeta1+(0.5)*(rp1/rf2)**2*fpeta1


a12os=1+eta1*(rp1/rp2)**3+(1.5)*gpeta1*(rp1/rp2)+(1.5)*fpeta1
     $*(rp1/rp2)**2


a21so=1+(1/eta1)*(rp2/rp1)**3+(1.5)*(gpeta1/eta1)*(rp2/rp1)**2
     &+(1.5)*(fpeta1/eta1)*(rp2/rp1)

      a11oo=2+(1.5)*(1/eta1)*fpeta1*gpeta1

 2    f=K1-exp(-phi1*a11of-phi2*a12of+a11oo*(1-K1)*chi1
     &+a12os*(1-K2)*chi2)
      g=K2-exp(-phi1*a21sf-phi2*a22sf+a21so*(1-K1)*chi1
     &+a22ss*(1-K2)*chi2)

      dfdK1=1+exp(-phi1*a11of-phi2*a12of+a11oo*(1-K1)*chi1
     &+a12os*(1-K2)*chi2)*a11oo*chi1
      dfdK2=exp(-phi1*a11of-phi2*a12of+a11oo*(1-K1)*chi1
     &+a12os*(1-K2)*chi2)*a12os*chi2
```

```
      dgdK1=exp(-phi1*a21sf-phi2*a22sf+a21so*(1-
K1)*chi1+a22ss*(1-K2)
     &*chi2)*a21so*chi1
      dgdK2=1+exp(-phi1*a21sf-phi2*a22sf+a21so*(1-
K1)*chi1+a22ss*(1-K2)
     &*chi2)*a22ss*chi2

      det=dfdK1*dgdK2-dgdK1*dfdK2

      delK1=(1/det)*(-dgdK2*f+dfdK2*g)
      delK2=(1/det)*(dgdK1*f-dfdK1*g)

      K1=K1+delK1
      K2=K2+delK2

      IF (abs(delK1).GT.0.0001 .AND. abs(delK2).GT.0.0001) THEN
         GO TO 2
      ENDIF

      WRITE (*,*) eta1,K1

      IF (eta1.LT.0.98) THEN
        eta1=eta1+0.02
        GO TO 1
      ENDIF

      STOP
      END

!************************************************************
!
!     Iterative Solver for Partition Coefficients
!     using Newton's Method with Two Prolate Spheroids
!     and Two Fibers
!
!     /mlazzara/partmodel/phinewtpro.f
!
!************************************************************

      PROGRAM PHISOLVE

      DOUBLE PRECISION K1,K2,chi1,chi2,phi1,phi2
      DOUBLE PRECISION rp1,rp2,rf1,rf2
      DOUBLE PRECISION a11pf,a12pf,a21pf,a22pf
      DOUBLE PRECISION a11pp,a12pp,a21pp,a22pp
      DOUBLE PRECISION delK1,delK2,det,f,g
      DOUBLE PRECISION dfdK1,dfdK2,dgdK1,dgdK2
      DOUBLE PRECISION feta1,feta2,geta1,geta2
      DOUBLE PRECISION eta1,eta2
      DOUBLE PRECISION d_acosh

      PARAMETER (rp1 = 20)
      PARAMETER (rp2 = 50)
      PARAMETER (rf1 = 20)
```

```
      PARAMETER (rf2 = 45)
!      PARAMETER (chi1 = 0.05)
      PARAMETER (chi2 = 0.0)
      PARAMETER (phi1 = 0.1)
      PARAMETER (phi2 = 0.0)
      PARAMETER (eta1 = 1.2)
      PARAMETER (eta2 = 1.05)

      open(unit=8,file='data.txt',status='unknown')

      WRITE (*,*) 'prolate'

      chi1=0
      K1=0
      K2=0

 1    feta1=1+(eta1**2)*(eta1**2-1)**(-0.5)*acos(eta1**(-1))
      feta2=1+(eta2**2)*(eta2**2-1)**(-0.5)*acos(eta2**(-1))

      geta1=eta1+(eta1**2-1)**(-0.5)*d_acosh(eta1)
      geta2=eta2+(eta2**2-1)**(-0.5)*d_acosh(eta2)

      a11pf=1+(rp1/rf1)*geta1+(0.5)*(rp1/rf1)**2*feta1
      a12pf=1+(rp1/rf2)*geta1+(0.5)*(rp1/rf2)**2*feta1
      a21pf=1+(rp2/rf1)*geta2+(0.5)*(rp2/rf1)**2*feta2
      a22pf=1+(rp2/rf2)*geta2+(0.5)*(rp2/rf2)**2*feta2

      a11pp=2+(1.5)*(1/eta1)*feta1*geta1

a12pp=1+((eta1*rp1)/(eta2*rp2))**3+(0.75)*(rp1/rp2)**2*(1/eta2)
     $*feta1*geta2+(0.75)*(rp1/rp2)*(1/eta2)*feta2*geta1

a21pp=1+((eta2*rp2)/(eta1*rp1))**3+(0.75)*(rp2/rp1)**2*(1/eta1)
     $*feta2*geta1+(0.75)*(rp2/rp1)*(1/eta1)*feta1*geta2
      a22pp=2+(1.5)*(1/eta2)*feta2*geta2

 2    f=K1-exp(-phi1*a11pf-phi2*a12pf+a11pp*(1-K1)*chi1
     &+a12pp*(1-K2)*chi2)
      g=K2-exp(-phi1*a21pf-phi2*a22pf+a21pp*(1-K1)*chi1
     &+a22pp*(1-K2)*chi2)

      dfdK1=1+exp(-phi1*a11pf-phi2*a12pf+a11pp*(1-K1)*chi1
     &+a12pp*(1-K2)*chi2)*a11pp*chi1
      dfdK2=exp(-phi1*a11pf-phi2*a12pf+a11pp*(1-K1)*chi1
     &+a12pp*(1-K2)*chi2)*a12pp*chi2

      dgdK1=exp(-phi1*a21pf-phi2*a22pf+a21pp*(1-K1)*chi1
     &+a22pp*(1-K2)*chi2)*a21pp*chi1
      dgdK2=1+exp(-phi1*a21pf-phi2*a22pf+a21pp*(1-K1)
     &*chi1+a22pp*(1-K2)*chi2)*a22pp*chi2

      det=dfdK1*dgdK2-dgdK1*dfdK2

      delK1=(1/det)*(-dgdK2*f+dfdK2*g)
```

```
      delK2=(1/det)*(dgdK1*f-dfdK1*g)

      K1=K1+delK1
      K2=K2+delK2

      IF (abs(delK1).GT.0.0001 .AND. abs(delK2).GT.0.0001) THEN
         GO TO 2
      ENDIF

      WRITE (*,*) chi1,K1

      IF (chi1.LT.0.20) THEN
        chi1=chi1+0.01
        GO TO 2
      ENDIF

      STOP
      END

!*************************************************************
!
!     Iterative Solver for Partition Coefficients
!     using Newton's Method with Two Oblate Spheroids
!     and Two Fibers
!
!     /mlazzara/partmodel/phinewtobl.f
!
!*************************************************************

      PROGRAM PHISOLVE

      DOUBLE PRECISION K1,K2,chi1,chi2,phi1,phi2
      DOUBLE PRECISION rp1,rp2,rf1,rf2
      DOUBLE PRECISION a11of,a12of,a21of,a22of
      DOUBLE PRECISION a11oo,a12oo,a21oo,a22oo
      DOUBLE PRECISION delK1,delK2,det,f,g
      DOUBLE PRECISION dfdK1,dfdK2,dgdK1,dgdK2
      DOUBLE PRECISION fpeta1,fpeta2,gpeta1,gpeta2
      DOUBLE PRECISION eta1,eta2
      DOUBLE PRECISION d_acosh

      PARAMETER (rp1 = 40)
      PARAMETER (rp2 = 50)
      PARAMETER (rf1 = 20)
      PARAMETER (rf2 = 80)
      PARAMETER (chi1 = 0.0)
      PARAMETER (chi2 = 0.0)
      PARAMETER (phi1 = 0.1)
      PARAMETER (phi2 = 0.0)
!      PARAMETER (eta1 = 0.8)
      PARAMETER (eta2 = 0.9)

      open(unit=8,file='data.txt',status='unknown')
```

```
      WRITE (*,*) 'oblate'

      eta1=0.05
      K1=0
      K2=0

 1    fpeta1=1+(eta1**2)*(1-eta1**2)**(-0.5)*d_acosh(eta1**(-1))
      fpeta2=1+(eta2**2)*(1-eta2**2)**(-0.5)*d_acosh(eta2**(-1))

      gpeta1=eta1+(1-eta1**2)**(-0.5)*acos(eta1)
      gpeta2=eta2+(1-eta2**2)**(-0.5)*acos(eta2)

      a11of=1+(rp1/rf1)*gpeta1+(0.5)*(rp1/rf1)**2*fpeta1
      a12of=1+(rp1/rf2)*gpeta1+(0.5)*(rp1/rf2)**2*fpeta1
      a21of=1+(rp2/rf1)*gpeta2+(0.5)*(rp2/rf1)**2*fpeta2
      a22of=1+(rp2/rf2)*gpeta2+(0.5)*(rp2/rf2)**2*fpeta2

      a11oo=2+(1.5)*(1/eta1)*fpeta1*gpeta1

a12oo=1+((eta1*rp1)/(eta2*rp2))**3+(0.75)*(rp1/rp2)**2*(1/eta2)
     $*fpeta1*gpeta2+(0.75)*(rp1/rp2)*(1/eta2)*fpeta2*gpeta1

a21oo=1+((eta2*rp2)/(eta1*rp1))**3+(0.75)*(rp2/rp1)**2*(1/eta1)
     $*fpeta2*gpeta1+(0.75)*(rp2/rp1)*(1/eta1)*fpeta1*gpeta2
      a22oo=2+(1.5)*(1/eta2)*fpeta2*gpeta2

 2    f=K1-exp(-phi1*a11of-phi2*a12of+a11oo*(1-K1)*chi1
     &+a12oo*(1-K2)*chi2)
      g=K2-exp(-phi1*a21of-phi2*a22of+a21oo*(1-K1)*chi1
     &+a22oo*(1-K2)*chi2)

      dfdK1=1+exp(-phi1*a11of-phi2*a12of+a11oo*(1-K1)*chi1
     &+a12oo*(1-K2)*chi2)*a11oo*chi1
      dfdK2=exp(-phi1*a11of-phi2*a12of+a11oo*(1-K1)*chi1
     &+a12oo*(1-K2)*chi2)*a12oo*chi2

      dgdK1=exp(-phi1*a21of-phi2*a22of+a21oo*(1-K1)*chi1
     &+a22oo*(1-K2)*chi2)*a21oo*chi1
      dgdK2=1+exp(-phi1*a21of-phi2*a22of+a21oo*(1-K1)
     &*chi1+a22oo*(1-K2)*chi2)*a22oo*chi2

      det=dfdK1*dgdK2-dgdK1*dfdK2

      delK1=(1/det)*(-dgdK2*f+dfdK2*g)
      delK2=(1/det)*(dgdK1*f-dfdK1*g)

      K1=K1+delK1
      K2=K2+delK2

      IF (abs(delK1).GT.0.0001 .AND. abs(delK2).GT.0.0001) THEN
         GO TO 2
      ENDIF

      WRITE (*,*) eta1,K1
```

```
      IF (eta1.LT.0.95) THEN
        eta1=eta1+0.05
        GO TO 1
      ENDIF

      STOP
      END


!*****************************************************************
!
!      Iterative Solver for Partition Coefficients
!      using Newton's Method with One Prolate Spheroid,
!      Two Spheres, and Two Fibers
!
!      /mlazzara/partmodel/phipro2sph.f
!
!*****************************************************************

      PROGRAM PHISOLVE

      DOUBLE PRECISION K1,K2,K3,chi1,chi2,chi3,phi1,phi2
      DOUBLE PRECISION rp1,rp2,rp3,rf1,rf2
      DOUBLE PRECISION a11pf,a12pf,a21sf,a22sf,a31sf,a32sf
      DOUBLE PRECISION a11pp,a12ps,a13ps
      DOUBLE PRECISION a21sp,a22ss,a23ss
      DOUBLE PRECISION a31sp,a32ss,a33ss
      DOUBLE PRECISION delK1,delK2,delK3,det,f,g,h
      DOUBLE PRECISION dfdK1,dfdK2,dfdK3
      DOUBLE PRECISION dgdK1,dgdK2,dgdK3
      DOUBLE PRECISION dhdK1,dhdK2,dhdK3
      DOUBLE PRECISION feta1,geta1
      DOUBLE PRECISION eta1
      DOUBLE PRECISION d11,d12,d13,d21,d22,d23,d31,d32,d33
      DOUBLE PRECISION d_acosh

      PARAMETER (rp1 = 21.2)     ! in Angstrom units
      PARAMETER (rp2 = 47.1)
!      PARAMETER (rp3 = 52)
      PARAMETER (rf1 = 16.4)
      PARAMETER (rf2 = 15)
      PARAMETER (chi1 = 0.09)  ! chi = 0.0564 upstream for GB's
exps
      PARAMETER (chi2 = 0.01)
      PARAMETER (chi3 = 0.0)
      PARAMETER (phi1 = 0.06)
      PARAMETER (phi2 = 0.00)    ! fine fiber
      PARAMETER (eta1 = 3.3)

      open(unit=8,file='data.txt',status='unknown')

      WRITE (*,*) '3 solutes - 1 prolate, 2 spherical'
```

```
      rp3=20              !  Angstroms

      K1=0
      K2=0
      K3=0

 1    feta1=1+(eta1**2)*(eta1**2-1)**(-0.5)*acos(eta1**(-1.0))
      geta1=eta1+(eta1**2-1)**(-0.5)*d_acosh(eta1)

      a11pf=1+(rp1/rf1)*geta1+(0.5)*(rp1/rf1)**2*feta1
      a12pf=1+(rp1/rf2)*geta1+(0.5)*(rp1/rf2)**2*feta1
      a21sf=(1+(rp2/rf1))**2
      a22sf=(1+(rp2/rf2))**2
      a31sf=(1+(rp3/rf1))**2
      a32sf=(1+(rp3/rf2))**2

      a11pp=2+(1.5)*(1/eta1)*feta1*geta1

a12ps=1+eta1*(rp1/rp2)**3+(1.5)*geta1*(rp1/rp2)+(1.5)*feta1
     $*(rp1/rp2)**2.0

a13ps=1+eta1*(rp1/rp3)**3+(1.5)*geta1*(rp1/rp3)+(1.5)*feta1
     $*(rp1/rp3)**2.0


a21sp=1+(1/eta1)*(rp2/rp1)**3+(1.5)*(geta1/eta1)*(rp2/rp1)**2
     $+(1.5)*(feta1/eta1)*(rp2/rp1)
      a22ss=8
      a23ss=(1+(rp2/rp3))**3


a31sp=1+(1/eta1)*(rp3/rp1)**3+(1.5)*(geta1/eta1)*(rp3/rp1)**2
     $+(1.5)*(feta1/eta1)*(rp3/rp1)
      a32ss=(1+(rp3/rp2))**3
      a33ss=8

 2    f=K1-exp(-phi1*a11pf-phi2*a12pf+a11pp*(1-K1)*chi1
     &+a12ps*(1-K2)*chi2+a13ps*(1-K3)*chi3)
      g=K2-exp(-phi1*a21sf-phi2*a22sf+a21sp*(1-K1)*chi1
     &+a22ss*(1-K2)*chi2+a23ss*(1-K3)*chi3)
      h=K3-exp(-phi1*a31sf-phi2*a32sf+a31sp*(1-K1)*chi1
     &+a32ss*(1-K2)*chi2+a33ss*(1-K3)*chi3)

      dfdK1=1+exp(-phi1*a11pf-phi2*a12pf+a11pp*(1-K1)
     &*chi1+a12ps*(1-K2)*chi2+a13ps*(1-K3)*chi3)*a11pp*chi1
      dfdK2=exp(-phi1*a11pf-phi2*a12pf+a11pp*(1-K1)
     &*chi1+a12ps*(1-K2)*chi2+a13ps*(1-K3)*chi3)*a12ps*chi2
      dfdK3=exp(-phi1*a11pf-phi2*a12pf+a11pp*(1-K1)
     &*chi1+a12ps*(1-K2)*chi2+a13ps*(1-K3)*chi3)*a13ps*chi3

      dgdK1=exp(-phi1*a21sf-phi2*a22sf+a21sp*(1-K1)*chi1
     &+a22ss*(1-K2)*chi2+a23ss*(1-K3)*chi3)*a21sp*chi1
      dgdK2=1+exp(-phi1*a21sf-phi2*a22sf+a21sp*(1-K1)*chi1
     &+a22ss*(1-K2)*chi2+a23ss*(1-K3)*chi3)*a22ss*chi2
```

```
 dgdK3=exp(-phi1*a21sf-phi2*a22sf+a21sp*(1-K1)*chi1
&+a22ss*(1-K2)*chi2+a23ss*(1-K3)*chi3)*a23ss*chi3

 dhdK1=exp(-phi1*a31sf-phi2*a32sf+a31sp*(1-K1)*chi1
&+a32ss*(1-K2)*chi2+a33ss*(1-K3)*chi3)*a31sp*chi1
 dhdK2=exp(-phi1*a31sf-phi2*a32sf+a31sp*(1-K1)*chi1
&+a32ss*(1-K2)*chi2+a33ss*(1-K3)*chi3)*a32ss*chi2
 dhdK3=1+exp(-phi1*a31sf-phi2*a32sf+a31sp*(1-K1)*chi1
&+a32ss*(1-K2)*chi2+a33ss*(1-K3)*chi3)*a33ss*chi3

 det=dfdK1*(dgdK2*dhdK3-dhdK2*dgdK3)-dfdK2*(dgdK1*dhdK3
&-dhdK1*dgdK3)+dfdK3*(dgdK1*dhdK2-dhdK1*dgdK2)

 d11=dgdK2*dhdK3-dhdK2*dgdK3
 d12=dgdK1*dhdK3-dhdK1*dgdK3
 d13=dgdK1*dhdK2-dhdK1*dgdK2
 d21=dfdK2*dhdK3-dhdK2*dfdK3
 d22=dfdK1*dhdK3-dhdK1*dfdK3
 d23=dfdK1*dhdK2-dhdK1*dfdK2
 d31=dfdK2*dgdK3-dgdK2*dfdK3
 d32=dfdK1*dgdK3-dgdK1*dfdK3
 d33=dfdK1*dgdK2-dgdK1*dfdK2

 delK1=(1/det)*(-d11*f+d21*g-d31*h)
 delK2=(1/det)*(d12*f-d22*g+d32*h)
 delK3=(1/det)*(-d13*f+d23*g-d33*h)

 K1=K1+delK1
 K2=K2+delK2
 K3=K3+delK3

 IF (abs(delK1).GT.0.0001 .AND. abs(delK2).GT.0.0001 .AND.
& abs(delK3).GT.0.0001) THEN
    GO TO 2
 ENDIF

 WRITE (*,*) rp3,K3

 IF (rp3.LT.50) THEN
   rp3=rp3+2
   GO TO 1
 ENDIF


 STOP
 END
```

```
!*************************************************************
!
!     FFT solution for transient diffusion from a 1D solid
!     to a stirred solution of infinite volume
!
!     /mlazzara/fftsolutions/infinitefft.f
!
!*************************************************************

      PROGRAM FFT1D

!*************************************************************
!     VARIABLE DECLARATIONS
!*************************************************************

      DOUBLE PRECISION x,y,z,a,b,gamma,lamn
      DOUBLE PRECISION an,term1,term2,term3
      DOUBLE PRECISION term4,alpha,pi
      DOUBLE PRECISION A,L,D,xtil,ttil
      DOUBLE PRECISION sumsol,sumliq
      DOUBLE PRECISION cm,cl,co,phi

      INTEGER n

      L=0.3             ! centimeters
      xtil=0.05*L
      ttil=3600*0

      D=0.53*6e-7       ! centimeters**2/s
      pi=3.14159

      gamma=1

      phi=0.7
      c0=2.0              ! g/dl


!*************************************************************
!    COMPUTING FFT SOLUTION FOR SOLID AND LIQUID PHASES
!*************************************************************

 1    sumsol=0.0
      sumliq=0.0

      DO n=0,30
         lamn=(n+0.5)*pi
         term1=(2**0.5)*lamn*sin(lamn)/(lamn**2)
         term2=(lamn**2)*ttil*D/L**2
         term3=1-exp(-term2)
         term4=(2**0.5)*cos(lamn*xtil/L)
         sumsol=sumsol+term1*term3*term4
      ENDDO

      cm=sumsol*c0*phi
```

```
      WRITE (*,*) ttil/3600,cm/(c0*phi)

      IF (ttil.LT.200*3600) THEN
        ttil=ttil+4*3600
        GO TO 1
      ENDIF

      STOP
      END

!************************************************************
!
!     FFT solution for transient diffusion from a 1D solid
!     to a stirred solution of finite volume
!
!     /mlazzara/fftsolutions/coupledfft.f
!
!************************************************************

      PROGRAM FFT1D

!************************************************************
!     VARIABLE DECLARATIONS
!************************************************************

      DOUBLE PRECISION x,y,z,a,b,gamma,lam(15)
      DOUBLE PRECISION an,term1,term2,term3l,term3s
      DOUBLE PRECISION term4,alpha,M,fc,c
      DOUBLE PRECISION A,L,D,xtil,ttil
      DOUBLE PRECISION sumsol,sumliq
      DOUBLE PRECISION cm,cl,co,phi

      INTEGER n

!************************************************************
!
!     FINDING THE EIGENVALUES FROM CHARACTERISTIC EQUATION
!
!     char equation : lambda(n) = -gamma*tan(lambda(n))
!
!************************************************************

      L=0.3          ! centimeters
      xtil=0.01*L
      ttil=3600*0

      D=0.53*6e-7       ! centimeters**2/s

      n=1
      gamma=1.0

      alpha=1
      M=1
```

```
      phi=0.7
      c0=2       ! g/dl

 1    a=(2*n-1)*3.14159/2.0
      b=(2*n+1)*3.14159/2.0

      a=a+0.0005
      b=b-0.0005

 2    c=(a+b)/2.0

      fc=gamma*tan(c)+c

      IF (fc.LT.0) THEN
         a=c
      ENDIF

      IF (fc.GT.0) THEN
         b=c
      ENDIF

      IF (abs(fc).GT.0.00001) THEN
         GOTO 2
      ENDIF

      lam(n)=c

      IF (n.LT.15) THEN
         n=n+1
         GOTO 1
      ENDIF


!************************************************************
!    COMPUTING FFT SOLUTION FOR SOLID AND LIQUID PHASES
!************************************************************

 3    sumsol=0.0
      sumliq=0.0

      DO n=1,15
         an=(0.5+sin(2*lam(n))/(4*lam(n))+(1/gamma)*
     $(cos(lam(n))**2))**(-0.5)
         term1=ttil*D*(lam(n)**2)/(L**2)
         term2=exp(-term1)
         term3l=cos(lam(n))*an**2
         term3s=cos(lam(n)*xtil/L)*an**2
         term4=cos(lam(n))/gamma
         sumsol=sumsol+term2*term3s*term4
         sumliq=sumliq+term2*term3l*term4
      ENDDO

      sumsol=sumsol+gamma/(gamma+1)
```

```
      sumliq=sumliq+gamma/(gamma+1)

      cm=sumsol*c0*phi
      cl=sumliq*c0

!      WRITE (*,*) ttil/3600,'sol',cm,'liq',cl
      WRITE (*,*) ttil/3600, cm/(gamma*c0*phi/(gamma+1))

      IF (ttil.LT.200*3600) THEN
         ttil=ttil+4*3600
         GO TO 3
      ENDIF

      STOP
      END

!*************************************************************
!
!     FFT solution of transient diffusion for an
!     equilibrating agarose prism, infinite solution volume
!
!     /mlazzara/fftsolutions/prismfft.f
!
!*************************************************************


      DOUBLE PRECISION ct,phi,c0,D
      DOUBLE PRECISION x,y,z,t,sum,kappa,pi
      DOUBLE PRECISION a,b,c
      INTEGER n,m,l

      pi=3.14159
      D=0.53*6e-7 ! cm2/s
      a=0.3       ! cm
      b=0.3        ! cm
      c=0.15        ! cm
      phi=0.7
      c0=2
      sum=0
      kappa=0

      t=2*3600

1       x=0.015
        y=0.06
        z=0.03

        n=1
        m=1
        l=1

        DO n=1,40,2
         DO m=1,40,2
          DO l=1,40,2
```

```
            kappa=(n**2+(m*a/b)**2+(l*a/c)**2)*(pi**2)*D/(a**2)
            sum=sum+exp(-kappa*t)*sin(n*pi*x/a)*
     $sin(m*pi*y/b)*sin(l*pi*z/c)/(n*m*l)
          ENDDO
         ENDDO
        ENDDO

        ct=phi*c0*(1-(64.0/(pi**3))*sum)

        WRITE (*,*) t/3600,ct

        IF (t.LT.60*60*20) THEN
           t=t+60*60*.1
           sum=0
           GO TO 1
        ENDIF

        STOP
        END

!************************************************************
!
!     FFT solution of transient diffusion for an
!     equilibrating agarose prism, infinite solution volume
!
!     **calculating apparent partitiong coeff versus time**
!
!     /mlazzara/fftsolutions/apppart.f
!
!************************************************************

      DOUBLE PRECISION ct,phi,c0,D
      DOUBLE PRECISION x,y,z,tau,sum,kappa,pi
      DOUBLE PRECISION a,b,c,h(21,21),g(21),temp(21)
      DOUBLE PRECISION xspace,yspace,zspace
      DOUBLE PRECISION partapp,cmavg

      INTEGER i,n,m,l,r,s,t

      pi=3.14159
      D=0.53*6e-7    ! cm^2/s
      a=0.3          ! cm
      b=0.3          ! cm
      c=0.3         ! cm
      phi=0.7
      c0=2.0           ! g/dL
      sum=0
      kappa=0

      xspace=a/20.0
      yspace=b/20.0
      zspace=c/20.0

      tau=3600*0.5
```

```
!     FIRST CALCULATE h(y,z) at 441 points

 1    DO s=1,21
       DO t=1,21
        DO r=1,21

          sum=0.0

          x=(r-1)*xspace
          y=(s-1)*yspace
          z=(t-1)*zspace

          DO n=1,40,2
           DO m=1,40,2
            DO l=1,40,2
              kappa=(n**2+(m*a/b)**2+(l*a/c)**2)*
     $(pi**2)*D/(a**2)
              sum=sum+exp(-kappa*tau)*sin(n*pi*x/a)*
     $sin(m*pi*y/b)*sin(l*pi*z/c)/(n*m*l)
           ENDDO
          ENDDO
         ENDDO

         ct=phi*c0*(1-(64.0/(pi**3))*sum)

         temp(r)=ct

        ENDDO          ! for r=1,21

        h(s,t)=0.0

         DO i=2,20,2
            h(s,t)=h(s,t)+4*temp(i)
         ENDDO
         DO i=3,19,2
            h(s,t)=h(s,t)+2*temp(i)
         ENDDO

         h(s,t)=(1.0/3.0)*xspace*(h(s,t)+temp(1)+temp(21))

       ENDDO
      ENDDO

!     NOW CALCULATE g(z) at 21 points

      DO t=1,21

         g(t)=0.0
         z=(t-1)*zspace

         DO i=2,20,2
            g(t)=g(t)+4*h(i,t)
         ENDDO
```

```
   DO i=3,19,2
      g(t)=g(t)+2*h(i,t)
   ENDDO

   g(t)=(1.0/3.0)*yspace*(g(t)+h(1,t)+h(21,t))

ENDDO

! NOW INTEGRATE OVER z

cmavg=0.0

DO i=2,20,2
   cmavg=cmavg+4*g(i)
ENDDO
DO i=3,19,2
   cmavg=cmavg+2*g(i)
ENDDO

cmavg=(1.0/3.0)*zspace*(cmavg+g(1)+g(21))
cmavg=cmavg/(a*b*c)

partapp=cmavg/c0

WRITE (*,*) tau/3600,partapp

IF (tau.LT.60*60*20) THEN
  tau=tau+60*60*0.5
  sum=0
  GO TO 1
ENDIF


STOP
END
```

```
!*********************************************************
!
!     Iterative Solver for Partition Coefficients
!     using Newton's Method with One Prolate Spheroid,
!     One Sphere, and Two Fibers
!
!     /mlazzara/partmodel/sieving.f
!
!     *calculates chi_L of BSA at specified Pe
!
!*********************************************************

      PROGRAM SIEVING

      DOUBLE PRECISION K1,K2,chi1,chi2,phi1,phi2
      DOUBLE PRECISION rp1,rp2,rf1,rf2
      DOUBLE PRECISION a11pf,a12pf
      DOUBLE PRECISION a11pp
      DOUBLE PRECISION delK1,delK2,det,f,g
      DOUBLE PRECISION dfdK1,dfdK2,dgdK1,dgdK2
      DOUBLE PRECISION feta1,geta1
      DOUBLE PRECISION eta1
      DOUBLE PRECISION a12ps,a21sp,a21sf,a22sf,a22ss
      DOUBLE PRECISION d_acosh
      DOUBLE PRECISION phidil,phi0,phiL,theta,Kc,Pe
      DOUBLE PRECISION chiL,chi0

      PARAMETER (rp1 = 21.2)     ! in Angstrom units
      PARAMETER (rp2 = 30)
      PARAMETER (rf1 = 10)
      PARAMETER (rf2 = 45)
!      PARAMETER (chi1 = 0.0)   ! conc = 0.0564
      PARAMETER (chi2 = 0.0)
      PARAMETER (phi1 = 0.2)
      PARAMETER (phi2 = 0)    ! fine fiber
      PARAMETER (eta1 = 3.3)
      PARAMETER (Pe = 10)

      open(unit=8,file='data.txt',status='unknown')

      chi0=0.0

 1    chi1=0                        !  Angstrom units

      K1=0
      K2=0

 2    a21sf=(1+(rp2/rf1))**2
      a22sf=(1+(rp2/rf2))**2

      a22ss=8

      feta1=1+(eta1**2)*(eta1**2-1)**(-0.5)*acos(eta1**(-1.0))
      geta1=eta1+(eta1**2-1)**(-0.5)*d_acosh(eta1)
```

```
      a11pf=1+(rp1/rf1)*geta1+(0.5)*(rp1/rf1)**2*feta1
      a12pf=1+(rp1/rf2)*geta1+(0.5)*(rp1/rf2)**2*feta1

      a11pp=2+(1.5)*(1/eta1)*feta1*geta1


a12ps=1+eta1*(rp1/rp2)**3+(1.5)*geta1*(rp1/rp2)+(1.5)*feta1
     $*(rp1/rp2)**2.0


a21sp=1+(1/eta1)*(rp2/rp1)**3+(1.5)*(geta1/eta1)*(rp2/rp1)**2
     $+(1.5)*(feta1/eta1)*(rp2/rp1)
!      WRITE (*,*) a21sp*(4.0/3.0)*3.14158*eta1*rp1**3

 3    f=K1-exp(-phi1*a11pf-phi2*a12pf+a11pp*(1-K1)*chi1
     &+a12ps*(1-K2)*chi2)
      g=K2-exp(-phi1*a21sf-phi2*a22sf+a21sp*(1-K1)*chi1
     &+a22ss*(1-K2)*chi2)

      dfdK1=1+exp(-phi1*a11pf-phi2*a12pf+a11pp*(1-K1)
     &*chi1+a12ps*(1-K2)*chi2)*a11pp*chi1
      dfdK2=exp(-phi1*a11pf-phi2*a12pf+a11pp*(1-K1)
     &*chi1+a12ps*(1-K2)*chi2)*a12ps*chi2

      dgdK1=exp(-phi1*a21sf-phi2*a22sf+a21sp*(1-K1)*chi1
     &+a22ss*(1-K2)*chi2)*a21sp*chi1
      dgdK2=1+exp(-phi1*a21sf-phi2*a22sf+a21sp*(1-K1)*chi1
     &+a22ss*(1-K2)*chi2)*a22ss*chi2

      det=dfdK1*dgdK2-dgdK1*dfdK2

      delK1=(1/det)*(-dgdK2*f+dfdK2*g)
      delK2=(1/det)*(dgdK1*f-dfdK1*g)


      K1=K1+delK1
      K2=K2+delK2

      IF (abs(delK1).GT.0.0001 .AND. abs(delK2).GT.0.0001) THEN
         GO TO 3
      ENDIF

!      WRITE (*,*) chi1,K1

      IF (chi1.EQ.0) THEN
         phidil=K1
      ENDIF

      IF (chi1.LT.chi0  ) THEN
        chi1=chi0
        GO TO 2
      ENDIF
```

```
      phi0=K1
      phiL=phidil

      Kc=0.75

5     theta=phi0*Kc/(1-(1-phiL*Kc)*exp(-Pe))
      chiL=theta*chi0

      chi1=chiL

      K1=0
      K2=0

4     f=K1-exp(-phi1*a11pf-phi2*a12pf+a11pp*(1-K1)*chi1
     &+a12ps*(1-K2)*chi2)
      g=K2-exp(-phi1*a21sf-phi2*a22sf+a21sp*(1-K1)*chi1
     &+a22ss*(1-K2)*chi2)

      dfdK1=1+exp(-phi1*a11pf-phi2*a12pf+a11pp*(1-K1)
     &*chi1+a12ps*(1-K2)*chi2)*a11pp*chi1
      dfdK2=exp(-phi1*a11pf-phi2*a12pf+a11pp*(1-K1)
     &*chi1+a12ps*(1-K2)*chi2)*a12ps*chi2

      dgdK1=exp(-phi1*a21sf-phi2*a22sf+a21sp*(1-K1)*chi1
     &+a22ss*(1-K2)*chi2)*a21sp*chi1
      dgdK2=1+exp(-phi1*a21sf-phi2*a22sf+a21sp*(1-K1)*chi1
     &+a22ss*(1-K2)*chi2)*a22ss*chi2

      det=dfdK1*dgdK2-dgdK1*dfdK2

      delK1=(1/det)*(-dgdK2*f+dfdK2*g)
      delK2=(1/det)*(dgdK1*f-dfdK1*g)

      K1=K1+delK1
      K2=K2+delK2

      IF (abs(delK1).GT.0.0001 .AND. abs(delK2).GT.0.0001) THEN
         GO TO 4
      ENDIF

      IF (abs(K1-phiL).GT.0.001) THEN
         phiL=phiL+0.1*(K1-phiL)
         GO TO 5
      ENDIF

      WRITE (*,*) chiL

      IF (chi0.LT.0.2) THEN
         chi0=chi0+0.01
         GO TO 1
      ENDIF

      STOP
      END
```

```
!*************************************************************
!
!     Powell's Method Code
!
!     /mlazzara/powells/glenmod5.f
!
!*************************************************************

      implicit real*4(a-h,o-z), integer(i-n)
      common/data1/tetbm(50000),phi(50000),tetslit(50000),pe(5000
      0)
      common/data2/rs(50000),sv(50000),flw(50000),xm0(20),xm1(20)
      common/ data3/ ndata,nparamsfit,xdel,void,gbmeq,cix, rfx
      common/ array/ params(4),theta(16),thetac(16)
      common/ results/ res(50000),avres,rms,tetabmth(50000)
      dimension p(4),xi(4,4),stnderr2(4),covar(4,4)
      dimension fjv(5000),fji(5000),ci(5000)

C     INPUT PARAMETERS

      nparamsmax = 2
      nparamsfit = 2

      ftol = 1.0e-7

      WRITE (*,*) 'Initial value for a = '
      READ (*,*) a
      WRITE (*,*) 'Initial value for b = '
      READ (*,*) b

!      a=0.1
!      b=0.1

      WRITE (*,*) ' '
      WRITE (*,*) 'Initial guesses'
      WRITE (*,*) 'a =',a,'b =',b
      WRITE (*,*) ' '
C     DEPOSIT ALL PARAMETERS (TO BE FIXED AND TO BE FIT) IN
PARAMS(I)
      params(1) = a
      params(2) = b
c      params(3) = c
c      params(4) = d
c      params(5)= e
c      params(6)= f

      do 240 i=1,nparamsmax
         p(i) = params(i)
         do 230 j=1,nparamsfit
            xi(i,j) = 0.0
            if (i.eq.j) xi(i,j) = p(i)*0.1
 230      continue
 240   continue
```

```
C     OBTAIN BEST FIT OF P VECTOR TO DATA

      print *, 'Beginning powell fitting . . .'
      call powell(p,xi,nparamsfit,nparamsmax,ftol,iter,fret)
      print *, 'Done.'
      WRITE (*,*) ' '

C     RESET FIT PARAMETERS IN PARAMS TO VALUES IN P
      do 260 i=1,nparamsmax
         params(i)=p(i)
 260   continue

C     FINAL VALUES
      a = params(1)
      b = params(2)

! 280   continue
       do 281 i=1,nparamsfit
          print*,'parameter ',i,' is : ',params(i)
          write(2,*)'parameter ',i,' is :',params(i)
 281   continue

      print*,'  '
      print*,'value of function',fret
      WRITE (*,*) 'number of iterations',iter
      WRITE (*,*) ' '

      WRITE (*,*) '   data          calculated         Kc
Kd'
      WRITE (*,*) '  ------------------------------------------
-------'
      WRITE (*,*) ' '

       DO i=1,16
          rstokes=20+(i-1)*2
          WRITE (*,*) theta(i)-0.0113,thetac(i)
       ENDDO

      end
**************************************************************
*****
C     FUNCTION TO CALCULATE CHI-SQUARE VALUES FOR A GIVEN
*     PARAMETER VECTOR

      function chisq(pms)
      implicit real*4(a-h,o-z), integer(i-n)
      DOUBLE PRECISION vel,kappa,visc,temp,delta
      DOUBLE PRECISION Peclet
      DOUBLE PRECISION phiKc,phiKd,rstokes,part(16)
      DOUBLE PRECISION Rf1,Rf2,phi1,phi2
      DOUBLE PRECISION F,dp,littlef,S,Kc,Kd
      common/ data1/
tetbm(50000),phi(50000),tetslit(50000),pe(50000)
```

```
      common/
data2/rs(50000),sv(50000),flw(50000),xm0(20),xm1(20)
      common/ data3/ ndata,nparamsfit,xdel,void,gbmeq,cix
      common/ array/ params(4),theta(16),thetac(16)
      common/ results/ res(50000),avres,rms,tetabmth(50000)
      dimension pms(4)

C     ASSIGN CURRENT VALUE OF FITTED PARAMETERS

      chisq = 0.0
      ntotal = ndata

      vel=1.72e-6      ! m/s
      kappa=1.38e-23   ! Boltzman constant
      visc=.8516e-3    ! Pa s
      temp=300         ! Kelvin
      delta=6.02e-6    ! m

      theta(1)=0.58
      theta(2)=0.503
      theta(3)=0.421
      theta(4)=0.349
      theta(5)=0.279
      theta(6)=0.226
      theta(7)=0.182
      theta(8)=0.146
      theta(9)=0.121
      theta(10)=0.0975
      theta(11)=0.0814
      theta(12)=0.0666
      theta(13)=0.0565
      theta(14)=0.0481
      theta(15)=0.0414
      theta(16)=0.0358

      do 10 i=1,nparamsfit
         params(i)=pms(i)
         if (pms(i) .lt. 0.0) chisq = 1.0e30
 10   continue

C     THIS SECTION NOT GENERAL:  MAKE ASSIGNMENTS FROM PARAMS
      A=params(1)
      B=params(2)
c      C=params(3)
c      D=params(4)
c      E=params(5)
c      F=params(6)

       avres = 0

       Rf1=10          ! in Angstroms
       Rf2=35         ! in Angstroms

       phi1=0.1
```

```
        phi2=0.0

        dp=1.15*100    ! Darcy permeability of GBM in A**2

        DO i=1,16
       rstokes=20+(i-1)*2        ! Angstroms
          littlef=phi1*(1+rstokes/Rf1)**2+phi2*(1+rstokes/Rf2)**2
          S=exp(-0.84*littlef**1.09)
          F=(1+rstokes/sqrt(dp)+(1/9.0)*(rstokes/sqrt(dp))**2)**-
1
          part(i)=exp(-phi1*(1+rstokes/Rf1)**2-
phi2*(1+rstokes/Rf2)**2)
          Dinf=(kappa*temp)/(6*3.14159*visc*rstokes*1e-10)
          Kd=F*S
          Kc=a*exp(-b*rstokes)
!          WRITE (*,*) rstokes,Kd,Kc
          phiKd=exp(-a*rstokes)
          phiKc=exp(-b*rstokes)
       Peclet=(phiKc*vel*delta)/(phiKd*Dinf)
       thetac(i)=(phiKc)/(1-(1-phiKc)*exp(-Peclet))
       chisq=chisq+(1.0/16.0)*((thetac(i)-theta(i)+0.0113)
     $/(theta(i)-0.0113))**2
         ENDDO
         chisq=chisq**(0.5)

       return
! 660   FORMAT (A4,F7.3,A4,F7.3,A4,F7.3,A4,F7.3,A4,F7.3)
       end

**************************************************************
***********

C      POWELL'S ROUTINE

* subroutine powell *

       SUBROUTINE POWELL(P,XI,N,NP,FTOL,ITER,FRET)
       PARAMETER (NMAX=40,ITMAX=400)
       DIMENSION P(4),XI(4,4),PT(nmax),PTT(nmax),XIT(nmax)
       FRET = chisq(P)
       DO 11 J=1,N
         PT(J)=P(J)
11     CONTINUE
       ITER=0
1      ITER=ITER+1
       FP=FRET
       IBIG=0
       DEL=0.
       DO 13 I=1,N
         DO 12 J=1,N
           XIT(J)=XI(J,I)
12       CONTINUE
         FPTT=FRET
         CALL LINMIN(P,XIT,N,FRET)
```

```
        IF(ABS(FPTT-FRET).GT.DEL)THEN
          DEL=ABS(FPTT-FRET)
          IBIG=I
        ENDIF
13    CONTINUE
      IF(2.*ABS(FP-FRET).LE.FTOL*(ABS(FP)+ABS(FRET)))RETURN
      IF(ITER.EQ.ITMAX) then
         print*, 'Powell exceeding maximum iterations.'
         return
      endif
      DO 14 J=1,N
        PTT(J)=2.*P(J)-PT(J)
        XIT(J)=P(J)-PT(J)
        PT(J)=P(J)
14    CONTINUE
      FPTT =chisq(PTT)
      IF(FPTT.GE.FP)GO TO 1
      T=2.*(FP-2.*FRET+FPTT)*(FP-FRET-DEL)**2-DEL*(FP-FPTT)**2
      IF(T.GE.0.)GO TO 1
      CALL LINMIN(P,XIT,N,FRET)
      DO 15 J=1,N
        XI(J,IBIG)=XIT(J)
15    CONTINUE
      GO TO 1
      END

* subroutine linmin *

      SUBROUTINE LINMIN(P,XI,N,FRET)
      PARAMETER (NMAX=80,TOL=1.E-4)
      EXTERNAL F1DIM
      DIMENSION P(n),XI(n)
      COMMON /F1COM/ NCOM,PCOM(NMAX),XICOM(NMAX)
      NCOM=N
      DO 11 J=1,N
        PCOM(J)=P(J)
        XICOM(J)=XI(J)
11    CONTINUE
      AX=0.
      XX=1.
      CALL MNBRAK(AX,XX,BX,FA,FX,FB)
      FRET=BRENT(AX,XX,BX,TOL,XMIN)
      DO 12 J=1,N
        XI(J)=XMIN*XI(J)
        P(J)=P(J)+XI(J)
12    CONTINUE
      RETURN
      END

* subroutine mnbrak

      SUBROUTINE MNBRAK(AX,BX,CX,FA,FB,FC)
      PARAMETER (GOLD=1.618034, GLIMIT=100., TINY=1.E-20)
```

```
      FA=f1dim(AX)
      FB=f1dim(BX)
      IF(FB.GT.FA)THEN
        DUM=AX
        AX=BX
        BX=DUM
        DUM=FB
        FB=FA
        FA=DUM
      ENDIF
      CX=BX+GOLD*(BX-AX)
      FC=f1dim(CX)
1     IF(FB.GE.FC)THEN
        R=(BX-AX)*(FB-FC)
        Q=(BX-CX)*(FB-FA)
        U=BX-((BX-CX)*Q-(BX-AX)*R)/(2.*SIGN(MAX(ABS(Q-
R),TINY),Q-R))
        ULIM=BX+GLIMIT*(CX-BX)
        IF((BX-U)*(U-CX).GT.0.)THEN
          FU=f1dim(U)
          IF(FU.LT.FC)THEN
            AX=BX
            FA=FB
            BX=U
            FB=FU
            RETURN
          ELSE IF(FU.GT.FB)THEN
            CX=U
            FC=FU
            RETURN
          ENDIF
          U=CX+GOLD*(CX-BX)
          FU=f1dim(U)
        ELSE IF((CX-U)*(U-ULIM).GT.0.)THEN
          FU=f1dim(U)
          IF(FU.LT.FC)THEN
            BX=CX
            CX=U
            U=CX+GOLD*(CX-BX)
            FB=FC
            FC=FU
            FU=f1dim(U)
          ENDIF
        ELSE IF((U-ULIM)*(ULIM-CX).GE.0.)THEN
          U=ULIM
          FU=f1dim(U)
        ELSE
          U=CX+GOLD*(CX-BX)
          FU=f1dim(U)
        ENDIF
        AX=BX
        BX=CX
        CX=U
        FA=FB
```

```
          FB=FC
          FC=FU
          GO TO 1
        ENDIF
        RETURN
        END

* function brent *

        FUNCTION BRENT(AX,BX,CX,TOL,XMIN)
        PARAMETER (ITMAX=1000,CGOLD=.3819660,ZEPS=1.0E-10)

        A=MIN(AX,CX)
        B=MAX(AX,CX)
        V=BX
        W=V
        X=V
        E=0.
        FX=f1dim(X)
        FV=FX
        FW=FX
        DO 11 ITER=1,ITMAX
          XM=0.5*(A+B)
          TOL1=TOL*ABS(X)+ZEPS
          TOL2=2.*TOL1
          IF(ABS(X-XM).LE.(TOL2-.5*(B-A))) GOTO 3
          IF(ABS(E).GT.TOL1) THEN
            R=(X-W)*(FX-FV)
            Q=(X-V)*(FX-FW)
            P=(X-V)*Q-(X-W)*R
            Q=2.*(Q-R)
            IF(Q.GT.0.) P=-P
            Q=ABS(Q)
            ETEMP=E
            E=D
            IF(ABS(P).GE.ABS(.5*Q*ETEMP).OR.P.LE.Q*(A-X).OR.
     *         P.GE.Q*(B-X)) GOTO 1
            D=P/Q
            U=X+D
            IF(U-A.LT.TOL2 .OR. B-U.LT.TOL2) D=SIGN(TOL1,XM-X)
            GOTO 2
          ENDIF
1         IF(X.GE.XM) THEN
            E=A-X
          ELSE
            E=B-X
          ENDIF
          D=CGOLD*E
2         IF(ABS(D).GE.TOL1) THEN
            U=X+D
          ELSE
            U=X+SIGN(TOL1,D)
          ENDIF
          FU= f1dim(U)
```

```
        IF(FU.LE.FX) THEN
          IF(U.GE.X) THEN
            A=X
          ELSE
            B=X
          ENDIF
          V=W
          FV=FW
          W=X
          FW=FX
          X=U
          FX=FU
        ELSE
          IF(U.LT.X) THEN
            A=U
          ELSE
            B=U
          ENDIF
          IF(FU.LE.FW .OR. W.EQ.X) THEN
            V=W
            FV=FW
            W=U
          ELSE IF(FU.LE.FV .OR. V.EQ.X .OR. V.EQ.W) THEN
            V=U
            FV=FU
          ENDIF
        ENDIF
11    CONTINUE
      PAUSE 'Brent exceed maximum iterations.'
3     XMIN=X
      BRENT=FX
      RETURN
      END

* function f1dim *

      FUNCTION F1DIM(X)
      PARAMETER (NMAX=80)
      COMMON /F1COM/ NCOM,PCOM(NMAX),XICOM(NMAX)
      DIMENSION XT(nmax)
      DO 11 J=1,NCOM
        XT(J)=PCOM(J)+X*XICOM(J)
11    CONTINUE
      F1DIM = chisq(XT)
      RETURN
      END

      FUNCTION EPART(rs,rf,qs,gbmeq,ci,void)
      double precision n, tau,B,as,agbm

c      rs=20.
c      rf=2.e-9
c      qs=-0.0489
c      gbmeq=-7.6
```

```
c       ci=0.01
c       void=.93
        phi=-log(void)
        xrs=rs/1e10
        temp=300.
        eps=78.3*8.854e-12
        as=xrs*96500*qs/(8.314*temp*eps)
        agbm=xrs*96500*(48250*gbmeq/phi*rf)/(8.314*temp*eps)
        kap=(ci*2*1000.*96500.**2/(8.314*temp*eps))**.5
        tau=xrs*kap
        B=rf/xrs
        h=0.
        epart=0
        dh=1.e-10
        l=0
 100    continue
        l=l+1
        n=h*kap
        gh=2*phi*(h+xrs+rf)/(rf**2)*exp(-
phi*(h+xrs+rf)**2/(rf**2))
        EA=as*agbm*2.3523*tau**-1.2472*B**.7599
        EB=exp(-1.0956*n)
        EC=as**2*.357*tau**-.9512*B**.5052
        ED=exp(-3.7684*n)
        EE=agbm**2*.4473*tau**-1.1512*B**.931
        EF=exp(-2.4987*n)
        E=(8.314*temp/96500)**2*eps*xrs/(temp*1.38e-23)*
     $(EA*EB+EC*ED+EE*EF)
c        print*,n,E,EA*EB+EC*ED+EE*EF
c         write (*,111)'gh=',gh,'E=',E
        epart=epart+exp(-E)*gh*dh
c        print*, exp(-E)*gh*dh,n
        if (l.gt.50)then
        if (exp(-E)*gh*dh.lt.1e-6) then
           goto 200
        endif
        endif
        h=h+dh
        goto 100
 200    continue
 111     format(a4,f16.3,a4,f16.3)

c       print*,'part=', epart
        return
        end
```

REFERENCES

1. Abrhamson DR. Structure and development of the glomerular capillary wall and basement membrane *Am J Physiol Renal Physiol* 253 F783-F794, 1987.

2. Al-Malah K, McGuire J and Sproull R. A macroscopic model for the single-component protein adsorption isotherm. *J Colloid Interface Sci* 170: 261-268, 1995.

3. Anderson JL and Brannon JH. Concentration dependence of the distribution coefficient for macromolecules in porous media. *J Polym Sci* 19: 405-421, 1981.

4. Anderson JL and Malone DM. Mechanism of osmotic flow in porous membranes. *Biophys J* 14: 957-982, 1974.

5. Arnott S, Fulmer A, Scott WE, Dea ICM, Moorhouse R and Rees DA. The agarose double helix and its function in agarose gel structure. *J Mol Biol* 90: 269-284, 1974.

6. Baylis C, Ichikawa I, Willis WT, Wilson CB and Brenner BM. Dynamics of glomerular ultrafiltration. Ix. Effects of plasma protein concentration. *Am J Physiol Renal Fluid Electrolyte Physiol* 232: F58-F71, 1977.

7. Bertolatus JA and Klinzman D. Macromolecular sieving by glomerular basement membrane in vitro: Effect of polycation or biochemical modifications. *Microvasc Res* 41: 311-327, 1991.

8. Blouch K, Deen WM, Fauvel JP, Bialek J, Derby G and Myers BD. Molecular configuration and glomerular size selectivity in healthy and nephrotic humans. *Am J Physiol Renal Physiol* 42: F430-F437, 1997.

9. Bohrer MP, Patterson GD and Carroll PJ. Hindered diffusion of dextran and ficoll in microporous membranes. *Macromolecules* 17: 1170-1173, 1984.

10. Bolton GR and Deen WM. Limitations in the application of fiber-matrix models to glomerular basement membrane. In: *Membrane transport and renal physiology*, edited by Layton HE and Weinstein AM. New York: Springer-Verlag, 2001.

11. Bolton GR, Deen WM and Daniels BS. Assessment of the charge selectivity of glomerular basement membrane using ficoll sulfate. *Am J Physiol Renal Physiol* 43: F889-F896, 1998.

12. Brannon JH and Anderson JL. Concentration effects on partitioning of dextrans and serum albumin in porous glass. *J Polym Sci: Polym Phys Ed* 20: 857-865, 1982.

13. Bray J and Robinson GB. Influence of charge on filtration across renal basement membrane films in vitro. *Kidney Int* 25: 527-533, 1984.

14. Buck KKS, Gerhardt NI, Dungan SR and Phillips RJ. The effect of solute concentration on equilibrium partitioning in polymeric gels. *J Colloid Interface Sci* 234: 400-409, 2001.

15. Burkitt HG, Young B and Heath JW. *Wheater's Functional Histology*. Edinburgh: Churchill Livingstone, 1993.

16. Burne MJ, Adal Y, Cohen N, Panagiotopoulos S, Jerums G and Comper WD. Anomalous decrease in dextran sulfate clearance in the diabetic rat kidney. *Am J Physiol Renal Physiol* 274: F700-F708, 1998.

17. Burne MJ, Vyas SV, Smit MF, Pratt LM and Comper WD. Competition between polyanions in glomerular binding and renal clearance. *Arch Biochem Biophys* 340: 257-264, 1997.

18. Campbell NA. *Biology*. Redwood City: The Benjamin/Cummings Publishing Company, Inc., 1990.

19. Casassa EF. Equilibrium distribution of flexible polymer chains between a macroscopic solution phase and small voids. *J Polym Sci: Polym Lett* 5: 773, 1967.

20. Chang RLS, Deen WM, Robertson CR and Brenner BM. Permselectivity of the glomerular capillary wall. Iii. Restricted transport of polyanions. *Kidney Int* 8: 212-218, 1975.

21. Clague DS, Kandhai BD, Zhang R and Sloot PMA. Hydraulic permeability of (un)bounded fibrous media using the lattice boltzmann method. *Phys Rev E* 61: 616-625, 2000.

22. Clague DS and Phillips RJ. A numerical calculation of the hydraulic permeability of three-dimensional disordered fibrous media. *Phys Fluids* 9: 1562-1572, 1997.

23. Cochrane SM, Byrne JC and Robinson GB. The permselectivity of glomerular basement membrane can be compromised by glycation or by exposure to low levels of hypochlorite. *Biochim Biophys Acta* 1361: 217-228, 1997.

24. Cochrane SM and Robinson GB. In vitro glycation of glomerular basement membrane alters its permeability: A possible mechanism in diabetic complications. *FEBS Lett* 375: 41-44, 1995.

25. Comper WD and Glasgow EF. Charge selectivity in kidney ultrafiltration. *Kidney Int* 47: 1242-1251, 1995.

26. Comper WD, Lee ASN, Tay M and Adal Y. Anionic charge concentration of rat kidney glomeruli and glomerular basement membrane. *Biochem J* 289: 647-652, 1993.

27. Comper WD, Tay M, Wells X and Dawes J. Desulfation of dextran sulfate during kidney ultrafiltration. *Biochem J* 297: 31-34, 1994.

28. Cotran RS, JKumar V and Collins T. *Robbins pathologic basis of disease*. Philadelphia: W.B. Saunders Compnay, 1999.

29. Curry FE and Michel CC. A fiber matrix model of capillary permeability. *Microvasc Res* 20: 96-99, 1980.

30. Curry FE, Rutledge JC and Lenz JF. Modulation of microvessel wall charge by plasma glycoprotein orosomucoid. *Am J Physiol Heart Circ Physiol* 257: H1354-H1359, 1989.

31. Daniels BS. Increased albumin permeability in vitro following alterations of glomerular charge is mediated by the cells of the filtration barrier. *J Lab Clin Med* 124: 224-230, 1994.

32. Daniels BS, Deen WM, Mayer G, Meyer T and Hostetter T. Glomerular permeability barrier in the rat: Functional assessment by in vitro methods. *J Clin Invest* 92: 929-936, 1993.

33. Daniels BS, Hauser EH, Deen WM and Hostetter TH. Glomerular basement membrane: In vitro studies of water and protein permeability. *Am J Physiol Renal Physiol* 262: F919-926, 1992.

34. Davidson MG and Deen WM. Equilibrium partitioning of flexible macromolecules between bulk solution and cylindrical pores. *Macromolecules* 20: 1141-1146, 1987.

35. Davidson MG and Deen WM. Hindered diffusion of water-soluble macromolecules in membranes. *Macromolecules* 21: 3474-3481, 1988a.

36. Davidson MG and Deen WM. Hydrodynamic theory for the hindered transport of flexible macromolecules in porous membranes. *J Membr Sci* 35: 167-192, 1988b.

37. DeBelder AN and Granath K. Preparation and properties of fluorescin-labeled dextrans. *Carbohydr Res* 30: 375-378, 1973.

38. Deen WM. Hindered transport of large molecules in liquid-filled pores. *AIChE J* 33: 1409-1425, 1987.

39. Deen WM. *Analysis of transport phenomena.* New York: Oxford University Press, 1998.

40. Deen WM, Lazzara MJ and Myers BD. Structural determinants of glomerular permeability. *Am J Physiol Renal Physiol* 281: F579-F596, 2001.

41. Djabourov M, Clark AH, Rowlands DW and Ross-Murphy SB. Small-angle x-ray scattering characterization of agarose sols and gels. *Macromol Rev* 22: 180-188, 1989.

42. Drummond MC and Deen WM. Stokes flow through a row of cylinders between parallel walls: Model for the glomerular slit diaphragm. *J Biomech Eng* 116: 184-189, 1994a.

43. Drummond MC and Deen WM. Structural determinants of glomerular hydraulic permeability. *Am J Physiol Renal Physiol* 266: F1-F12, 1994b.

44. Drummond MC and Deen WM. Hindered transport of macromolecules through a single row of cylinders: Application to glomerular filtration. *J Biomech Eng* 117: 414-422, 1995.

45. Drummond MC, Kristal B, Myers BD and Deen WM. Structural basis for reduced glomerular filtration capacity in nephrotic humans. *J Clin Invest* 94: 1187-1195, 1994.

46. Dubin PL and Principi JM. Optimization of size-exclusion separation of proteins on a superose column. *J Chromatogr* 479: 159-164, 1989.

47. Edwards A, Daniels BS and Deen WM. Hindered transport of macromolecules in isolated glomeruli. Ii. Convection and pressure effects in basement membrane. *Biophys J* 72: 214-222, 1997a.

48. Edwards A, Daniels BS and Deen WM. Ultrastructural model for size selectivity in glomerular filtration. *Am J Physiol Renal Physiol* 276: F892-F902, 1999.

49. Edwards A, Deen WM and Daniels BS. Hindered transport of macromolecules in isolated glomeruli. I. Diffusion across intact and cell-free capillaries. *Biophys J* 72: 204-213, 1997b.

50. Ellis EN, Steffes MW, Chavers B and Mauer SM. Observations of glomerular epithelial cells structure in patients with type i diabetes mellitus. *Kidney Int* 32: 736-741, 1987.

51. Fanti LA and Glandt ED. Partitioning of spherical particles into fibrous matrices 1. Density-functional theory. *J Colloid Interface Sci* 135: 385-395, 1990a.

52. Fanti LA and Glandt ED. Partitioning of spherical particles into fibrous matrices 2. Monte carlo simulation. *J Colloid Interface Sci* 135: 396-404, 1990b.

53. Furukawa T, Ohno S, Oguchi H, Hora K, Tokunaga S and Furuta S. Morphometric study of glomerular slit diaphragms fixed by rapid-freezing and freeze substitution. *Kidney Int* 40: 621-624, 1991.

54. Giddings CJ, Hucera E, Russel CP and Myers MN. Statistical theory for the equilibrium distribution of rigid molecules in inert porous networks. Exclusion chromatography. *J Phys Chem* 72: 43697-44408, 1968.

55. Glandt ED. Distribution equilibrium between a bulk phase and small pores. *AIChE J* 27: 51-59, 1981.

56. Guasch A, Deen WM and Myers BD. Charge-selectivity of the glomerular filtration barrier in healthy and nephrotic humans. *J Clin Invest* 92: 2274-2282, 1993.

57. Happel J and Brenner H. Low reynolds number hydrodynamics. Dordrecht: Nijhoff, 1983, p. 222, 224.

58. Haraldsson B and Rippe B. Orosomucoid as one of the serum components contributing to normal capillary permselectivity in rat skeletal muscle. *Acta Physiol Scand* 129: 127-135, 1987.

59. Haraldsson BS, Johnsson EKA and Rippe B. Glomerular permselectivity is dependent on adequate serum concentrations of orosomucoid. *Kidney Int* 41: 310-316, 1992.

60. Holthofer H, Ahola H, Solin M-L, Wang S, Palmen T, Luimula P, Miettinen A and Kerjaschki D. Nephrin localizes at the podocyte filtration slit area and is characteristically spliced in the human kidney. *Am J Path* 155: 1681-1687, 1999.

61. Hora K, Ohno S, Ogushi H, Furukawa T and Furuta S. Three-dimensional study of glomerular slit diaphragm by the quick-freezing and deep-etching replica method. *Eur J Cell Biol* 53: 402-406, 1990.

62. Jackson GW and James DF. The permeability of fibrous media. *Can J Chem Eng* 64: 364-374 1986.

63. Jansons KM and Phillips CG. On the application of geometric probability theory to polymer networks and suspensions. *J Colloid Interface Sci* 137: 75-91, 1990.

64. Johnson EM. *Partitioning and diffusion of macromolecules in charged gels* (Ph.D.). Cambridge, MA: Massachusetts Institute of Technology, 1995.

65. Johnson EM, Berk DA, Jain RK and Deen WM. Diffusion and partitioning of proteins in charged agarose gels. *Biophys J* 68: 1561-1568, 1995.

66. Johnson EM, Berk DA, Jain RK and Deen WM. Hindered diffusion in agarose gels: Test of effective medium model. *Biophys J* 70: 1017-1023, 1996.

67. Johnson EM and Deen WM. Electrostatic effects on the equilibrium partitioning of spherical colloids in random fibrous media. *J Colloid Interface Sci* 178: 749-756, 1996.

68. Johnsson E and Haraldsson B. Addition of purified orosomucoid preserves the glomerular permeability for albumin in isolated perfused rat kidneys. *Acta Physiol Scand* 147: 1-8, 1993.

69. Johnston ST and Deen WM. Hindered convection of proteins in agarose gels. *J Membr Sci* 153: 271-279, 1999.

70. Johnston ST and Deen WM. Hindered convection of ficoll and proteins in agarose gels. *Ind Eng Chem Res* 41: 340-346, 2002.

71. Johnston ST, Smith KA and Deen WM. Concentration polarization in stirred ultrafiltration cells. *AIChE J* 47: 1115-1125, 2001.

72. Kanwar YS and Farquhar MG. Anionic sites in the glomerular basement membrane: In vivo and in vitro localization to the laminae rarae by cationic probes. *J Cell Biol* 81: 137-153, 1979.

73. Kanwar YS and Venkatachalam MA. Ultrastructure of glomerulus and juxtaglomerular apparatus. In: *Handbook of physiology renal physiology*. Bethesda, MD: Am Physiol Soc, 1992, p. 3-40.

74. Kapur V, Charkoudian J and Anderson JL. Transport of proteins through gel-filled porous membranes. *J Membr Sci* 131: 143-153, 1997.

75. Kondo H. Rat kidney glomerular basement membrane visualized in situ by embedment-free sectioning and subsequent platinum-carbon replication. *J Electron Microsc Tech* 14: 63-69, 1990.

76. Kong DD, Kosar TF, Dungan SR and Phillips RJ. Measurement of hindered diffusion of proteins and nonionic micelles in agarose gels by holographic interferometry. *AIChE J* 43: 25-32, 1997.

77. Lafayette RA, Druzin M, Sibley R, Derby G, Malik T, Huie P, Polhemus C, Deen WM and Myers BD. Nature of glomerular dysfunction in pre-eclampsia. *Kidney Int* 54: 1240-1249, 1998.

78. Laurent TC. Determination of the structure of agarose gels by gel chromatography. *Biochim Biophys Acta* 136: 199-205, 1967.

79. Laurent TC and Killander J. A theory of gel filtration and its experimental verification. *J Chromatog* 14: 317-330, 1964.

80. Laurie GW, Leblond CP, Inoue S, Martin GR and Chung A. Fine structure of the glomerular basement membrane and immunolocalization of five basement membrane components to the lamina densa (basal lamina) and its extensions in both glomeruli and tubules of the rat kidney. *Am J Anat* 169: 463-481, 1984.

81. Lazzara MJ, Blankschtein D and Deen WM. Effects of multisolute steric interactions on membrane partition coefficients. *J Colloid Interface Sci* 226: 112-122, 2000.

82. Lazzara MJ and Deen WM. Effects of plasma proteins on sieving of tracer macromolecules in glomerular basement membrane. *Am J Physiol Renal Physiol* 281: F860-F868, 2001.

83. Lea PJ, Silverman M, Hegele R and Hollenberg MJ. Tridimensional ultrastructure of glomerular capillary endothelium revealed by high-resolution scanning electron microscopy. *Microvasc Res* 38: 296-308, 1989.

84. Lenkkeri U, Mannikko M, McCready P, Lamerdin J, Gribouval O, Niaudet P, Antignac C, Kashtan C, Holmberg C, Olsen A, Kestila M and Tryggvason K. Structure of the gene for congenital nephrotic syndrome of the finnish type (nphs1) and characterization of mutations. *Am J Hum Genet* 64: 51-61, 1999.

85. Limbach KW, Nitsche JM and Wei J. Partitioning of nonspherical molecules between bulk solution and porous solids. *AIChE J* 35: 42-52, 1989.

86. Lin NP and Deen WM. Effects of long-range polymer-pore interactions on the partitioning of linear polymers. *Macromolecules* 23: 2947-2955, 1990.

87. Lindstrom KE, Johnson E and Haraldsson B. Glomerular charge selectivity for proteins larger than serum albumin as revealed by lactate dehydrogenase isoforms. *Acta Physiol Scand* 162: 481-488, 1998.

88. Luft JH. Fine structures of capillary and endocapillary layer as revealed by ruthenium red. *Fed Proc* 25: 1773-1783, 1966.

89. Maddox DA, Deen WM and Brenner BM. Glomerular filtration. In: *Handbook of physiology*. Bethesda, MD: Am Physiol Soc, 1992, p. 545-638.

90. Mann GE. Alterations of myocardial capillary permeability by albumin in the isolated, perfused rabbit heart. *J Physiol* 319: 311-323, 1981.

91. Mason JC, Curry FE and Michel CC. The effects of proteins upon the filtration coefficient of individually perfused frog mesenteric capillaries. *Microvasc Res* 13: 185-202, 1977.

92. Maunsbach AB. Absorption of 125i-labeled homologous albumin by rat kidney proximal tubule cells. *J Ultrstruct Res* 15: 197-241, 1966.

93. Mayer G, Lafayette RA, Oliver J, Deen WM, Myers BD and Meyer TW. Effects of angiotensin ii receptor blockade on remnant glomerular permselectivity. *Kidney Int* 43: 346-353, 1993.

94. McDonagh PF. Both protein and blood cells reduce coronary microvascular permeability to macromolecules. *Am J Physiol Heart Circ Physiol* 245: H698-H706, 1983.

95. Meyer PL. *Introductory probability and statistical applications*. Reading, MA: Addison-Wesley, 1965.

96. Michel CC. Capillary permeability and how it may change. *J Physiol* 404: 1-29, 1988.

97. Michel CC, Phillips ME and Turner MR. The effects of native and modified bovine serum albumin on the permeability of frog mesenteric capillaries. *J Physiol* 360: 333-346, 1985.

98. Mitchell BD and Deen WM. Theoretical effects of macromolecule concentration and charge on membrane rejection coefficients. *J Membrane Sci* 19: 75-100, 1984.

99. Mitchell BD and Deen WM. Effect of concentration on the rejection coefficients of rigid macromolecules in track-etch membranes. *J Colloid Interface Sci* 113: 132-142, 1986.

100. Nikas YJ, Liu CL, Srivastava T, Abbott NL and Blankschtein D. Protein partitioning in two-phase aqueous nonionic micellar solutions. *Macromolecules* 25: 4797-4806, 1992.

101. Ogston AG. The spaces in a uniform random suspension of fibers. *Trans Faraday Soc* 54: 1754-1757, 1958.

102. Ogston AG, Preston BN and Wells JD. On the transport of compact particles through solutions of chain polymers. *Proc R Soc Lond A* 333: 297-316, 1973.

103. Ohlson M, Sorensson J and Haraldsson B. Glomerular size and charge selectivity in the rat as revealed by fitc-ficoll and albumin. *Am J Physiol Renal Physiol* 279: F84-F91, 2000.

104. Ohlson M, Sorensson J and Haraldsson B. A gel-membrane model of glomerular charge and size selectivity in series. *Am J Physiol Renal Physiol* 280: F396-F405, 2001.

105. Oliver JD, Anderson S, Troy JL, Brenner BM and Deen WM. Determination of glomerular size-selectivity in the normal rat with ficoll. *J Am Soc Nephrol* 3: 214-228, 1992.

106. Oncley JL, Stratchard G and Brown A. Physical-chemical characteristics of certain of the proteins of normal human plasma. *J Phys Colloid Chem* 51: 184, 1947.

107. Osicka TM and Comper WD. Glomerular charge selectivity for anionic and neutral horseradish peroxidase. *Kidney Int* 47: 1630-1637, 1995.

108. Osicka TM and Comper WD. Tubular inhibition destroys charge selectivity for anionic and neutral horseradish peroxidase. *Biochim Biophys Acta* 1381: 170-178, 1998.

109. Osicka TM, Pratt LM and Comper WD. Glomerular capillary wall permeability to albumin and horseradish peroxidase. *Nephrology* 2: 199-212, 1996.

110. Pappenheimer JR, Renkin EM and Borrero LM. Filtration, diffusion and molecular sieving through peripheral capillary membranes. *Am J Physiol* 167: 13-46, 1951.

111. Peters T. Serum albumin. In: *Advances in protein chemistry*, edited by Anfinsen CB, Edsall JT and Richards FM: Academic Press, Inc., 1985.

112. Phillips RJ. A hydrodynamic model for hindered diffusion of proteins and micelles in hydrogels. *Biophys J* 79: 3350-3353, 2000.

113. Potschka M. Universal calibration of gel permeation chromatography and determination of molecular shape in solution. *Anal Biochem* 162: 47-64, 1987.

114. Reisner J, Kriz W, Kretzler M and Mundel P. The glomerular slit diaphragm is a modified adherens junction. *J Am Soc Nephrol* 11: 1-8, 2000.

115. Remuzzi A, Perico N, Amuchastegui CS, Malanchini B, Mazerska M, Battaglia C, Bertani T and Remuzzi G. Short- and long-term effect of angiotensin ii receptor blockade in rats with experimental diabetes. *J Am Soc Nephrol* 4: 40-49, 1993.

116. Rennke HG, Patel Y and Venkatachalam MA. Glomerular filtration of proteins: Clearance of anionic, neutral, and cationic horseradish peroxidase in the rat. *Kidney Int* 13: 324-328, 1978.

117. Rippe B and Folkow B. Capillary permeability to albumin in normotensive and spontaneously hypertensive rats. *Acta Physiol Scand* 101: 72-83, 1977.

118. Robinson GB and Walton HA. Ultrafiltration through basement membrane. In: *Renal basement membranes in health and disease*, edited by Price RG and Hudson BG. London: Academic, 1987, p. 147-161.

119. Robinson GB and Walton HA. Glomerular basement membrane as a compressible ultrafilter. *Microvasc Res* 38: 36-48, 1989.

120. Rodewald R and Karnovsky MJ. Porous substructure of the glomerular slit diaphragm in the rat and mouse. *J Cell Biol* 60: 423-433, 1974.

121. Rostgaard J and Qvortrup K. Electron microscopic demonstrations of filamentous molecular sieve plugs in capillary fenestrae. *Microvasc Res* 53: 1-13, 1997.

122. Ruotsalainen V, Ljungberg P, Wartiovaara J, Lenkkeri U, Kestila M, Jalanko H, Holmberg C and Tryggvason K. Nephrin is specifically located at the slit diaphragm of glomerular podocytes. *PNAS USA* 96: 7962-7967, 1999.

123. Ryan GB. The glomerular filtration barrier. In: *Advances in renal physiology*, edited by Lote CJ. New York: Liss, 1986, p. 1-32.

124. Ryan GB and Karnovsky MJ. Distribution of endogenous albumin in the rat glomerulus: Role of hemodynamic factors in glomerular barrier function. *Kidney Int* 9: 36-45, 1976.

125. Saksena S and Zydney AL. Influence of protein-protein interactions on bulk mass transport during ultrafiltration. *J Membrane Sci* 125: 93, 1997.

126. Shea SM and Morrison AB. A stereological study of the glomerular filter in the rat: Morphometry of the slit diaphragm and basement membrane. *J Cell Biol* 67: 436-443, 1975.

127. Shirahama T and Cohen AS. The role of mucopolysaccharides in vesicle architecture and endothelial transport. An electron microscope study of myocardial blood vessels. *J Cell Biol* 52: 198-206, 1972.

128. Simionescu M and Siomionescu N. Functions of the endothelial cell surface. *Annu Rev Physiol* 48: 279-293, 1986.

129. Smith FG and Deen WM. Electrostatic effects on the partitioning of spherical colloids between dilute bulk solution and cylindrical pores. *J Colloid Interface Sci* 91: 571-590, 1983.

130. Sorensson J. *Properties of the endothelial cells and the glomerular barrier* (Ph.D.). Gothenburg, Sweden: Gothenburg University, 2000.

131. Sorensson J, Ohlson M, Lindstrom K and Haraldsson B. Glomerular charge selectivity for horseradish peroxidase at low and normal ionic strengths. *Acta Physiol Scand* 163: 83-91, 1998.

132. Squarer A, Ambalavanan S, Kristal B, Deen WM, Sibley R, Anderson L and Myers BD. Mechanisms of progressive glomerular injury in membranous nephropathy. *J Am Soc Nephrol* 9: 1389-1398, 1998.

133. Squire PG, Moser P and O'Konski CT. The hydrodynamic properties of bovine serum albumin monomer and dimer. *Biochem* 7: 4261-4272, 1968.

134. Takami H, Naramoto A, Shigematsu H and Ohno S. Ultrastructure of glomerular basement membrane by quick-freeze deep-etch methods. *Kidney Int* 39: 659-664, 1991.

135. Tanford C. Physical chemistry of macromolecules. New York: Wiley, 1961, p. 359.

136. Tay M, Comper WD and Singh AK. Charge selectivity in kidney ultrafiltration is associated with glomerular uptake of transport probes. *Am J Physiol Renal Physiol* 260: F549-F554, 1991.

137. Tisher C and Madsen KM. Anatomy of the kidney. In: *The kidney* (3rd ed.), edited by Brenner BM and Rector J, F.C. Philadelphia: W.B. Saunders Company, 1986, p. 3-60.

138. Tojo A and Hitoshi E. Intrarenal handling of proteins in rats using fractional micropuncture technique. *Am J Physiol Renal Physiol* 263: F601-F606, 1992.

139. Tryggvason K. Unraveling the mechanisms of glomerular ultrafiltration: Nephrin, a key component of the slit diaphragm. *J Am Soc Nephrol* 10: 2440-2445, 1999.

140. Tucker BJ and Blantz RC. Effects of glomerular filtration dynamics on the glomerular permeability coefficient. *Am J Physiol Renal Fluid Electrolyte Physiol* 240: F245-254, 1981.

141. Vogel KG. Glycosaminoglycans and proteoglycans. In: *Extracellular matric assembly and structure*, edited by Yurchenco PD. San Diego, CA: Academic, 1994, p. 243-279.

142. Vyas SV, Burne MJ, Pratt LM and Comper WD. Glomerular processing of dextran sulfate during transcapillary transport. *Arch Biochem Biophys* 332: 205-212, 1996.

143. Vyas SV, Parker J-A and Comper WD. Uptake of dextran sulfate by glomerular intracellular vesicles during kidney ultrafiltration. *Kidney Int* 47: 945-950, 1995.

144. Walton HA, Byrne J and Robinson GB. Studies of the permeation properties of glomerular basement membrane: Cross-linking renders glomerular basement membrane permeable to protein. *Biochim Biophys Acta* 1138: 173-183, 1992.

145. Watson PD. Effects of blood-free and protein-free perfusion on cfc in the isolated cat hindlimb. *Am J Physiol Heart Circ Physiol* 245: H911-H919, 1983.

146. Webber WA and Blackbourne J. The permeability of the immature glomerulus to large molecules. *Lab Invest* 23: 1-7, 1970.

147. White JA and Deen WM. Equilibrium partitioning of flexible macromolecules in fibrous membranes and gels. *Macromolecules* 33: 8504-8511, 2000.

148. White JA and Deen WM. Effects of solute concentration on equilibrium partitioning of flexible macromolecules in fibrous membranes and gels. *Macromolecules* 34: 8278-8285, 2001.

149. Yurchenco PD and Ruben GC. Basement membrane strucutre in situ: Evidenve for lateral association in the type iv collagen network. *J Cell Biol* 105: 2559-2568, 1987.

150. Zimmerman SB and Trach SO. Excluded volume effects on the partition of macromolecules between two liquid phases. *Biopolymers* 30: 703-718, 1990.